Incomplete Dynamic Measurement in Structural Damage Assessment

By

Pui Shan, MAK

Master of Philosophy

in

the Civil and Structural Engineering Department

The Hong Kong Polytechnic University

January 2001

Abstract

Abstract of thesis entitled:

Incomplete Dynamic Measurement in Structural Damage Assessment

Submitted by Pui Shan, MAK

for the degree of Master of Philosophy

at The Hong Kong Polytechnic University in January 2001

The structural damage assessment strategy adopted in this thesis is to localize the damage sites first using incomplete measured mode shapes, and to quantify the structural damage extent later using measured frequencies which are less contaminated by measurement noise and with better accuracy than mode shapes.

Modal strain energy change (*MSEC*) has been proved to be more sensitive to structural damage than natural frequencies and mode shapes. The parameter *MSEC* is used in the correlation matching of the Multiple Damage Location Assurance Criterion (*MDLAC*) to localize the damage. The sensitivity of *MSEC* is a function of the analytical property matrices, natural frequencies and mode shapes of the original structure. The incomplete measured mode shapes before and after damage and the analytical stiffness matrix are required to calculate the experimental *MSEC* which are then normalized. The potential damage sites are identified as those elements with higher *MDLAC* values. The *MDLAC* values on the different combinations of the potential damage sites are further computed. The final damage sites are located corresponding to the combination with the largest *MDLAC* value. Simulation studies of the damage localization method are based on a three-storey plane frame.

After localization of the damage sites, the damage extent of the final damage sites can be determined using the measured natural frequencies. A structural damage quantification method is developed using only the first order sensitivity terms in which a linear sequential filtering technique is used to relate the analytical and experimental sets of eigenvalues including the measurement noise matrix. An unbiased minimum variance error estimation method is used for an optimal solution. Weight linear least squares method is used to solve the identification equation.

Simulation studies on the damage quantification method are conducted on the same three-storey plane frame.

The accuracy of identification using only the first order terms will be reduced when dealing with large damage, and the damage quantification method including the second order terms in the Taylor's expansion is proposed. Simulation studies on the three-storey plane frame are again performed.

In these two damage quantification methods, the formulation has the capability to estimate a larger set of eigenvalues from a smaller set of measured eigenvalues. The effectiveness of the eigenvalue expansion is also studied using the three-storey plane frame.

After simulation studies, a dynamic test is carried out in the laboratory on a five-storey steel plane frame to further verify the damage localization method and the damage quantification methods using first order and second order analysis. A method to select the modes for the identification is proposed.

Acknowledgements

I would like to express my appreciation to my chief supervisor, Dr. S. S. Law, for his valuable guidance and inspiration, both during my research and during the preparation of this dissertation. His insight and participation have greatly affected my attitude towards the acquisition of knowledge.

I also wish to express my gratitude to my co-supervision, Dr. C. F. Ng, for his supportive advice on my research project.

I would like to give special thanks to Mr. L. Yu and Mr. C. K. Iu for their suggestions.

I would especially indebted to all technical staff of the Civil and Structural Engineering Department of the Hong Kong Polytechnic University for their assistance in the laboratory work and computing work

I am sincerely grateful to my parents, my sisters and Frank Lam for their love, supports and understanding throughout my study.

Lastly, I would express my deepest appreciation to the Hong Kong Polytechnic University for its financial support.

Memorandum

The accompanying dissertation entitled "Incomplete Dynamic Measurement in Structural Damage Assessment" is submitted for the degree of Master of Philosophy in the Department of Civil and Structural Engineering of the Hong Kong Polytechnic University.

The dissertation is based on independent work carried out by the author from September 1998 to January 2001 under the supervision of Dr. S. S. Law. The work and ideas are original and all contributions from others are duly acknowledged in the text by reference.

Pui Shan, MAK

List of Publications

Papers resulting from this thesis:

1. Mak, P.S. and Law, S.S. "Structural damage assessment by elemental modal strain energy change". *Proceedings of the International Conference on Advances in Structural Dynamics*, ASD 2000, Hong Kong, Vol. 2, pp.1061-1068 (2000)
2. Mak, P.S. and Law, S.S. "Structural damage quantification on large damage". *IMAC-XIX: Conference on Structural Dynamics*, Orlando, FL, 2001 (submitted)
3. Mak, P.S. and Law, S.S. "Structural damage detection from linear sequential filtering technique". *Journal of Sound and Vibration* (submitted)
4. Law, S.S. and Mak, P.S. "Higher order sensitivity in structural damage quantification: Part I". *Journal of Engineering Mechanics, ASCE* (submitted)
5. Mak, P.S. and Law, S.S. "Higher order sensitivity in structural damage quantification: Part II". *Journal of Engineering Mechanics, ASCE* (submitted)

Contents

List of Tables

List of Figures

List of Notations

K	System stiffness matrix
K_j	The j-th elemental stiffness matrix
M	System mass matrix
Λ	Diagonal eigenvalue matrix
λ_k	The k-th eigenvalue of the system
$\widetilde{\lambda}_i$	The i-th "noisy" eigenvalue
Δf	Measured frequency change vector
δf	Analytical frequency change vector
Φ_k	The k-th mode shape of the system
$\widetilde{\Phi}_{ji}$	The j-th component of the i-th "noisy" mode shape
$\Delta\Phi$	Measured mode shape change vector
$\delta\Phi$	Analytical mode shape change vector
ΔMSE	Measured modal strain energy change vector
δMSE	Analytical modal strain energy change vector
δD	Damage extent vector
P	Gain matrix
C	Damage coefficient vector
D	Measurement matrix
γ	Random number
ρ	Noise level
$\widetilde{\bullet}$	Error
$\overline{\bullet}$	Measured value
$\hat{\bullet}$	Estimated value
Tr	Trace operation of matrix
$E(\bullet)$	Mean of variable
$E(\bullet\bullet^T)$	Variance of variable

MSE	Abbreviation of Modal Strain Energy
EMSE	Abbreviation of Elemental Modal Strain Energy
EMSE	Abbreviation of Elemental Modal Strain Energy
EMSEC	Abbreviation of Elemental Modal Strain Energy Change
MDLAC	Abbreviation of Multiple Damage Location Assurance Criterion

Chapter 1

Introduction

1.1 Importance of Structural Damage Assessment

Damage in a structure can be defined as a change in the physical properties of its structural components. When an element of the structure contains a damage, the stiffness of the damage element as well as the load-carrying capacity of that element will change. If the loading on the damage element is greater than that it can resist, the element will fail and the internal forces of the structure will be redistributed. As the internal force distribution is different from what is planned at the design stage, there is no safety guarantee in the structure. Also when the damage is at the connection of the structure, the assumed rigid connection may become semi-rigid or even pin in nature. It will also lead to redistribution of internal forces.

All load-carrying structures such as buildings, bridges and offshore platforms continuously accumulate damage during their service life. Then structures may be damaged if the actual loads exceed the design load. Bridges may be subjected to remarkably heavy traffic loading due to heavy trucks. Short-duration excess in loading may also cause damage, and the effective life of a bridge may be shortened. Offshore platforms are continuously exposed to the wave action, chemical corrosion and fatigue effect. In general, the occurrence of damage during the service life of a

structure is unavoidable. The only way to ensure the safety of human life and to reduce the loss of wealth is to detect the existence, location and extent of damage in the structure and to carry out remedial work.

A sound structural damage assessment method, which can detect the existence of damage, its location and extent, is important in the maintenance of a structural system. Many researchers have invested their effort in this area and a number of methods have been developed based on different approaches. However, all available methods are only applicable to some specified types of structure and under some specified assumptions, and the development of damage assessment method is still a very attractive research area.

1.2 Objective of the Thesis

Damage assessment process comprises of three stages including the identification of damage occurrence, location and extent. The detection of damage occurrence based on vibration measurement approach is not a difficult task and many techniques have been developed. The damage localization and extent assessment is more important and difficult. In the past, many damage assessment methods require the complete measured information to detect the damage. When the measured mode shapes are incomplete, the measured information is projected onto the unmeasured degrees-of-freedom to reconstruct the complete mode shapes. However, this mode shape expansion process introduces errors in the expanded mode shapes and increases

the difficulty in damage assessment. Also, few works have been done on the use of incomplete natural frequencies in damage assessment. Hence, this project focuses on the development of a method for the damage localization and quantification using incomplete measured information.

1.3 Scope of the Thesis

A Multiple Damage Assurance Criterion (*MDLAC*) method using incomplete Elemental Modal Strain Energy Change is proposed to localize the damage in Chapter 3. The measured information is applied directly in the proposed method without any expansion of the measured data or reduction of the model. The Multiple Damage Assurance Criterion (*MDLAC*) developed by Shi *et al.* (2000) originally makes use of incomplete measured mode shapes. The parameter Elemental Modal Strain Energy Change is applied instead of mode shapes in the correlation matching of the Multiple Damage Assurance Criterion (*MDLAC*) to localize the damage. The experimental Modal Strain Energy Change is calculated from the incomplete measured mode shapes before and after damage and the analytical stiffness matrix. The analytical sensitivity of the Modal Strain Energy Change is a function of the analytical stiffness matrix, mass matrix, eigenvalues and mode shapes of the undamaged structure. One element of the structure is assumed to be damaged and the *MDLAC* value of each element is calculated. The potential damage sites are identified in those elements with higher *MDLAC* values. Then the *MDLAC* values on the different combinations of the potential damage sites are re-calculated. The final damage sites correspond to the

combination with the highest *MDLAC* value. The effectiveness and robustness of this method is judged from the identification results on a three-storey plane frame. The Multiple Damage Assurance Criterion (*MDLAC*) method using incomplete mode shape is also studied for comparison with the proposed method.

After the estimation of the final damage sites, the damage extent in terms of the change of the stiffness matrix can be quantified using the measured eigenvalues which are less contaminated by measurement noise and have better accuracy than mode shapes. In the damage assessment problem, the change in vibration parameter is usually represented in a Taylor's expansion in terms of a change in the design variable. In general, the formulation of the identification equation includes only the first order terms in the Taylor's expansion. Hence, a damage quantification method using the first order sensitivity is developed in Chapter 4 in which a linear sequential filtering technique is used to relate the analytical and experimental sets of eigenvalues including the measurement noise matrix. An unbiased minimum variance error estimation method is applied to obtain the optimum solution of the damage extent. Weight linear least squares method is used to solve the identification equation. Numerical examples on the three-storey plane frame are studied for different scenarios of damage.

In practice, the accuracy of identification using the above technique reduces when dealing with large damage, and higher order terms in the Taylor's expansion are required. However, terms above second order are numerically small and their inclusive in the computation would increase the computational cost. Therefore, a damage quantification method using the second order terms in the Taylor's expansion

is proposed in Chapter 5. The same linear sequential filtering technique and the unbiased minimum variance error estimation method are used to generate the identification equation, and weight linear least squares method is used to solve the identification equation. Two necessary conditions for the optimal solution are generated from the formulation. The identification of both small and large damages using the first condition or both conditions are studied with a three-storey plane frame.

In these two damage quantification methods, the formulation has the capability to estimate a larger set of eigenvalues from a small number of measured eigenvalues. The accuracy of this eigenvalue expansion method is also studied for the plane frame with small and large damages in Chapter 6.

Finally, a dynamic test is carried out in the laboratory on a five-storey steel plane frame. The damage localization method and the two damage quantification methods are verified with the experimental data in Chapter 7.

The conclusions drawn on the work in this thesis and further recommendations are given in Chapter 8.

Chapter 2

Literature Review

2.1 Development of Structural Damage Assessment

A sound structural damage assessment method is very important for all load-carrying structures. A structure loses its function and even collapses without warning when it is continuously accumulating damage. The risk to human life would be a serious problem. A practice of damage assessment would guarantee an acceptable level of service condition of the structure. Hence, structural damage assessment for all load-carrying structures during their service life is advisable.

Many researchers have invested their effort on damage assessment and a number of methods have been developed based on different approaches. The existing approaches may be categorized into three classes, which are, modal analysis, system identification and neural network.

2.1.1 Modal Analysis

The modal parameters are usually used as damage indicators in structural damage assessment. The most common ones are natural frequencies, mode shapes and frequency respond function.

2.1.1.1 Natural frequency approaches

In general, natural frequencies can be obtained more accurately and reliably than mode shapes because they are less contaminated by measurement noise. Besides, the collection of the natural frequencies is easy and simple. Hence, many approaches are based on natural frequencies only for damage assessment.

Cawley and Adams (1979) proved that the ratio of the natural frequency change between any two modes is a function of the damage location only. Ju and Mimovich (1986,1987) used changes in natural frequencies to locate structural damage of a beam. Hearn and testa (1991) proposed a similar damage localization approach for welded steel frames and wire ropes. Later, Friswell *et al.* (1994) used a statistical tool to reduce the effect of the measurement errors and to improve the method proposed by Cawley and Adams. Messina *et al.* (1996) developed a Damage Location Assurance Criterion (*DLAC*), which is derived in a sensitivity and statistical approach to locate a single damage in the structure. Then they extended this method to detect multiple damages (Messina *et al.*, 1998). This criterion is based on the correlation between the measured and the analytical frequency changes. A new parameter called the Multiple Damage Location Assurance Criterion (*MDLAC*) is developed and is formulated as :

$$MDLAC(\{\delta D\}) = \frac{|\{\Delta f\}^T \cdot \{\delta f(\{\delta D\})\}|^2}{(\{\Delta f\}^T \cdot \{\Delta f\}) \cdot (\{\delta f(\{\delta D\})\}^T \cdot \{\delta f(\{\delta D\})\})} \tag{2.1}$$

where $\{\Delta f\}$ is the measured frequency change vector before and after the occurrence of damage in the structure, and its size is equal to the number of measured modes. $\{\delta f\}$ is the analytical frequency change vector for a damage of a known size $\{\delta D\}$, which is an arbitrary pattern of damage at one or more sites. The size of $\{\delta f\}$ is equal to the number of modes used, while the size of $\{\delta D\}$ is equal to the number of potential damage sites.

2.1.1.2 Mode shape approaches

In practice, natural frequency is not very sensitive to local damage. And the information it contains is insufficient to localize the structural damage. Mode shapes contain information distributed over the structure, and they are very attractive for structural damage assessment.

Allermang and Brown (1982) developed the Modal Assurance Criterion (*MAC*) which is traditionally used to quantify the comparison of experimental-based and analytical-based mode shapes. Lieven and Ewins (1988) localized the damage site by the Co-ordinate Modal Assurance Criterion (*COMAC*), which is correlating two sets of mode shapes before and after the occurrence of damage in the structure.

Moreover, some researchers found that modal strain energy is very sensitive to damage. Lim and Kashangake (1994) and Doebling *et al.* (1997) studied the performance of the modal strain energy in the identification of structural behaviour and in damage localization. Stubbs and Kim (1996) suggested using modal strain

energy to localize the damage and using analytical and post-damage measured mode shapes to quantify the damage. Shi *et al.* (1998) extended the work on Elemental Modal Strain Energy (*EMSE*) and proposed the Elemental Modal Strain Energy Change Ratio (*EMSECR*) as a damage indicator to localize the damage sites in the structure. An algorithm for quantifying the damage extent based on this energy change was also proposed.

2.1.1.3 Natural frequency and mode shape approaches

Many researchers have developed the damage assessment methods using both natural frequencies and mode shapes. Yuen (1985) proposed using measured frequencies and mode shapes to detect the damage by establishing the relationship between the eigenparameters, damage location and damage extent. Lin (1990) presented a flexibility matrix, which is determined using experimental data to detect the damage location. Approximate Parameter Change and Measured Damage Signature developed by Paul (1994) make use of the sensitivity technique based on the natural frequencies and mode shapes to detect the damage location. Topole and Stubbs (1995) localized and quantified the structural damage using mode shape orthogonality by a pseudo-inverse solution of a system.

2.1.2 System Identification

The main objective of system identification is to seek a refined finite element model (FEM) of the structure such that the measured and analytical modal properties are in agreement. Damage assessment algorithms can then be developed based on the

general framework of FEM refinement. The major algorithms used to solve the finite element model (FEM) refinement problem and structural damage assessment can be broadly classified into three different categories. They are optimal matrix update algorithms, sensitivity methods and control-based eigenstructure assignment techniques.

2.1.2.1 Optimal matrix update algorithms

In optimal matrix update formulation, perturbation matrices for the mass, stiffness, and/or damping matrices (property matrices) are determined based on the optimization of functions. Rodden (1967) is a prior researcher in optimal matrix updates using measured test data and he determined the structural influence coefficients of a structure using ground vibration test data. Brock (1968) examined the problem of determining a matrix that satisfied a set of measurements as well as enforcing symmetry and positive definiteness. Berman and Flannelly (1971) discussed the computation of the property matrices when the number of modes is not equal to the number of degrees-of-freedom of the model. Baruch and Bar Itzhack (1978) based on the minimal Frobenius-norm matrix adjustment to modify the structural stiffness matrix using measured frequencies and mode shapes. Berman and Nagy (1983) proposed a similar formulation to improve both the stiffness and mass matrices. In all the previous works, the zero/nonzero (sparsity) pattern of the original stiffness matrix may be destroyed. Kabe (1985), Kammer (1988) and Smith and Beattie (1991) developed algorithms that preserve the original stiffness matrix sparsity pattern and the original load paths of the structural model. Kaouk and Zimmerman (1992) developed the Minimum Rank Perturbation Theory (*MRPT*) for damage detection.

The update to each property matrix is of a minimum rank and is equal to the number of measured modes. The minimum rank constraint is consistent with the matrix changes in FEM to represent the situations of the structural damage. They also verified this method with experimental results (Kaouk and Zimmerman, 1993). Koh *et al.* (1995) proposed an improved-condensation method to detect local structural damage of multistory frame buildings in terms of changes in story stiffness.

2.1.2.2 Sensitivity methods

Sensitivity derivatives of the modal parameters with respect to physical design variables are widely used for the practical application in model refinement and damage assessment (Adelman and Haftka, 1986). The updated models remain consistent within the original finite element program framework when physical parameters are varying. Chen and Garba (1980) presented a method to refine the FEM using Jacobian sensitivity matrix. Hajela and Soeiro (1990) applied the nonlinear optimization to the damage assessment problem directly. Ricles and Kosmatke (1992) proposed an eigenvector sensitivity approach for damage assessment in elastic structures. The damage location is predicted using the residual modal force vectors and the damage extent is then estimated using the weight eigenvector sensitivity approach. Farhat and Hemez (1993) developed a sensitivity-based method that computes the sensitivity of the global structural mass and stiffness matrices at the structural element level. Later, this method is applied to a truss structure by Doebling *et al.* (1993).

2.1.2.3 Control-based eigenstructure assignment techniques

Control-based eigenstructure assignment techniques determine a pseudo-control that re-produces the measured modal properties with the initial structural model. Then, the pseudo-control is translated into matrix adjustments and applied to the initial FEM. Inman and Minas (1990) presented two techniques for FEM refinement. The first technique used both eigenvalue and eigenvector to produce the updated stiffness and damping matrices. An unconstrained numerical nonlinear optimization problem is proposed to enforce symmetry of the resulting model. The second technique used a state-space formulation from eigenvalue only to determine the state matrix which has the measured eigenvalues and which is closest to the original state matrix. Zimmerman and Widengren (1990) proposed a symmetric eigenstructure assignment technique to incorporate the eigenvalue and eigenvector into the FEM. Later, Zimmerman and Kaouk (1992) extended the eigenstructure assignment technique, called "subspace rotation algorithm", to localize and quantify the structural damage. Lim and Kashangaki (1994) proposed using best achievable eigenvectors to localize the structural damage.

2.1.3 Neural Network

Neural networks are viewed as alternative computation methods, which can be trained to process and correlate huge quantities of data. Wu *et al.* (1992) developed a three-layer neural network to localize the structural damage in a shear type frame model. The network was trained to detect the damage location and extent from Fourier spectra. However, this method is only effective to localize the damage in the

top floor members. Kudva *et al.* (1992) used the neural network to monitor aircraft structures and to detect the damage location and extent from stress data. Worden *et al.* (1993) proposed a multi-layer network to recognize the missing member in a cantilever latticework from stresses in horizontal and vertical members. Ceravolo *et al.* (1995) presented the "feedforward" neural networks to determine the damage location in an FEM truss model based on the modal analysis carried out on the structure in its undamaged and damaged conditions.

2.2 Approaches with Incomplete Measurements

The problem of incomplete measurements is pervasive across many areas of structural dynamics. Many researchers used experimental data and an analytical model to perform damage assessment and they faced a great problem. There is an inherent mismatch between the experimental and the analytical degrees-of-freedom. There are two categories of methods to deal with this problem, i.e., model reduction and/or mode shape expansion techniques and direct application of incomplete measurements.

2.2.1 Model Reduction and/or Mode Shape Expansion Techniques

Model reduction and/or mode shape expansion are critical techniques that bridge the gap in the mismatch between the experimental data and the analytical model. Guyan (1965) developed a condensation technique to reduce the stiffness and

mass matrices. Berman and Nagy (1983) and He and Ewins (1991) proved that all reduction techniques yield matrices where the connectivity of the original FEM is destroyed. This difficult is resolved by augmentation technique such that the experimental mode shapes are expanded to the dimension of the analytical model. Berger *et al.* (1984) presented an expansion scheme based on a Component Mode Synthesis (*CMS*) approach where forces and displacements are obtained by condensing the dynamic behaviour of the structure on a subset of "master" degrees-of-freedom. Smith and Beattie (1990) proposed an expansion algorithm by solving the orthogonal Procrustes problem. The experimental/analytical cross-orthogonality matrix is factored using the Singular Value Decomposition (*SVD*). Imregun and Ewins (1993) applied the mode shape expansion technique to the case of a large flexible space structure. Law *et al.* (1998) presented the Elemental Energy Quotient (*EEQ*) with mode shape expansion for damage localization. Moreover, Shi *et al.* (1995) presented a model reduction and expansion method using cross-orthogonal condition on relating the analytical data and incomplete experimental data. The cross orthogonality between the analytical and experimental eigenvectors has two advantages. Both the modal reduction and expansion can be considered simultaneously, and the computation of the method is simplified.

2.2.2 Direct Application of Incomplete Measurements

Unfortunately, the model reduction techniques destroy the connectivity of the original FEM and the mode shape expansion techniques induce errors in the expanded full mode shapes. The errors from these two techniques are inherent and they affect the accuracy of the damage assessment. The best solution is using the incomplete

measurements directly into the damage assessment method. Shi *et al.* (2000) proposed an approach correlating the incomplete sets of analytical and measured mode shapes to localize the structure damage. It is an extension of the Multiple Damage Location Assurance Criterion (*MDLAC*) method developed by Messina *et al.* (1998) by using incomplete mode shapes instead of natural frequencies. The formulation is given below.

$$MDLAC(\{\delta D\}) = \frac{|\{\Delta\Phi\}^T \cdot \{\delta\Phi(\{\delta D\})\}|^2}{(\{\Delta\Phi\}^T \cdot \{\Delta\Phi\}) \cdot (\{\delta\Phi(\{\delta D\})\}^T \cdot \{\delta\Phi(\{\delta D\})\})} \tag{2.2}$$

where $\{\Delta\Phi\}$ is the measured mode shape change vector before and after the occurrence of damage in the structure, and its size is the product of the number of measured modes and the number of sensor locations. $\{\delta\Phi\}$ is the analytical mode shape change vector at the same degrees-of-freedom for a damage of a known size $\{\delta D\}$, which is an arbitrary pattern of damage at one or more sites. The size of $\{\delta\Phi\}$ is equal to the product of number of modes used and the number of sensor locations, while the size of $\{\delta D\}$ is equal to the number of potential damage sites.

2.3 Sensor Placement Methods

For an incomplete measurements problem, the accuracy of a damage assessment method depends on whether or not the measurement points are associated with components of the structure that exhibit significant and important information. Hence, the selection of sensor placement is also a part of the damage assessment method with incomplete measurements.

Chen and Graba (1985) developed an optimal sensor placement approach by minimizing the covariance of a location estimator. The required solution is the set of sensor locations with the "best" parameter estimation. However, the optimal sensor locations are estimator dependent and an exhaustive search is executed for each specific estimator. Kammer (1991) presented an effective independence algorithm basing on a backward elimination to minimize the covariance of the Fisher Information matrix. The initial candidate set of sensor locations was quickly reduced to the number of available sensors. Hemez and Farhat (1994) extended the effective independence algorithm to select the sensor locations in terms of the strain energy contribution of the structure. Cobb and Liebst (1997) proposed an optimal sensor placement method for the purpose of determining the structure damage. However, the previous mentioned sensor placement methods do not suggest how to select target modes to make the analysis more effective. Kashangaki (1992) developed a sensitivity parameter as a quantitative measure of eigenvalue and eigenvector derivatives for damage assessment and, he suggested which modes should be selected to benefit the subsequent damage assessment.

2.4 Discussions

Many researchers have invested their effort in damage assessment problem and a number of methods have been developed based on different approaches. The approaches can be broadly classified as modal analysis, system identification and neural networks.

In optimal matrix update algorithms, minimization of the matrix norm of the difference between the original and refined stiffness matrices is justified in an engineering sense. However, damage typically results in the local stiffness reduction at one or a few location, whereas the matrix norm minimization would tend to disperse the changes throughout the entire stiffness matrix. This difference may affect its applicability for damage assessment.

Sensitivity methods can preserve the structural load path automatically through the model assembly using physical parameters. Moreover, elements in a property matrix away from the damage remain unaffected by using a localized set of physical parameters. However, the physical parameters must be chosen before a sensitivity analysis such that the properties of the damage component can be varied. This introduces a practical difficulty that the number of physical parameters becomes quite large. Besides, most sensitivity approaches are restricted to detect small parameter changes because higher order terms in the formulation are truncated. Hence, the linearizing formulation is not applicable in assessment of large parameter changes.

Many approaches for system identification, either optimal matrix update algorithms, sensitivity methods or control-based eigenstructure assignment techniques, become practical for damage assessment when the damage locations are known.

Neural networks can be trained to process and correlate huge quantities of data. The main drawback of a large-sized network is that an inconceivable amount of data is required to train it. Moreover, there are many difficulties in its management.

Several damage indicators for damage assessment were developed by correlating the measured modal parameters with the corresponding parameters of the finite element model. The damage assessment methods were developed based on natural frequencies, mode shapes or both natural frequencies and mode shapes. Measured frequencies are commonly used to detect the existence of the damage. They are easy to measure and less contaminated by measurement noise. However, natural frequency is not sensitive to damage because it is a global parameter of a structure. In practice, only a truncated set of natural frequencies is measured in the test structure. Hence, the measured frequencies are usually insufficient to localize the damage.

Many damage assessment approaches have been proposed using measured mode shapes. Later, some researchers suggested that modal strain energy is more sensitive than natural frequencies and mode shapes in damage assessment. In practice, the number of measured degrees-of-freedom in the test structure is much less than the number of total degrees-of-freedom in the finite element model. This introduces a great problem in correlating the experimental and analytical model. Model reduction

and mode shape expansion are the two common techniques to overcome this problem. However, model reduction techniques destroy the connectivity of the original FEM and the mode shape expansion techniques induce errors in the expanded full mode shapes. The errors from these two techniques are inherent and they affect the accuracy of the damage assessment. Therefore, using the incomplete measurements directly is an optimal approach for damage assessment.

A strategy is proposed in this dissertation to localize the damage using incomplete Elemental Modal Strain Energy Change. The measured information is applied directly in the proposed method without any expansion of the measured data or reduction of the model. The parameter Elemental Modal Strain Energy Change is applied instead of mode shapes in the correlation matching of the Multiple Damage Assurance Criterion (*MDLAC*) for damage localization.

Generally, damage causes the change of stiffness matrix only. And natural frequencies can be easily measured and are less contaminated by measurement noise. Sensitivity approach is direct and simple. Hence, two damage quantification methods are proposed using the derivatives for the natural frequency and mode shape with respect to a physical parameter. The first proposed method is based on the first order terms in the Taylor's expansion. And the other proposed method includes the second order terms in the Taylor's expansion.

Chapter 3

Damage Localization Method

3.1 Introduction

Damage often occurs in single or multiple local sites in a structure during its design life. The structure will lose its function and even collapse without warning when the damage continuously accumulates. The only way to ensure the safety of human life and to reduce the loss of wealth is to evaluate the integrity of the structure and to carry out the remedial work. The main objective in the damage detection process is to localize the damage sites as early as possible for structural maintenance. In this chapter, a damage localization method using incomplete Elemental Modal Strain Energy Change is proposed, and the Multiple Damage Location Assurance Criterion (*MDLAC*) developed by Shi *et al.* (2000) is used. Incomplete measured information is applied directly in the proposed method without expansion of the measured data or reduction of the model.

In this thesis, the parameter Elemental Modal Strain Energy Change (*EMSEC*) is used instead of mode shapes in the correlation matching of the Multiple Damage Location Assurance Criterion (*MDLAC*) to localize the damage. The sensitivity of Elemental Modal Strain Energy (*EMSE*) to localize the damage has been derived by Shi *et al.* (1998), and an improved sensitivity formulation (Shi *et al.*, submitted) on

the *EMSE* is also developed. One element of the structure is assumed to be damaged and the *MDLAC* value of each element is calculated. The potential damage sites are preliminarily identified in those elements with higher *MDLAC* values. The final damage sites are then determined by finding those combined sites among the potential damage sites with the highest *MDLAC* values. Damage in the structure is assumed to change the stiffness of individual elements only. Numerical examples in this chapter show that the *MDLAC* method performs better with the *EMSEC* in the correlation comparison than that from mode shapes in damage localization with or without noise effect.

3.2 Damage Localization Method using Incomplete Measurements

For the convenience of comparison, the damage localization approach by the Multiple Damage Location Assurance Criterion (Shi *et al.*, 2000) using incomplete mode shapes is briefly reviewed before the presentation of the new method.

3.2.1 Damage Localization Method using Incomplete Mode Shapes

The Modal Assurance Criterion (*MAC*) developed by Allermang and Brown (1982) is traditionally used to quantify the comparison of experimental-based and analytical-based mode shapes. Messina *et al.* (1996 and 1998) presented a sensitivity and statistical-based method called the Multiple Damage Location Assurance Criterion (*MDLAC*) using natural frequencies to localize structural damage. It is

formulated on the same basis as *MAC* for quantifying consistence correspondence between related vectors. However, mode shapes are more sensitive to the local structural damage than natural frequencies, and the *MDLAC* approach is further modified (Shi *et al.*, 2000) making use of incomplete mode shapes to localize the damage sites. The basic algorithm of *MDLAC* using natural frequencies or incomplete mode shapes is similar.

The incomplete mode shapes can be directly combined with the analytical counterparts at the same measured degrees-of-freedom to localize the damage sites using the correlation parameter *MDLAC*.

$$MDLAC(\{\delta D\}) = \frac{|\{\Delta\Phi\}^T \cdot \{\delta\Phi(\{\delta D\})\}|^2}{(\{\Delta\Phi\}^T \cdot \{\Delta\Phi\}) \cdot (\{\delta\Phi(\{\delta D\})\}^T \cdot \{\delta\Phi(\{\delta D\})\})} \tag{3.1}$$

in which,

$$\{\delta\Phi\} = \begin{Bmatrix} \delta\Phi_1 \\ \cdots \\ \delta\Phi_k \\ \cdots \\ \delta\Phi_m \end{Bmatrix} = \begin{bmatrix} \frac{\partial\{\Phi_1\}}{\partial D_1} & \cdots & \frac{\partial\{\Phi_1\}}{\partial D_L} \\ \cdots & \cdots & \cdots \\ \frac{\partial\{\Phi_k\}}{\partial D_1} & \cdots & \frac{\partial\{\Phi_k\}}{\partial D_L} \\ \cdots & \cdots & \cdots \\ \frac{\partial\{\Phi_m\}}{\partial D_1} & \cdots & \frac{\partial\{\Phi_m\}}{\partial D_L} \end{bmatrix} \{\delta D\} \tag{3.2}$$

$$\{\delta\Phi_k\} = \frac{\partial\{\Phi_k\}}{\partial D_1}\delta D_1 + \frac{\partial\{\Phi_k\}}{\partial D_2}\delta D_2 + \cdots + \frac{\partial\{\Phi_k\}}{\partial D_L}\delta D_L, \quad (k = 1,2,...,m) \tag{3.3}$$

where m is the number of selected modes to be monitored, and L is the number of the potential damage sites. $\{\Delta\Phi\}$ is the measured mode shape change vector before and

after the occurrence of damage in the structure, and its dimension is the product of the number of measured modes and the number of sensor locations. $\{\delta\Phi\}$ is the analytical mode shape change vector at the same degrees-of-freedom for the same structure with a damage of a known size $\{\delta D\}$, which is an arbitrary pattern of damage at one or more sites. The size of $\{\delta\Phi\}$ is equal to the product of the number of modes used and the number of sensor locations, while the size of $\{\delta D\}$ is equal to the number of potential damage sites.

The sensitivity of the k-th mode shape to the j-th elemental damage is given below (Shi *et al.*, submitted).

$$\frac{\partial\{\Phi_k\}}{\partial D_j} = [K]^{-1}[b_w]\{\{\Phi_k\}^T[K_j]\{\Phi_k\}[M]\{\Phi_k\} - [K_j]\{\Phi_k\}\} + \sum_{\substack{r=1 \\ r\neq k}}^{n^*} \frac{-\left(\frac{\lambda_k}{\lambda_r}\right)^W \{\Phi_r\}^T[K_j]\{\Phi_k\}}{\lambda_r - \lambda_k}\{\Phi_r\} \tag{3.4}$$

in which,

$$[b_w] = I + \lambda_k[M][K]^{-1} + (\lambda_k[M][K]^{-1})^2 + \cdots + (\lambda_k[M][K]^{-1})^{W-1} \tag{3.5}$$

where $[K_j]$ is the j-th elemental stiffness matrix; $\{\Phi_k\}$ and λ_k are the k-th analytical mode shape and eigenvalue respectively; W is the weight factor and is equal to one in this study; and n^* is the number of analytical modes used in the calculation (n^* should be equal to the total number of degrees-of-freedom. But in practice only a limited number of modes of the system are used).

3.2.2 Damage Localization Method using Incomplete *EMSEC*

Modal strain energy has been studied previously by Lim and Kashangake (1994) and Doebling *et al.* (1997) in the identification of structural behaviour and the damage location. Stubbs and Kim (1996) also used it as a damage indicator. Previous works compared the modal strain energy in the finite elements before and after the occurrence of damage. The proposed method is a modification of the *MDLAC* method (Shi *et al.*, 2000) by using incomplete Elemental Modal Strain Energy Change (*EMSEC*) instead of incomplete mode shapes. The Elemental Modal Strain Energy Change (*EMSEC*) for a damage scenario is computed using measured data. The sensitivity of the Elemental Modal Strain Energy (*EMSE*) is also computed using analytical data. Then the two sets of *EMSEC* from the analytical and the experimental models are compared in the form of the Multiple Damage Location Assurance (*MDLAC*) to determine the damage sites.

$$MDLAC(\{\delta D\}) = \frac{|\{\Delta MSE\}^T \cdot \{\delta MSE(\{\delta D\})\}|^2}{(\{\Delta MSE\}^T \cdot \{\Delta MSE\}) \cdot (\{\delta MSE(\{\delta D\})\}^T \cdot \{\delta MSE(\{\delta D\})\})} \tag{3.6}$$

in which,

$$\{\delta MSE\} = \begin{Bmatrix} \delta MSE_1 \\ \cdots \\ \delta MSE_k \\ \cdots \\ \delta MSE_m \end{Bmatrix} = \begin{bmatrix} \frac{\partial\{MSE_1\}}{\partial D_1} & \cdots & \frac{\partial\{MSE_1\}}{\partial D_L} \\ \cdots & \cdots & \cdots \\ \frac{\partial\{MSE_k\}}{\partial D_1} & \cdots & \frac{\partial\{MSE_k\}}{\partial D_L} \\ \cdots & \cdots & \cdots \\ \frac{\partial\{MSE_m\}}{\partial D_1} & \cdots & \frac{\partial\{MSE_m\}}{\partial D_L} \end{bmatrix} \{\delta D\} \tag{3.7}$$

$$\{\delta MSE_k\} = \frac{\partial\{MSE_k\}}{\partial D_1}\delta D_1 + \frac{\partial\{MSE_k\}}{\partial D_2}\delta D_2 + \cdots + \frac{\partial\{MSE_k\}}{\partial D_L}\delta D_L, \quad (k = 1,2,...,m) \tag{3.8}$$

where m is the number of selected modes to be monitored, and L is the number of potential damage sites. $\{\Delta MSE\}$ is the measured *MSEC* vector before and after the occurrence of damage in the structure; $\{\delta MSE\}$ is the analytical *MSEC* vector at the same selected elements with damage of a known size $\{\delta D\}$. The dimension of vectors $\{\Delta MSE\}$ and $\{\delta MSE\}$ is equal to the product of the number of modes used and the number of selected elements, while the dimension of $\{\delta D\}$ is equal to the number of potential damage sites. The *MDLAC* value of each element is calculated when only one element is assumed damaged at one time. That is, every element in the vector $\{\delta D\}$ equals to *0.0* except the element relating to the assumed damage site in calculating each set of *MDLAC* value, which can be set to any value in calculating each set of *MDLAC*. This is possible because this value will be cancelled out in the subsequent normalization by the highest *MDLAC* value of the group of elements of the structure. Then, those elements with a higher *MDLAC* value are preliminary identified to be the potential damage sites. The final damage sites can be localized as those combined sites with the largest *MDLAC* value.

The sensitivity of *MSE* of the k-th mode to damage at element j is given by equation (3.9) below (Shi *et al.*, submitted).

$$\frac{\partial\{MSE_i\}}{\partial D_j} = \sum_{r=1}^{L} 2\{\Phi_i\}^T[K_j]\left[[K]^{-1}[b_w]\{\{\Phi_i\}^T[K_r]\{\Phi_i\}[M]\{\Phi_i\} - [K_r]\{\Phi_i\}\} + \sum_{\substack{r=1 \\ r\neq i}}^{n^*} \frac{-\left(\frac{\lambda_i}{\lambda_r}\right)^W \{\Phi_r\}^T[K_r]\{\Phi_i\}}{\lambda_r - \lambda_i}\{\Phi_r\}\right] \tag{3.9}$$

in which,

$$[b_w] = I + \lambda_k[M][K]^{-1} + (\lambda_k[M][K]^{-1})^2 + \cdots + (\lambda_k[M][K]^{-1})^{W-1} \tag{3.10}$$

where $[K_j]$ is the j-th elemental stiffness matrix; $[K]$ and $[M]$ are the system stiffness and mass matrices respectively; $\{\Phi_k\}$ and λ_k are the k-th analytical mode shape and eigenvalue respectively; W is the weight factor and is equal to one in this study. The number of potential damage site, L, is taken equal to the total number of elements in the system; and n^* is the number of analytical modes used in the calculation. (n^* should be equal to the total number of degrees-of-freedom of the system. But in practice only a limited number of modes of the system are used).

3.3 Numerical Examples

3.3.1 The Simulated Structure and Its Properties

A symmetric three-storey plane frame shown in Figure 3.1 is used to demonstrate the damage localization method. Only vibration in the x-z plane is considered. It is 0.59 metre wide and 1.2 metres high divided into three storeys of 0.4 metre each. It consists of two columns and three horizontal interconnection beams.

The finite element model of the frame consists of 45 two-dimensional elements, 44 nodes and 126 degrees-of-freedom. The material properties of the frame are shown in Figure 3.1 and the physical properties are summarized in Table 3.1. There are 42 unconstrained nodes and two constrained nodes at the supports. Each unconstrained node has two translational (x-direction and z-direction) and one rotational (about y-axis) degrees-of-freedom in the plane under consideration. All degrees-of-freedom of each node are calculated using the FORTRAN programs. And there is no restriction on the elongation of the elements in the calculation. However, the z-direction displacement of the column nodes has very small contribution to vibration modes and they are not considered such that incomplete information on the mode shapes for the damage localization method is used. Besides, the interconnecting beams are assumed to vibrate without deformation in x-direction. Then, the translation in the x-direction of each beam node is equal to that of the corresponding column-beam connection node. And the rotational degrees-of-freedom of all the nodes are ignored because they are difficult to measure. Thus, all rotational degrees-of-freedom are not chosen to have incomplete information of the mode shapes for the damage localization method. Therefore, each node has only one degree-of-freedom significant motion during free vibration.

3.3.2 Vibration Properties of the Simulated Structure

The three-storey plane frame is studied for its free vibration properties without damping effect. The first fifteen modes are studied. The first three modes are global modes and the rests are local modes. The natural frequencies of the frame are listed in Table 3.2. The mode shapes of each mode are shown in Figure 3.2.

3.3.3 Damage Cases of the Simulated Structure

Damage in the structure is assumed to change the stiffness of individual elements only (a change in the elastic modulus) and the other properties are unchanged. There are three damage scenarios with small or large damage. The first scenario has a single damage in element 45. Element 45 is located at the edge of the third-level interconnecting beam. The second scenario contains damage in elements 17 and 32. Element 17 is located at the column in-between the base and the first level. Element 32 is located at the first-level interconnecting beam. The third scenario is with damage in elements 9, 13 and 39. Element 9 is located at the column in-between the first and second levels. Element 13 is located at the middle of the column in-between the second and third levels. Element 39 is located at the second-level interconnecting beam. The details of the three damage scenarios with small and large damages are listed in Tables 3.3 and 3.4 respectively.

3.3.4 Damage Localization without Noise Effect

The incomplete mode shapes from 18 translation degrees-of-freedom at the two ends of 9 finite elements are used. They are the horizontal translation degrees-of-freedom at nodes 3, 4, 8, 9, 13, 14, 19, 20, 24, 25, 29 and 30, and the vertical translation degrees-of-freedom at nodes 34, 35, 38, 39, 42 and 43. The elements selected for monitoring in the different states are elements 3, 8, 13, 18, 23, 28, 33, 38 and 43. They are at the middle of each length of the column and beam members, and are selected from engineering sense. Modes 1, 2, 3, 10, 11 and 12 are selected in the analysis because the first three modes are global modes with large column vibrations

and the last three modes are the first three local modes dominated with large beam vibration.

3.3.4.1 Results from MDLAC method using incomplete mode shapes

The damage localization results using the selected incomplete mode shapes for the three damage scenarios with small and large damages are shown in Figures 3.3(a) to 3.5(a) and Figures 3.6(a) to 3.8(a) respectively. For single damage (see Figures 3.3(a) and 3.6(a)), it is found that the damage site can be determined when the damage is small or large. For two damages (see Figures 3.4(a) and 3.7(a)), the damage on the column is localized but the damage on the interconnecting beam is not detected in both the small and large damage scenarios. For the case with three small damages (see Figure 3.5 (a)), element 9 is localized successfully but elements 13 and 39 are not located as damage sites. For the case with three large damages (see Figure 3.8(a)), elements 9 and 39 are localized but element 13 is not classified as potential damage site.

3.3.4.2 Results from MDLAC method using incomplete EMSEC

Figures 3.3(b) to 3.5(b) and Figures 3.6(b) to 3.8(b) give the damage localization results for the three damage scenarios with small and large damages respectively. The results from *EMSEC* can identify the actual damage elements as the potential damage sites with their numerical *MDLAC* values higher than 0.5 (except damage scenario S3, the threshold value is 0.4) within the group of all elements. However when incomplete mode shapes are used, the *MDLAC* method cannot localize

the actual damage elements in the potential damage sites for multiple damage scenarios as seen in Figures 3.4(a), 3.5(a), 3.7(a) and 3.8(a).

The *MDLAC* values on the different combinations of the potential damage sites are further computed. The final damage sites are located corresponding to the combination with the largest *MDLAC* value. The results obtained from using incomplete *EMSEC* without noise effect are shown in Table 3.5. The final damage sites are found to be the same as the actual damage elements for both small and large damages when noise effect is not included.

For the single damage scenarios S1 and L1 (see Figures 3.3(b) and 3.6(b)), the damage element 45 has the largest *MDLAC* value. However, some undamaged elements (elements 30 and 44), which are adjacent to the damage, contain a larger *MDLAC* value. The reason is that these adjacent elements share the same measured mode shapes of the damage element and have some damage characteristic. Moreover, some undamaged elements (elements 41 to 43), which are near the structural damage, also have a larger *MDLAC* value because their measured mode shapes are affected by the damage. The undamaged element 15 poses a larger *MDLAC* value. This is due to that the structure is symmetrical. Then the analytical *EMSEC* of elements 15 and 30 are similar and give a mistake in the damage localization. Element 14 also has a higher *MDLAC* value but this error cannot be explained.

For the two damage scenarios S2 and L2 (see Figures 3.4(b) and 3.7(b)), the damage element on column (element 17) has the largest *MDLAC* value and the damage element on beam (element 32) has a larger *MDLAC* value. Some undamaged

elements (elements 6, 16, 18, 31 and 33), which are adjacent or near the structural damages, also contain a larger *MDLAC* value due to the reason mentioned above. The undamaged element 21 has a larger *MDLAC* value because its analytical *EMSEC* is similar to that of element 6 which is symmetrically located on the other side of the frame and is near the damage. For identifying the potential damage sites, only one element of the structure is assumed to be damaged in the analytical *EMSEC*. Then, this analytical *EMSEC* is correlated to the experimental *EMSEC* and obtained a *MDLAC* value. However, the experimental *EMSEC* includes the effect from two damages. Therefore, the *MDLAC* value in some undamaged elements (elements 3, 15, 41 to 45) may have errors due to the coupling effects from several damage sites.

For the three damage scenarios S3 and L3 (see Figures 3.5(b) and 3.8(b)), one damage element on column (element 9) has the largest *MDLAC* value. The other damage element on column (element 13) and on beam (element 39) has a larger *MDLAC* value. This observation shows that the damage effect on the measured mode shapes by element 9 is more dominant than that by element 13 or element 39. Some undamaged elements (elements 7, 8 and 40), which are adjacent to or near the damages, also contain a larger *MDLAC* value with the same reason mentioned above.

3.3.5 Damage Localization with Noise Effect

Measured frequencies and mode shapes are always contaminated with the measurement noise. The ability of a damage localization method to localize damages using incomplete noisy information is very important. The noisy "measured"

eigenvalues and mode shapes (with superscript ~) are calculated according to the following equations.

$$\tilde{\lambda}_i = \lambda_i \cdot (1 + \gamma_i^{\lambda} \rho^{\lambda}) \tag{3.11}$$

$$\tilde{\Phi}_{ji} = \Phi_{ji} \cdot (1 + \gamma_{ji}^{\Phi} \rho^{\Phi}) \tag{3.12}$$

where λ_i is the i-th eigenvalue and Φ_{ji} is the j-th component of the i-th mode shape at any damage scenario. $\tilde{\lambda}_i$ and $\tilde{\Phi}_{ji}$ are the corresponding noisy eigenvalue and mode shape. γ_i^{λ} and γ_{ji}^{Φ} are random numbers with a mean equal to zero and a variance equal to one. ρ^{λ} and ρ^{Φ} are the noise level for the eigenvalue and mode shape. Messian *et al.* (1996) suggested a standard error of $\pm 0.15\%$ as a benchmark figure for natural frequencies measured in the laboratory with the impulse hammer technique. In contrast, the mode shape estimate have an error level as much as 20 times worse (Farrar and Cone, 1995) than those in the corresponding natural frequencies estimate. Therefore, the noise levels for the eigenvalue (ρ^{λ}) and mode shape (ρ^{Φ}) are assumed to be 0.15% and 3% respectively.

The incomplete and noisy mode shapes are then used to localize the structural damage sites by the *MDLAC* methods using mode shapes and using *EMSEC* in turn. Figures 3.9 to 3.11 give the damage localization results for the three damage scenarios with small damage. The results show that the noise has a large adverse effect in the *MDLAC* method using incomplete mode shapes or using incomplete *EMSEC* when the damage is small. Figures 3.12 to 3.14 give the damage localization results for the three damage scenarios with large damage. The results show that the *MDLAC*

methods using mode shape or *EMSEC* with noise effect have similar results to that without noise when the damage is large.

The potential damage sites and the final damage sites for the small and large damage scenarios using incomplete and noisy *EMSEC* are listed in Table 3.6. The threshold value of the elements identified as potential damage sites is 0.5 for damage scenarios S1, S2, L1 and L2. The threshold value is 0.3 and 0.45 for damage scenarios S3 and L3 respectively. It is found that the actual damage elements are grouped in the final set of damage sites. Hence, the *MDLAC* method using incomplete *EMSEC* with noise effect, though not able to match the actual damage sites, can significantly reduce the number of final damage sites for further examination in the subsequent stage of damage quantification.

By comparing Figures 3.3(b) to 3.5(b) and 3.9(b) to 3.11(b), it was reported that the localization results are greatly affected by the noise effect for small damages. The damage element does not contain the largest *MDLAC* value. The undamaged elements, which are adjacent to or near the damage, have a larger *MDLAC* value. However, some undamaged elements, which are far away from the structural damage, also have a larger *MDLAC* value due to the noise effect and the assumption of a single damage in the computation of the analytical *EMSEC* for identifying the potential damage sites.

For the case of large damages, the damage element has the largest *MDLAC* value for scenarios L1 and L3. However, the adjacent element (element 31) has the largest *MDLAC* value for scenario L2. The undamaged elements, which are adjacent

to or near the damage, also contain a larger *MDLAC* value because they exhibit some damage characteristic derived from the mode shape of the adjacent connecting node. The undamaged elements at the same position of the adjacent elements on the other column have a larger *MDLAC* value due to the symmetry of the structure.

3.3.6 Damage Localization with Larger Noise Level

For further investigating the noise effect on this proposed damage localization method, a higher noise level on the eigenvalue and mode shape are used. Two more noise levels are further investigated. Noise level A is 0.25% and 5% for the eigenvalue and mode shape respectively. And Noise level B is 0.5% and 10% for the eigenvalue and mode shape respectively. The noisy eigenvalue and mode shape are calculated using the equations in Section 3.3.5. The larger noise effect on the localization results is further studied with damage scenario L3.

The damage localization results from the *MDLAC* method using *EMSEC* for damage scenario L3 are shown in Figures 3.15 and 3.16 with noise level A and noise level B respectively. For damage scenario L3 with noise level A or noise level B, the threshold value is 0.3. The potential damage sites are elements 7, 8, 9, 13, 36, 38, 39, 40 and the final damage sites are elements 7, 13, 36, 40 for both cases. Unfortunately, only the actual damage element 13 is grouped in the final damage sites and the other two damage elements (elements 9 and 39) are not.

3.4 Conclusions

The Multiple Damage Location Assurance Criterion (*MDLAC*) derived directly from incomplete mode shapes is studied for its effectiveness to localize the damage in a structure. The elemental modal strain energy change (*EMSEC*) is used instead of mode shapes. The potential damage sites are identified by grouping those elements with their *MDLAC* values larger than a prescribed threshold value. The final damage sites can be determined by further calculating the *MDLAC* values for different combinations of the potential damage sites. The combination that gives the highest *MDLAC* value is the final damage state. A three-storey plane frame is used to demonstrate the damage localization methods using incomplete mode shape and using incomplete *EMSEC*. The effect of the measurement noise in the damage assessment methods is also studied. From Section 3.3.6, we found that the damage localization method using incomplete noisy *EMSEC* cannot localize the actual damage elements when a high noise level is used. Results show that the *MDLAC* method using incomplete *EMSEC* is more accurate and effective to localize the structural damages than that using incomplete mode shapes. For the proposed method, the damage element usually has the largest *MDLAC* value. The undamaged elements, which are adjacent to or near the damage, or at the same position of the adjacent elements on the other column, also contain a larger *MDLAC* value due to symmetry. However, some undamaged elements, which are far away from the structural damage, are also identified as potential sites due to noise effect.

Table 3.1 - Physical properties of column and beam elements

	Column Element	Beam Element
Axial Area, A (m^2)	142.40×10^{-6}	230.03×10^{-6}
Poison Ratio, ν	0.30	0.30
Moment of Inertia, I (m^4)	2.350×10^{-10}	1.976×10^{-8}

Table 3.2 - Natural frequencies of three-storey plane frame

Mode No.	Natural Frequency (Hz)
1	7.067
2	20.75
3	31.159
4	127.056
5	134.379
6	137.096
7	138.261
8	151.668
9	166.477
10	192.787
11	203.584
12	210.749
13	374.523
14	377.771
15	379.413

Table 3.3 - Damage scenarios with small damages for three-storey plane frame

Scenario S1		Scenario S2		Scenario S3	
Element No.	Damage	Element No.	Damage	Element No.	Damage
45	5%	17	5%	9	2%
		32	3%	13	3%
				39	3%

Table 3.4 - Damage scenarios with large damages for three-storey plane frame

Scenario L1		Scenario L2		Scenario L3	
Element No.	Damage	Element No.	Damage	Element No.	Damage
45	30%	17	30%	9	15%
		32	20%	13	20%
				39	20%

Table 3.5 - Potential and final damage sites by using incomplete *EMSEC*

	Potential Damage Sites	Final Damage Sites	*MDLAC* value
Scenario S1	14, 15, 30, 41-45	45	0.536
Scenario S2	3, 6, 15-18, 21, 31-33, 41-45	17, 32	0.480
Scenario S3	7-9, 13, 39	9, 13, 39	0.637
Scenario L1	14, 15, 30, 41-45	45	0.532
Scenario L2	3, 6, 15-18, 21, 31-33, 41-45	17, 32	0.495
Scenario L3	7, 9, 13, 39, 40	9, 13, 39	0.741

Table 3.6 - Potential and final damage sites by using incomplete and noisy *EMSEC*

	Potential Damage Sites	Final Damage Sites	*MDLAC* value
Scenario S1	2, 4, 10, 18, 25, 42-45	25, 44, 45	0.215
Scenario S2	6, 12-14, 16, 17, 21, 28, 29, 31-33, 35, 42, 43	17, 31, 32	0.407
Scenario S3	7, 9-11, 13, 24, 25, 36-40	9, 13, 25, 39, 40	0.342
Scenario L1	30, 41-45	45	0.386
Scenario L2	3, 6, 13, 16, 17, 21, 31-33, 35, 42-44	17, 31, 32	0.494
Scenario L3	7, 9, 13, 34, 36, 38-40	7, 9, 13, 39, 40	0.583

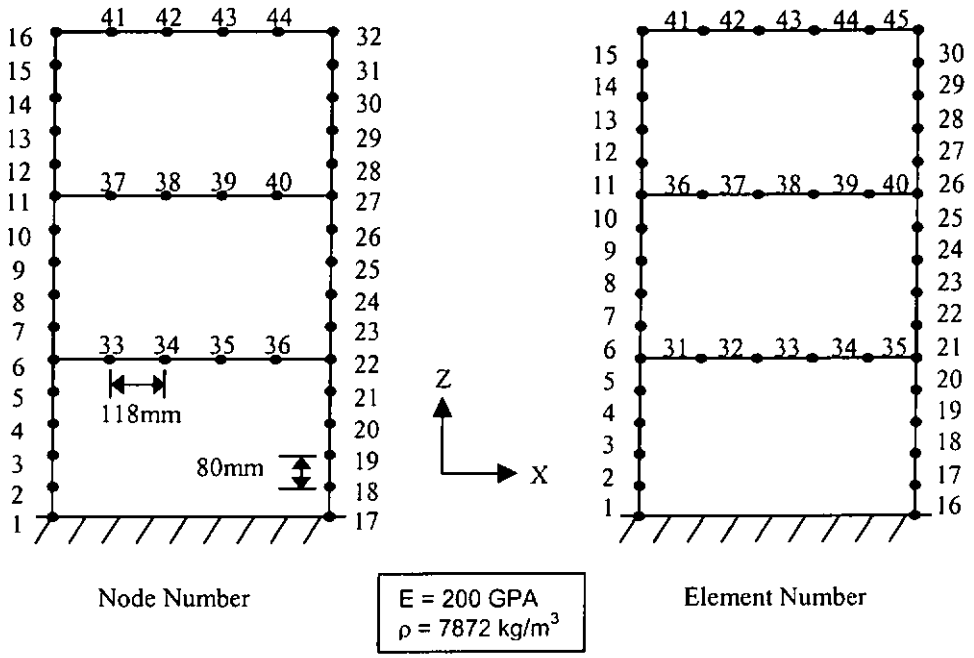

Figure 3.1 - Evaluation view of three-storey plane frame

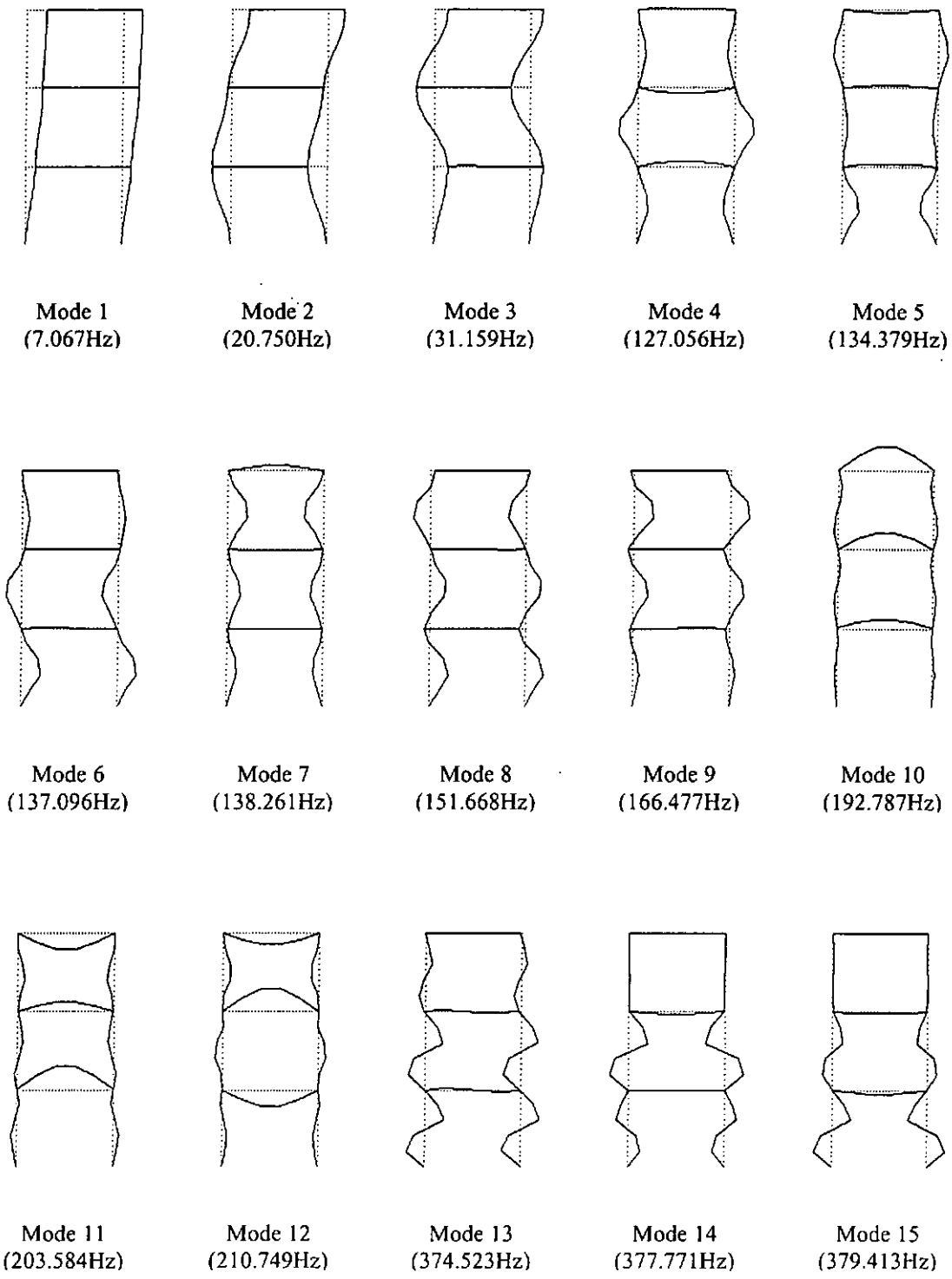

Figure 3.2 - Mode shapes of three-storey plane frame

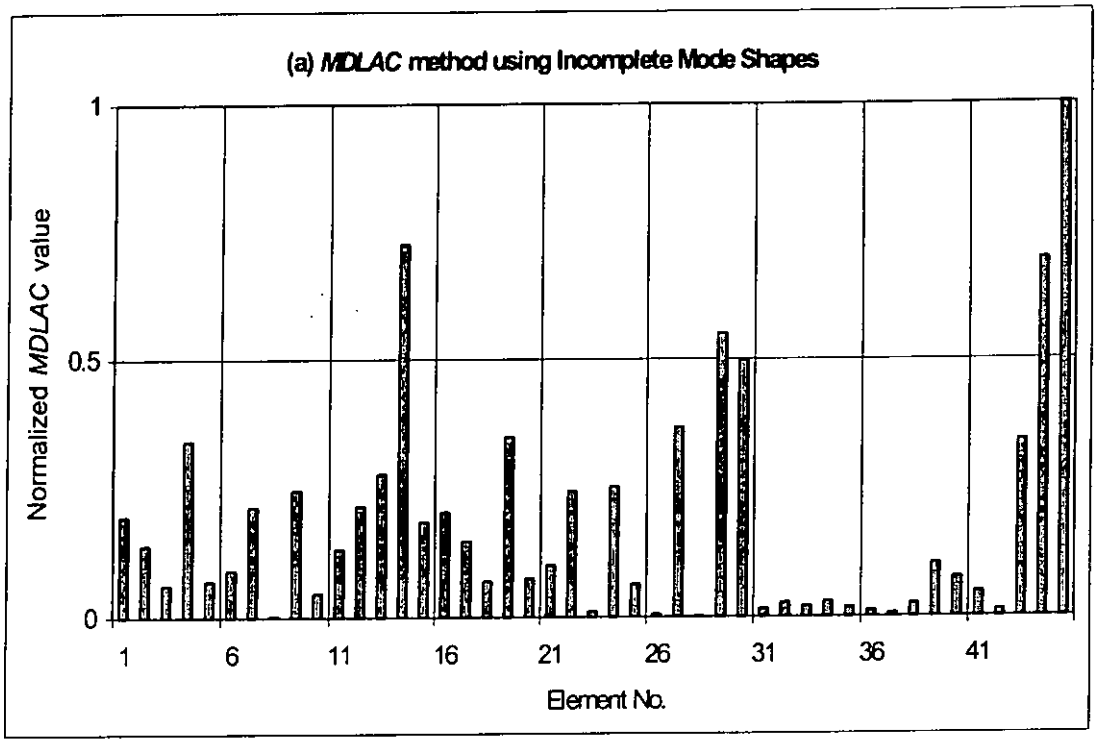

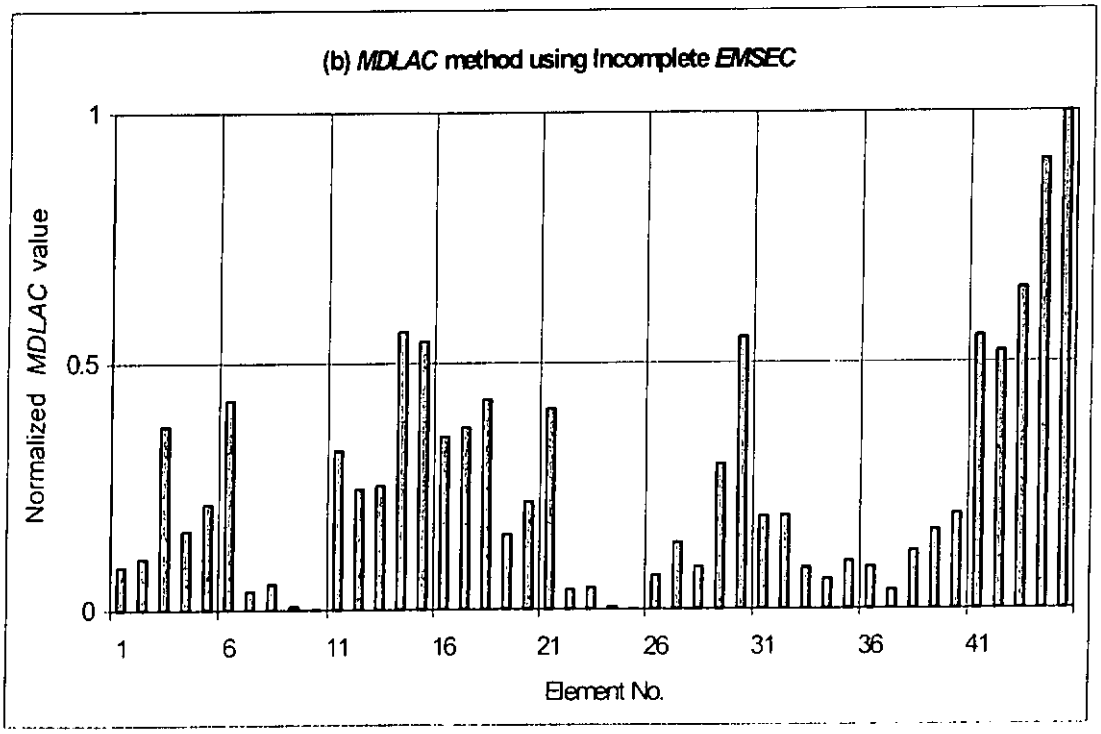

Figure 3.3 - Damage localization charts for scenario S1 without noise

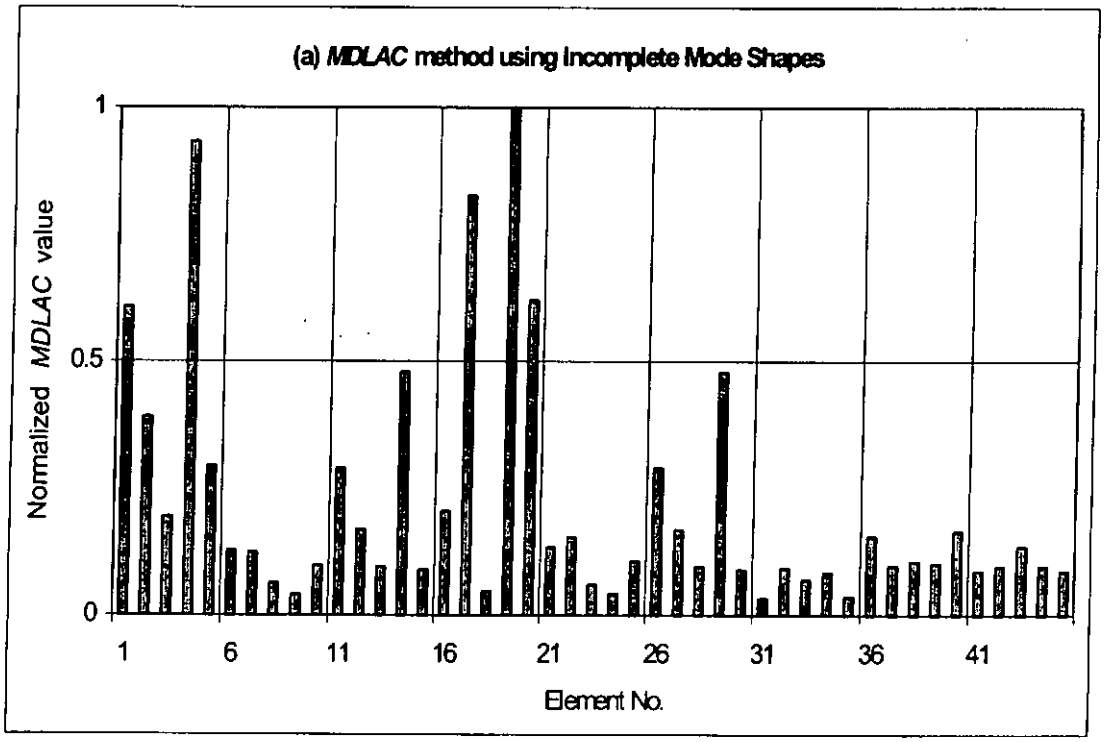

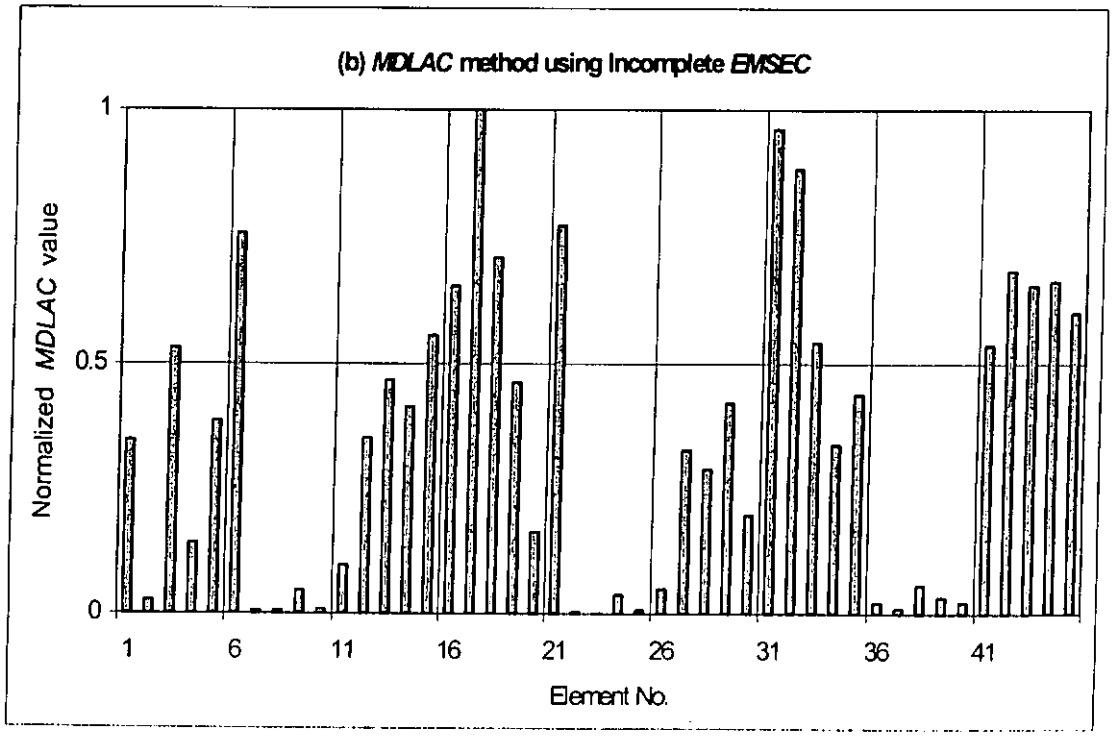

Figure 3.4 - Damage localization charts for scenario S2 without noise

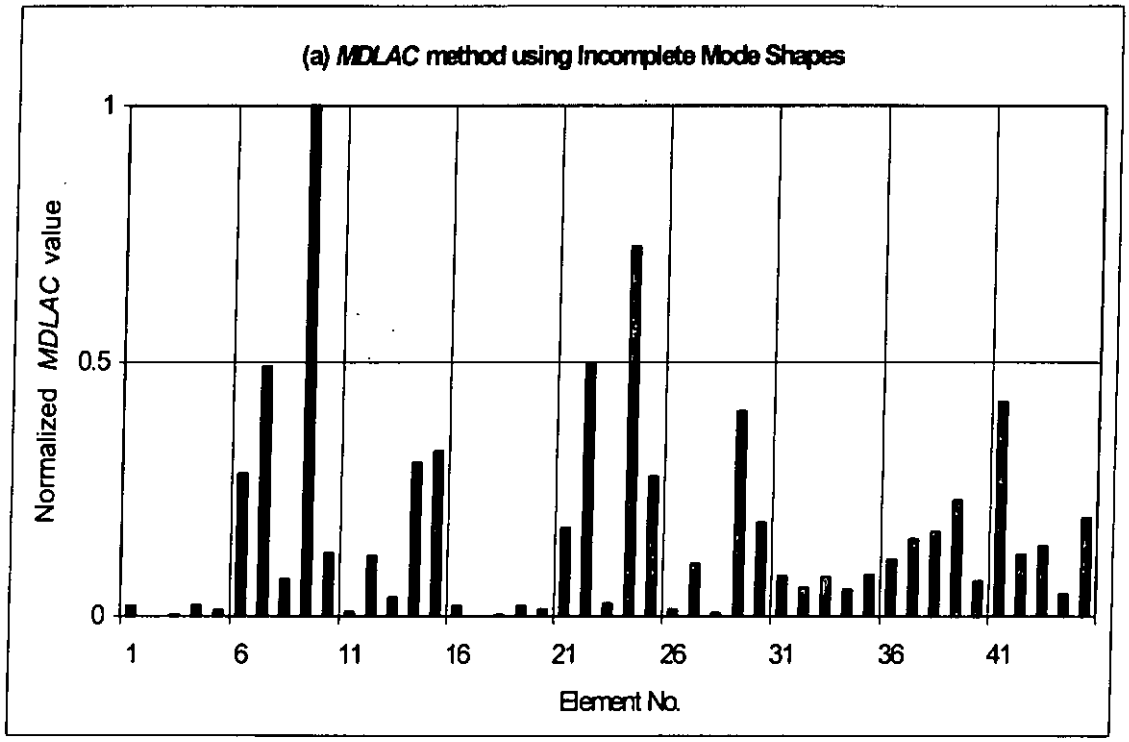

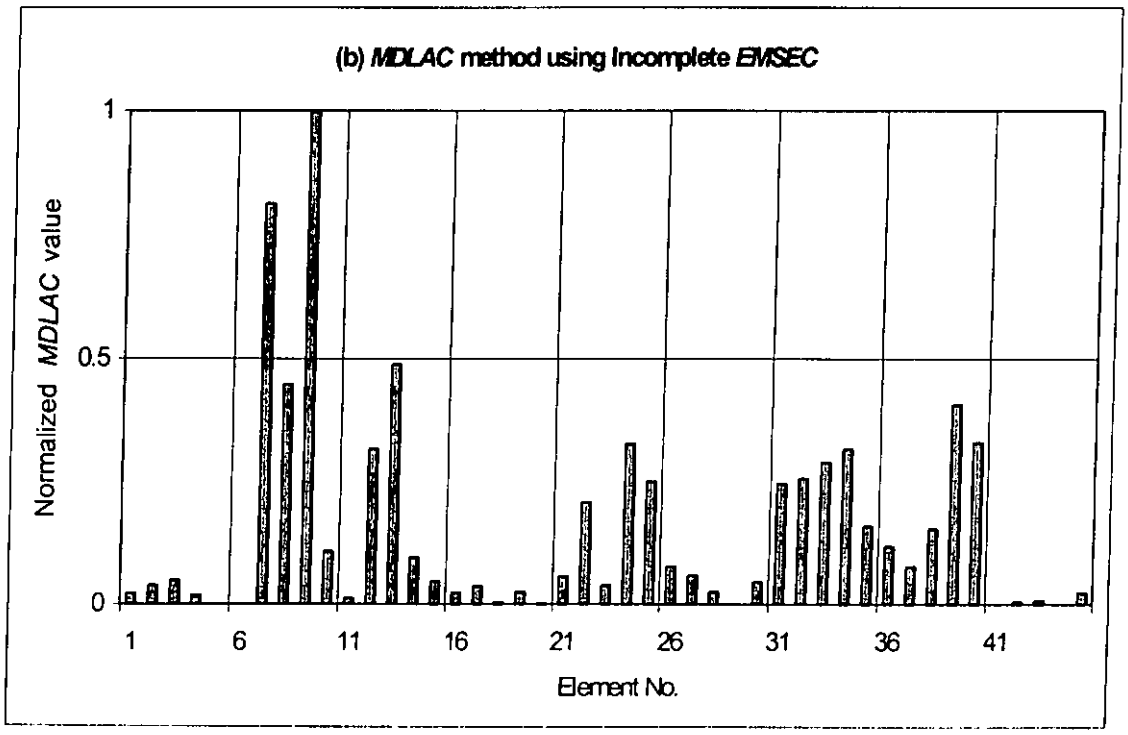

Figure 3.5 - Damage localization charts for scenario S3 without noise

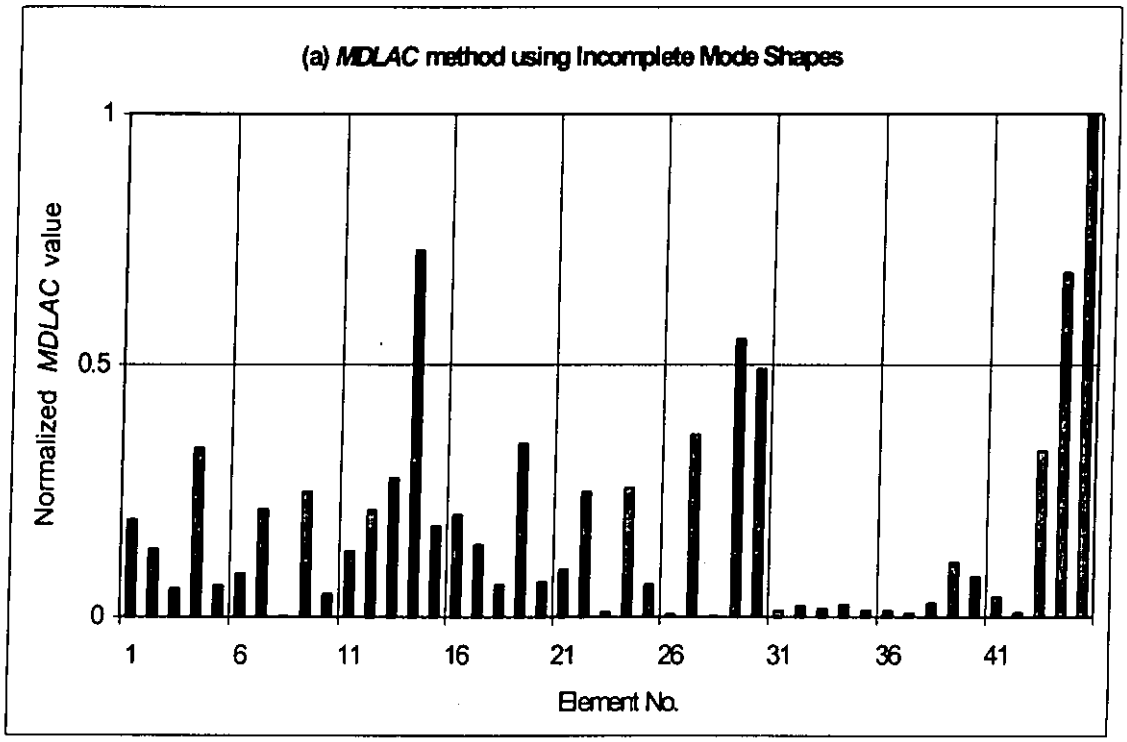

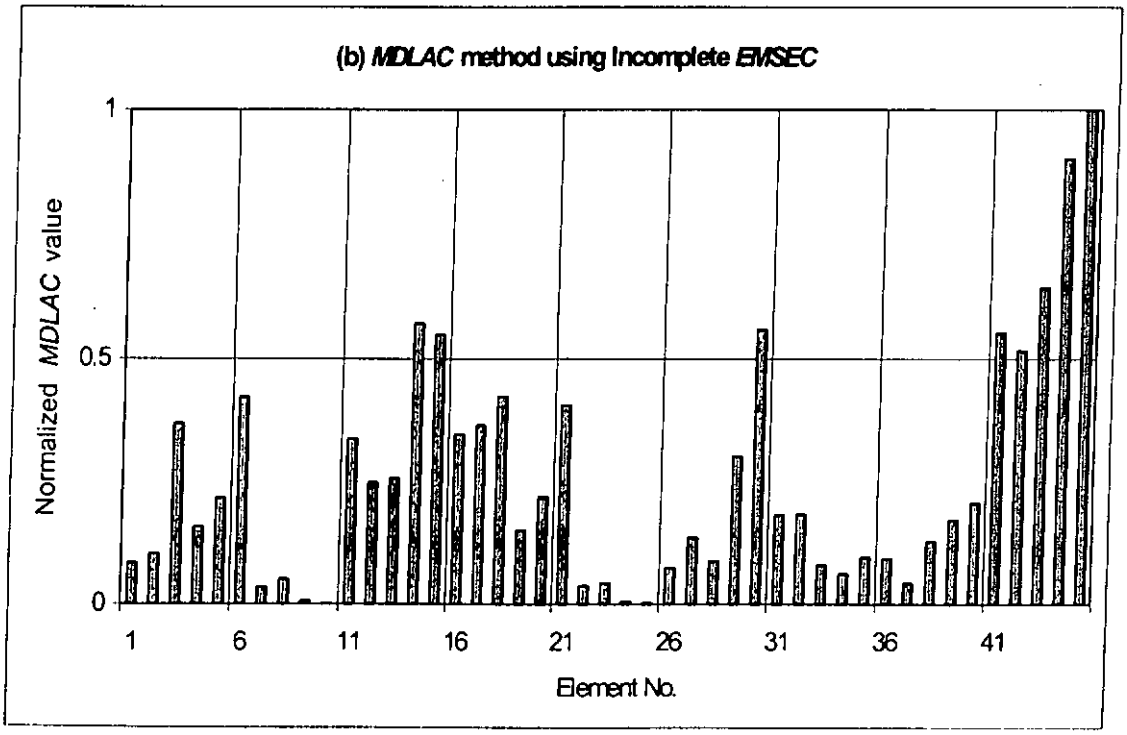

Figure 3.6 - Damage localization charts for scenario L1 without noise

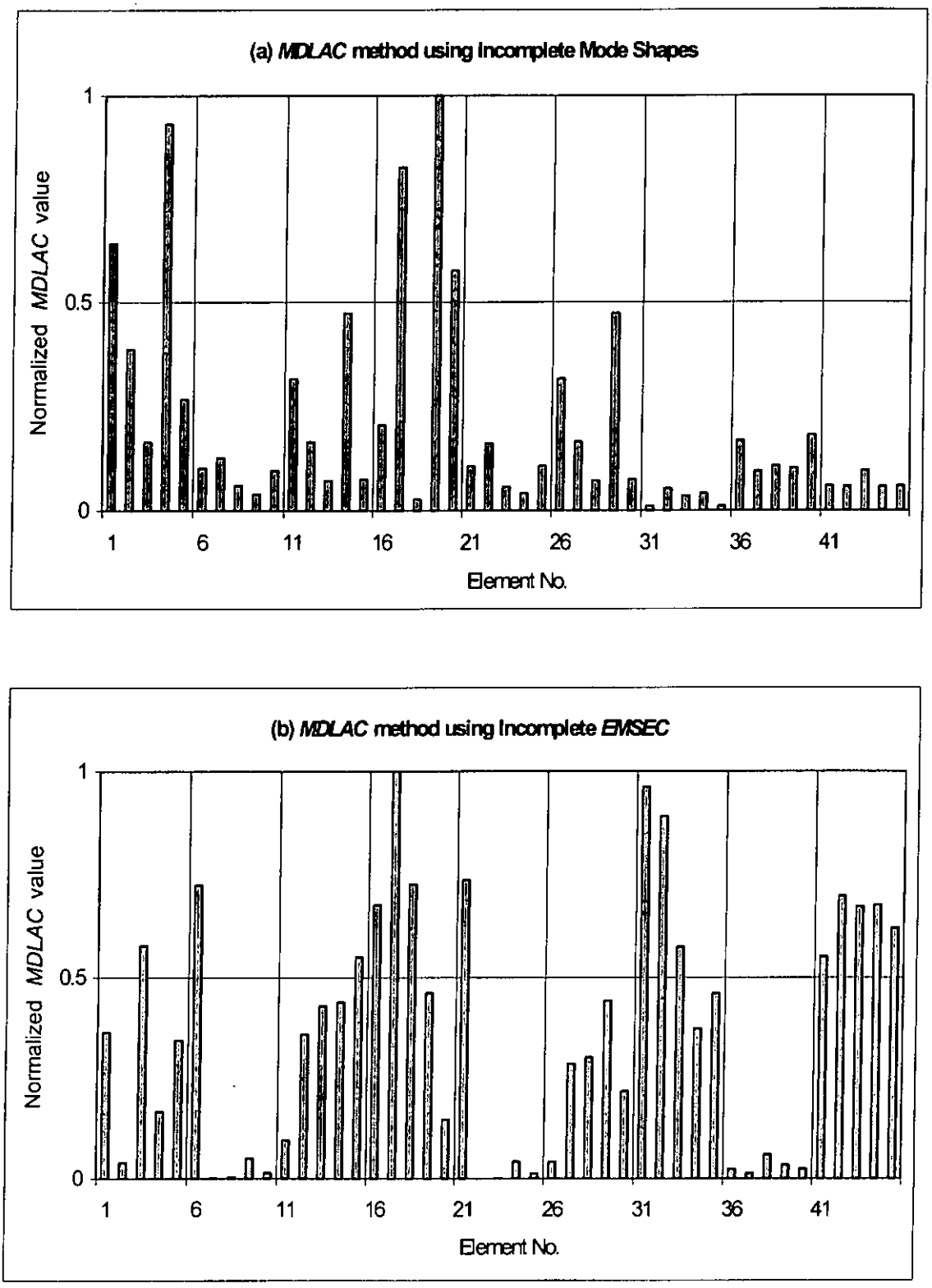

Figure 3.7 - Damage localization charts for scenario L2 without noise

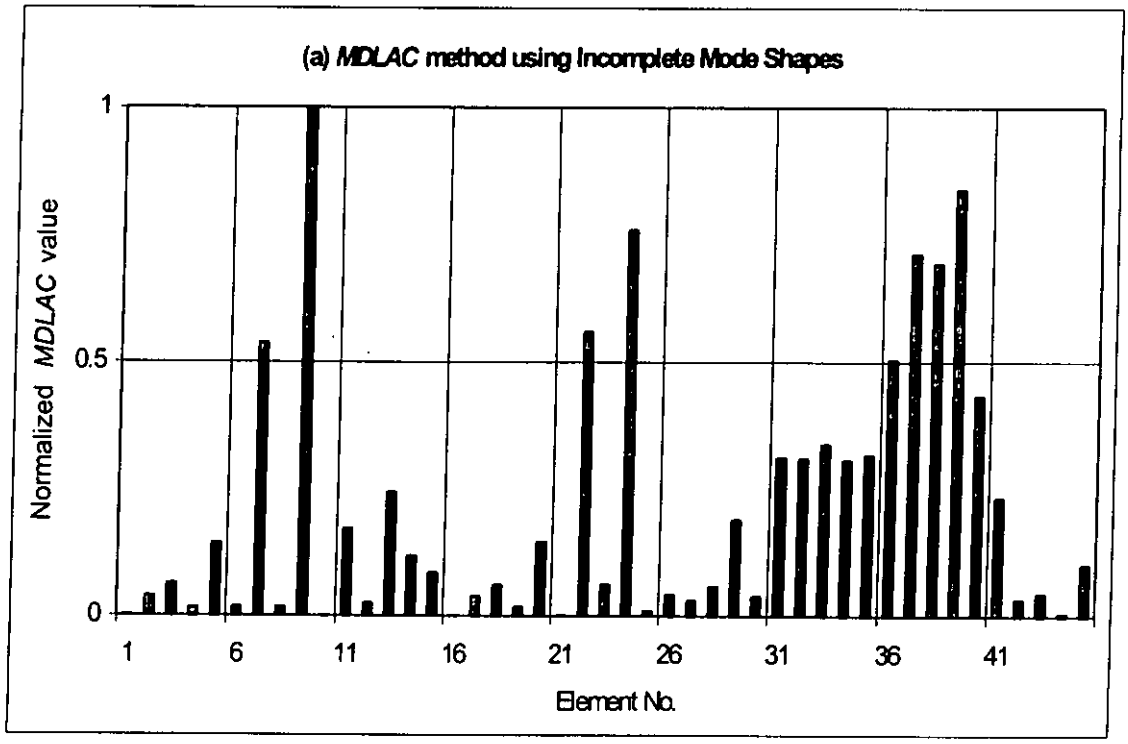

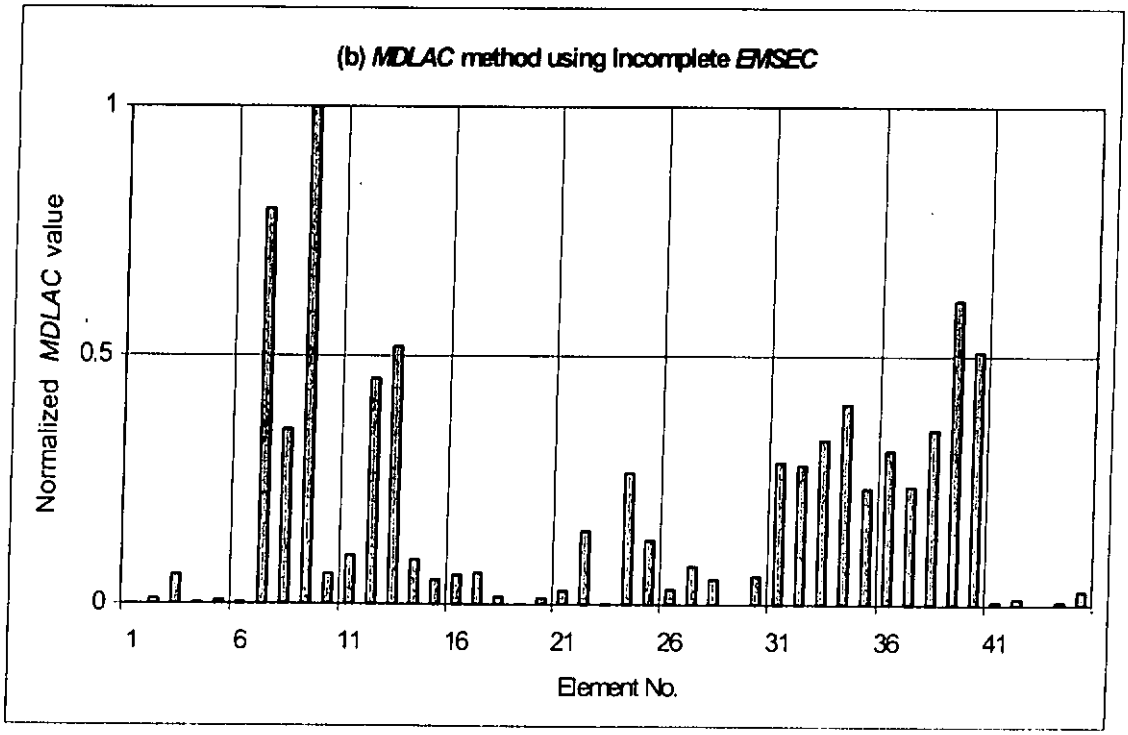

Figure 3.8 - Damage localization charts for scenario L3 without noise

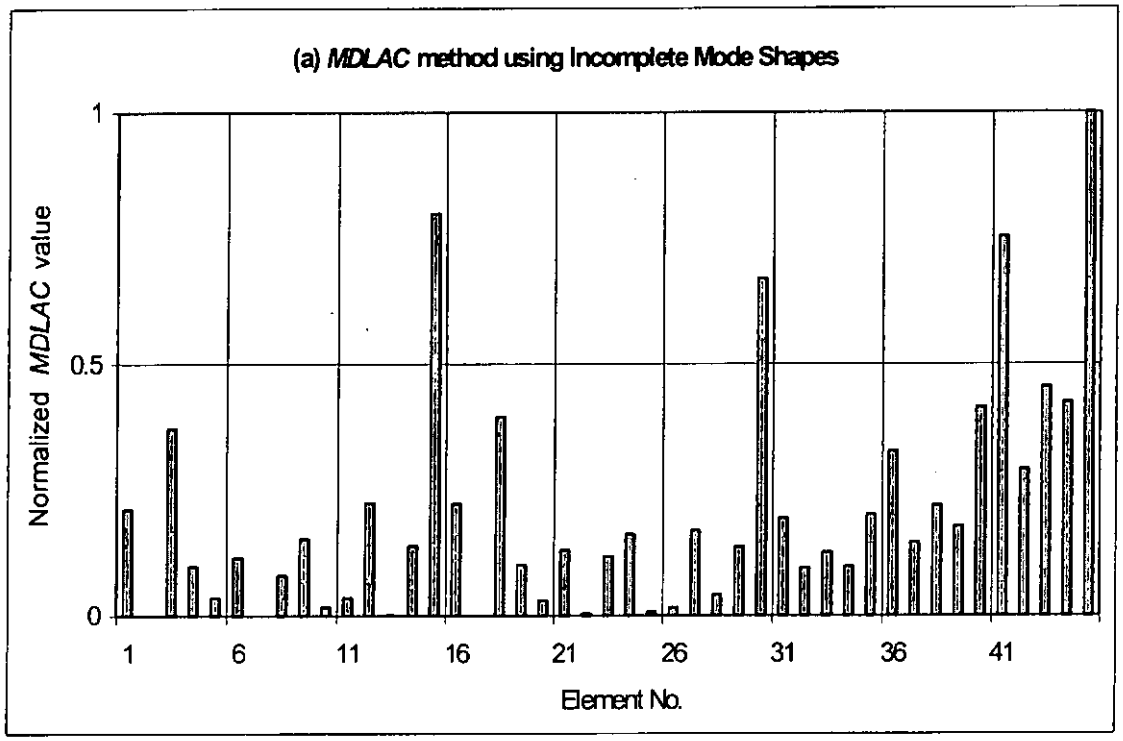

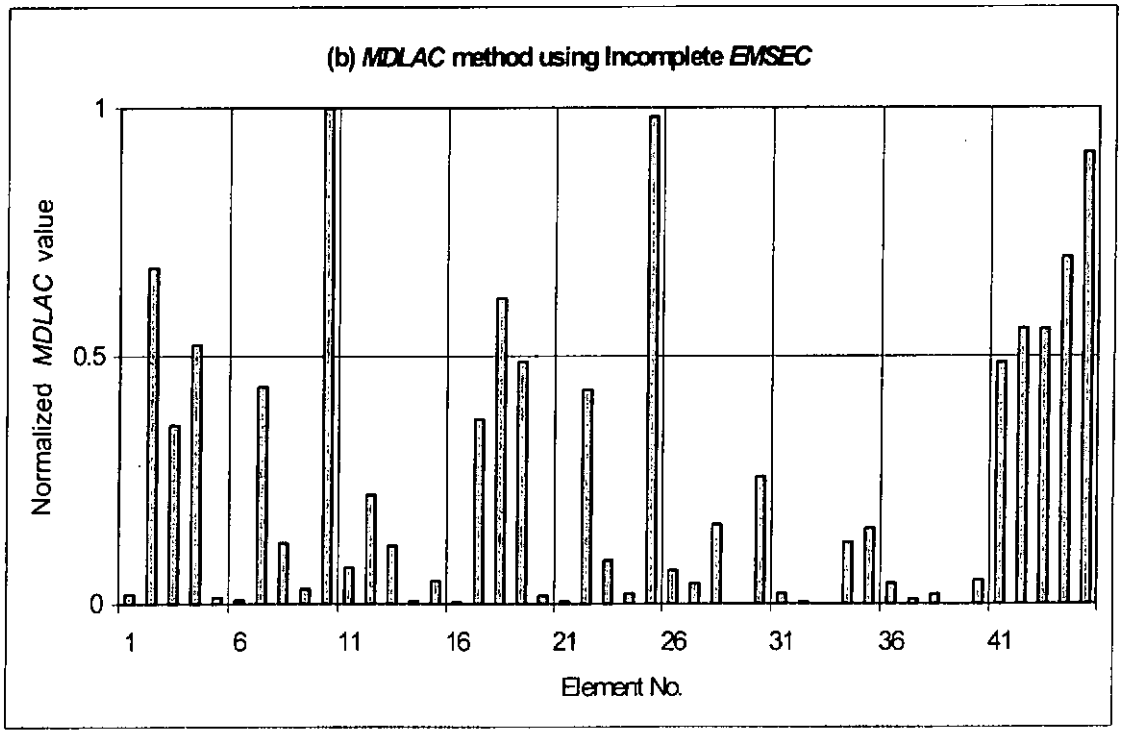

Figure 3.9 - Damage localization charts for scenario S1 with noise

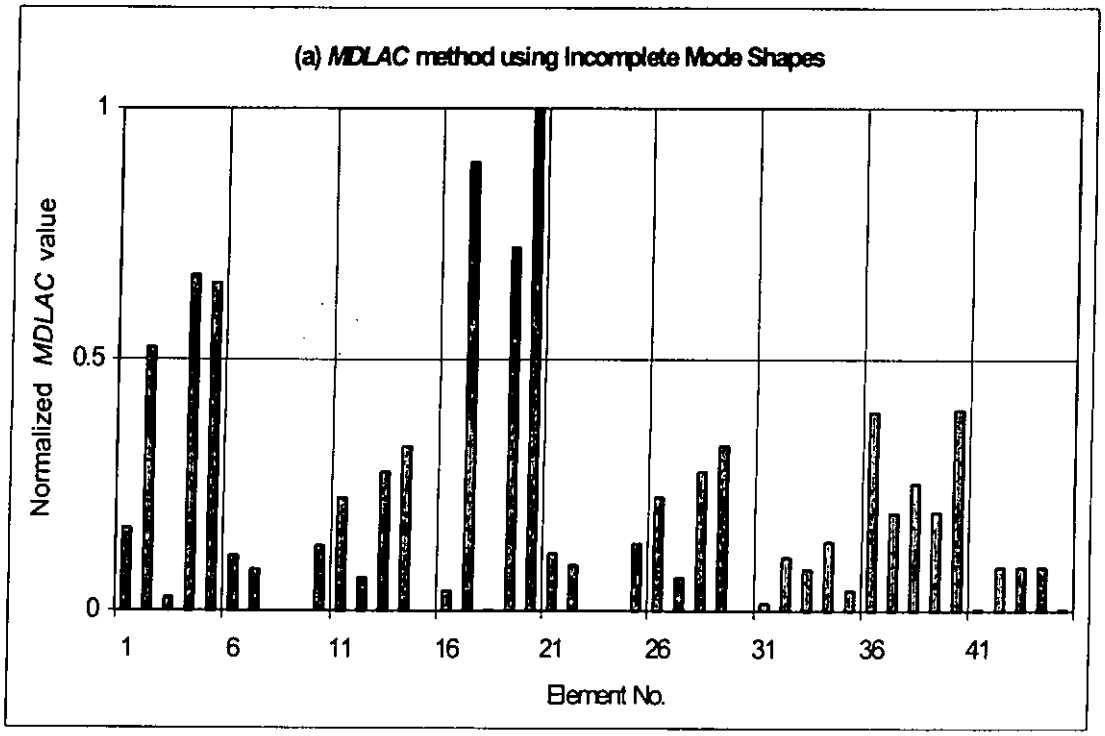

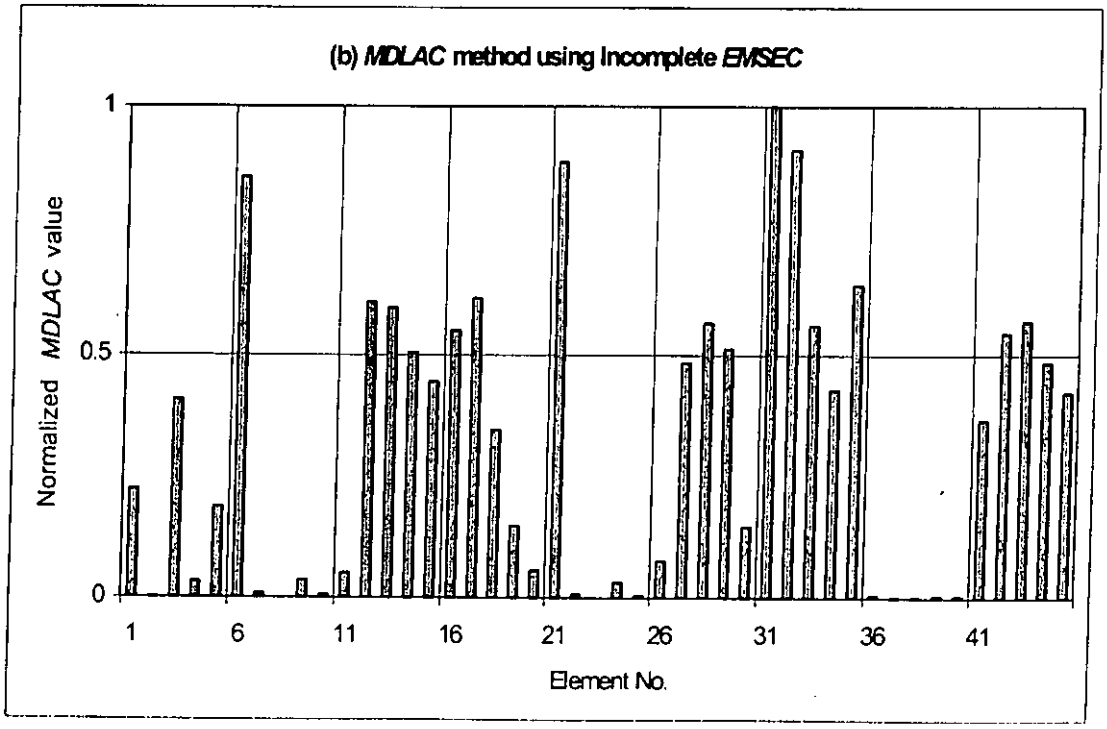

Figure 3.10 - Damage localization charts for scenario S2 with noise

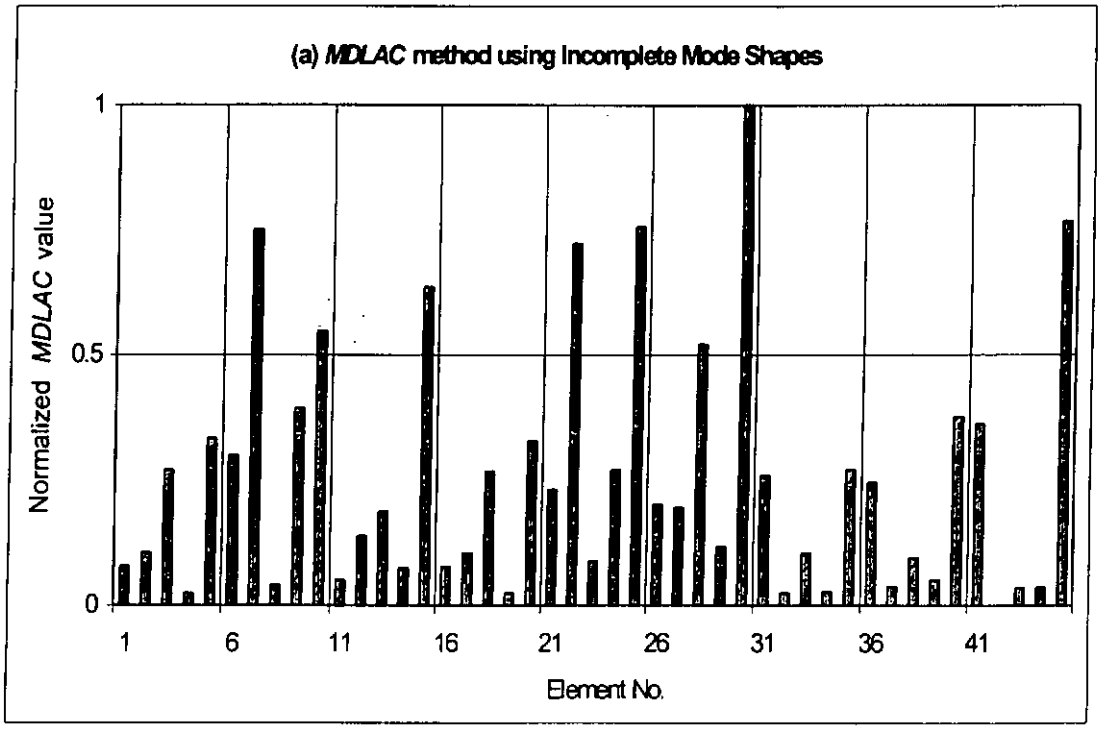

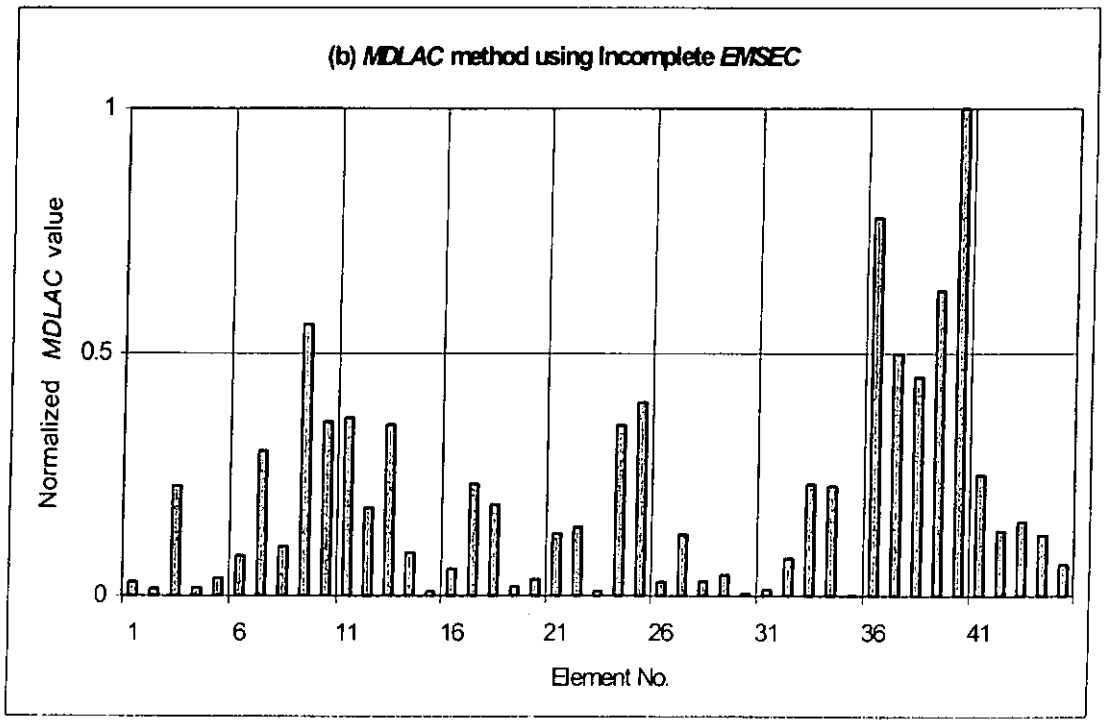

Figure 3.11 - Damage localization charts for scenario S3 with noise

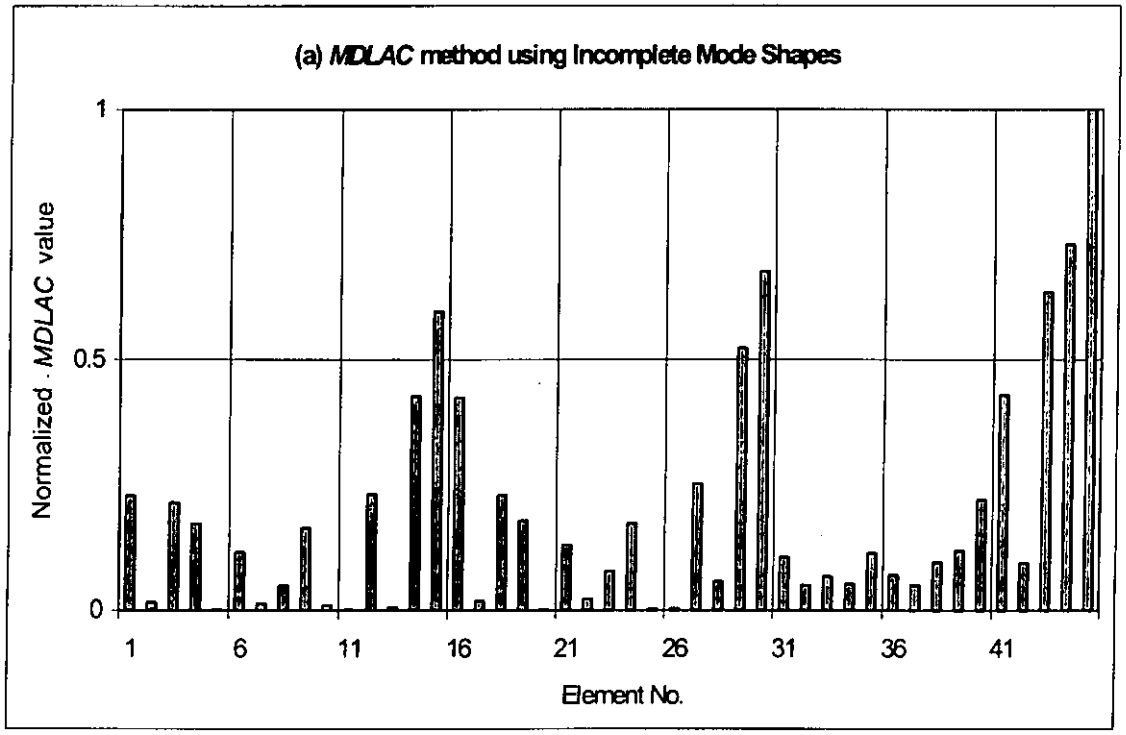

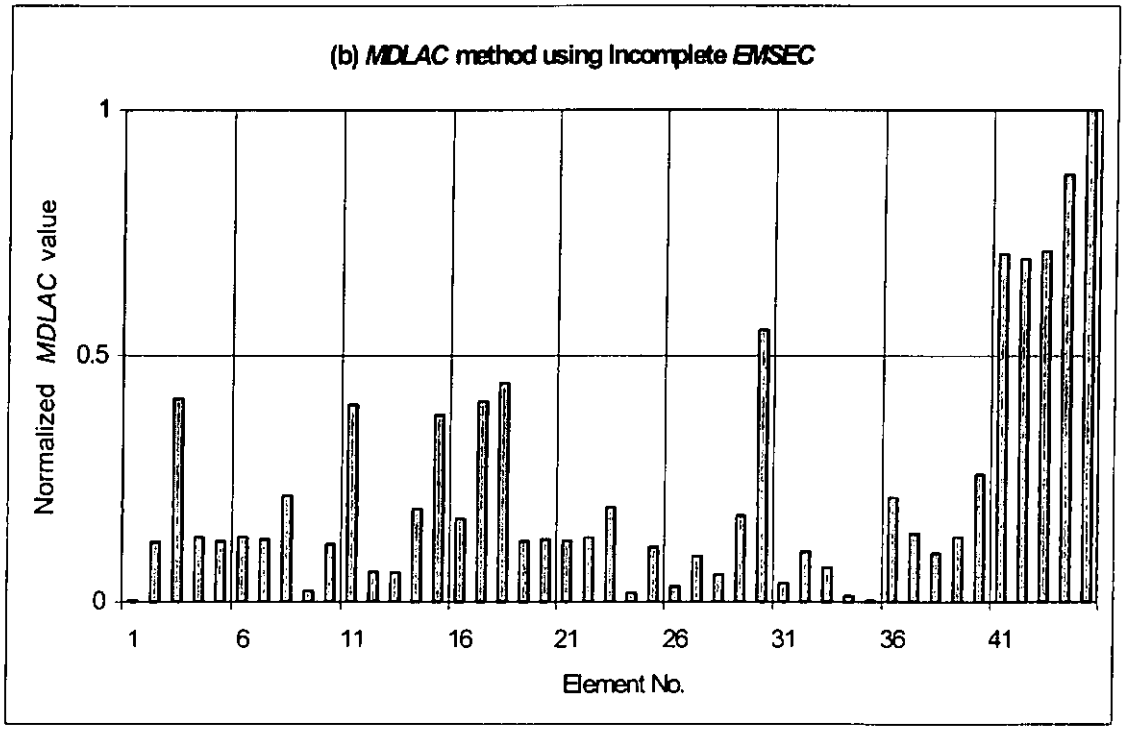

Figure 3.12 - Damage localization charts for scenario L1 with noise

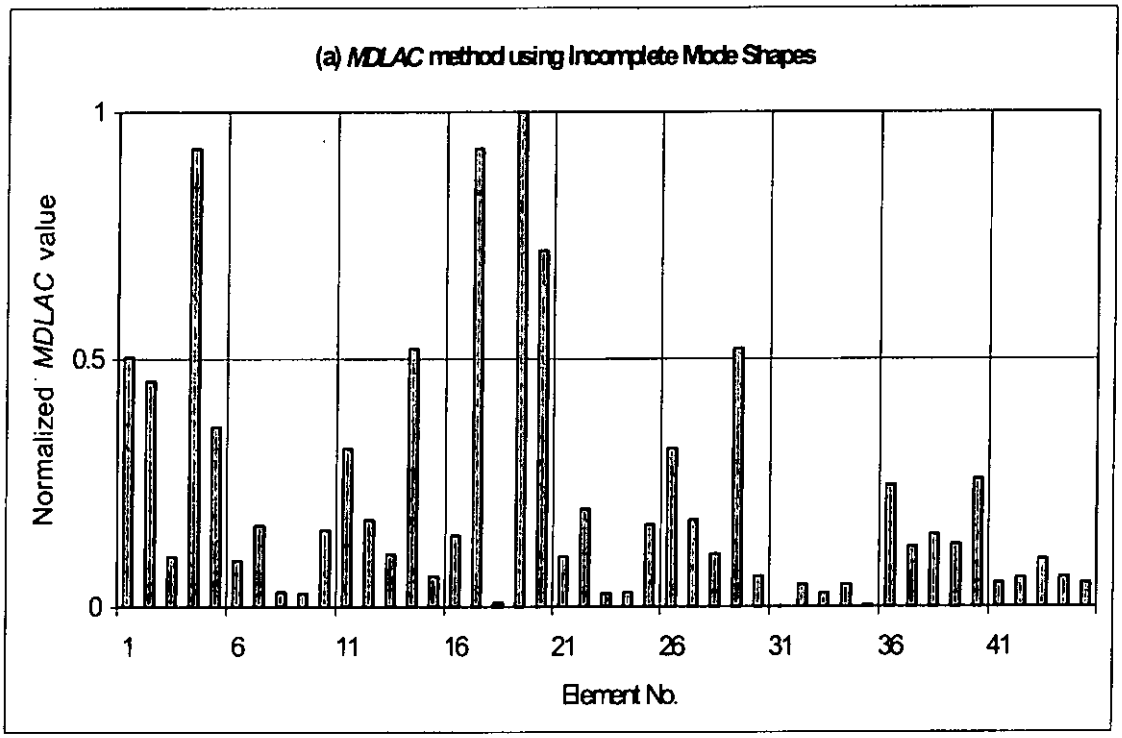

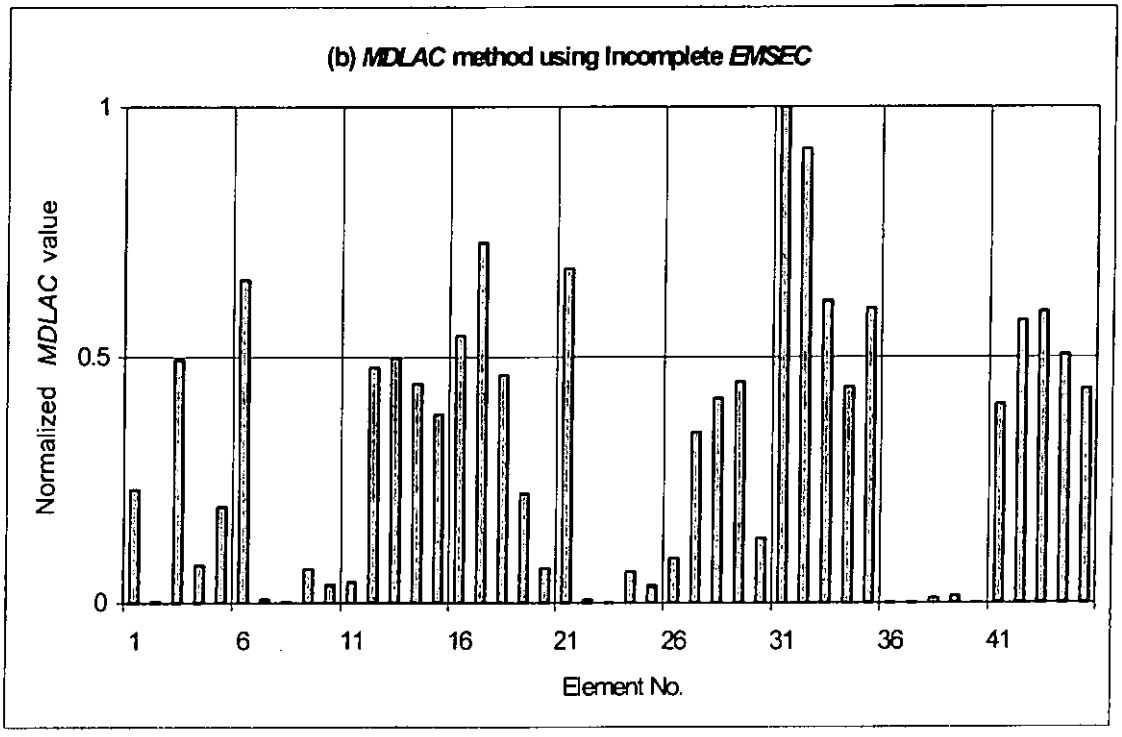

Figure 3.13 - Damage localization charts for scenario L2 with noise

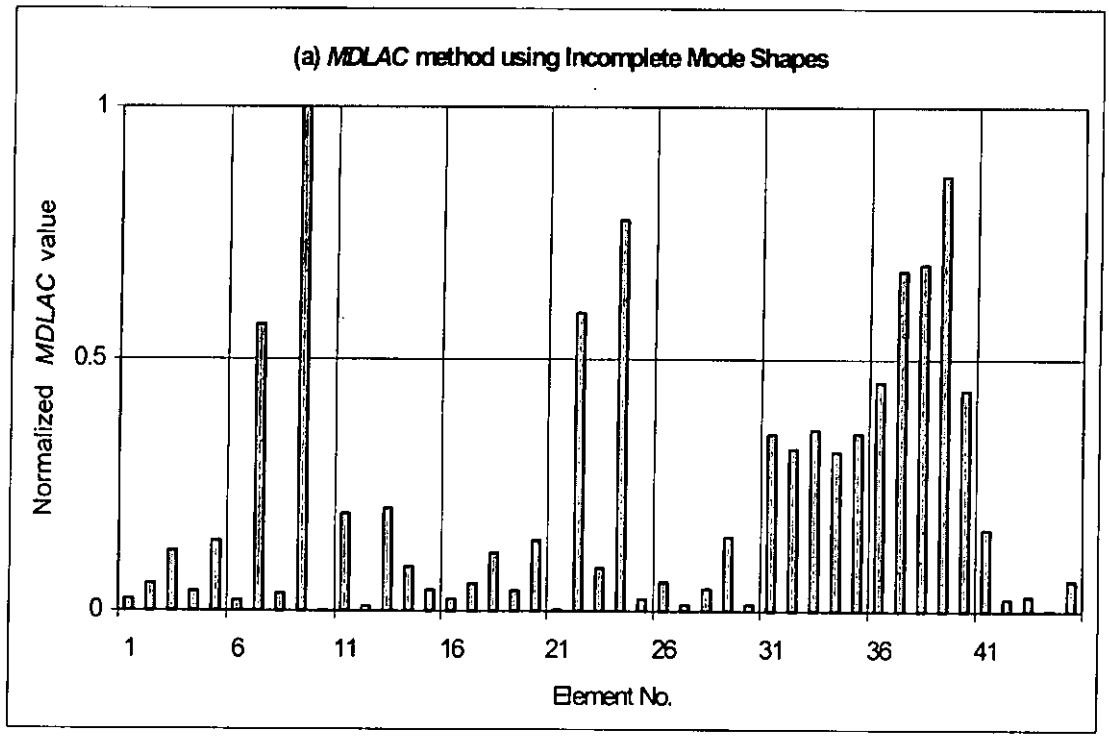

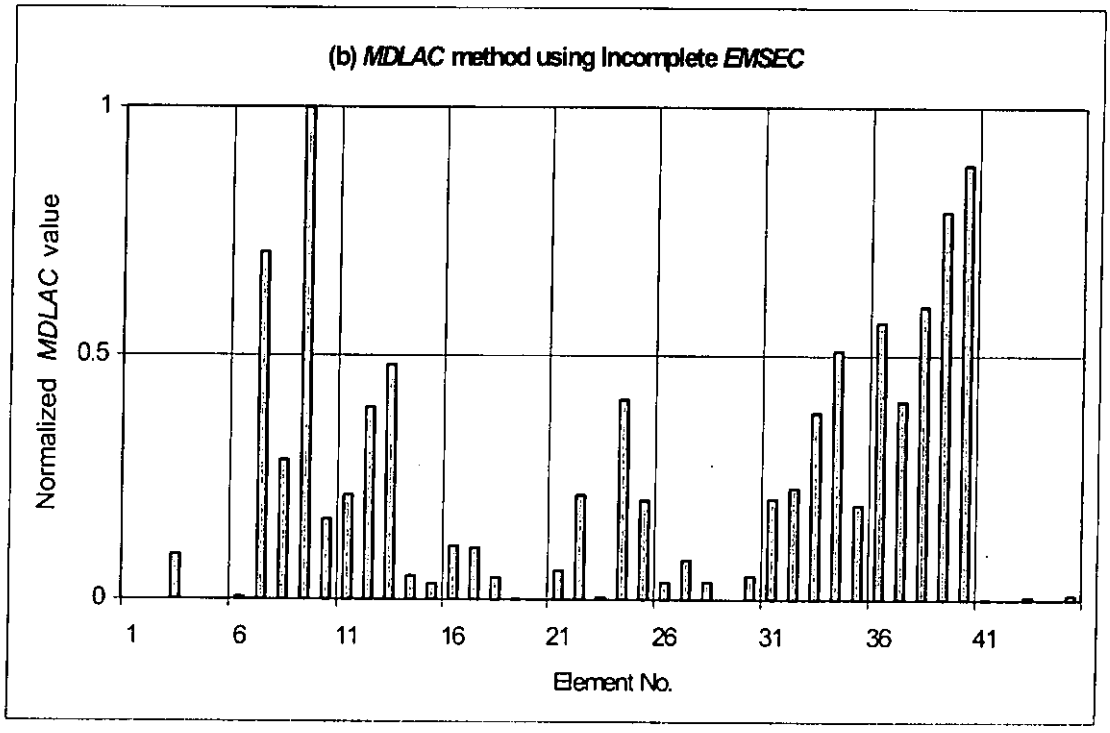

Figure 3.14 - Damage localization charts for scenario L3 with noise

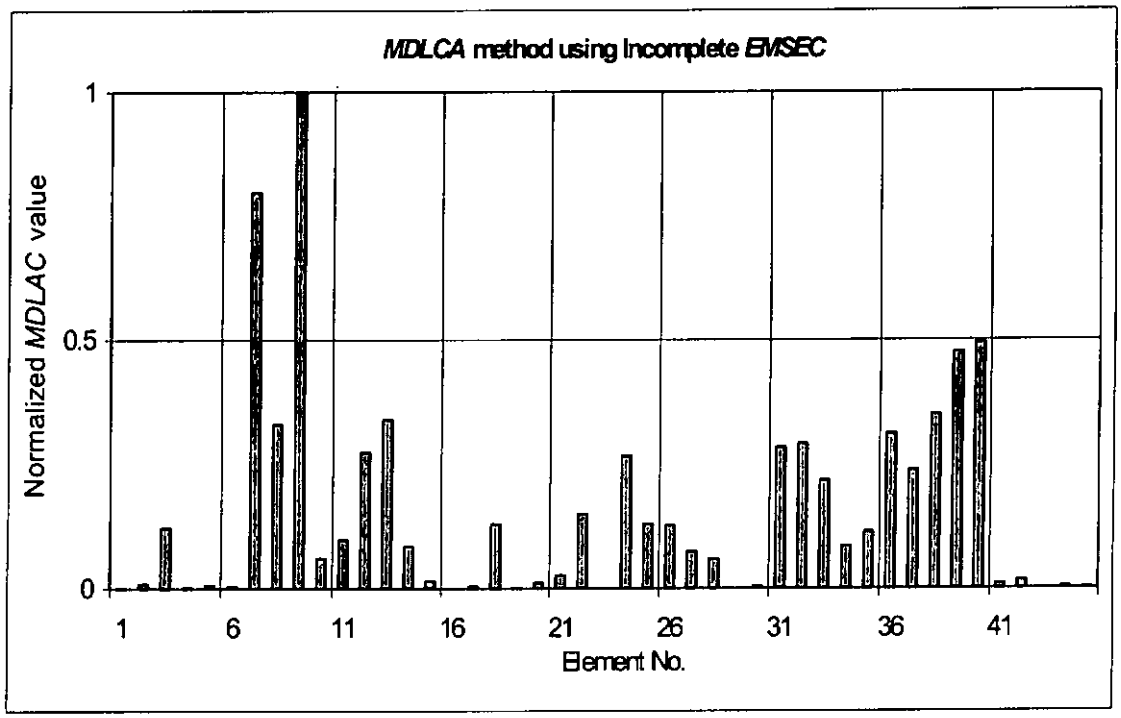

Figure 3.15 - Damage localization chart for scenario L3 with noise level A

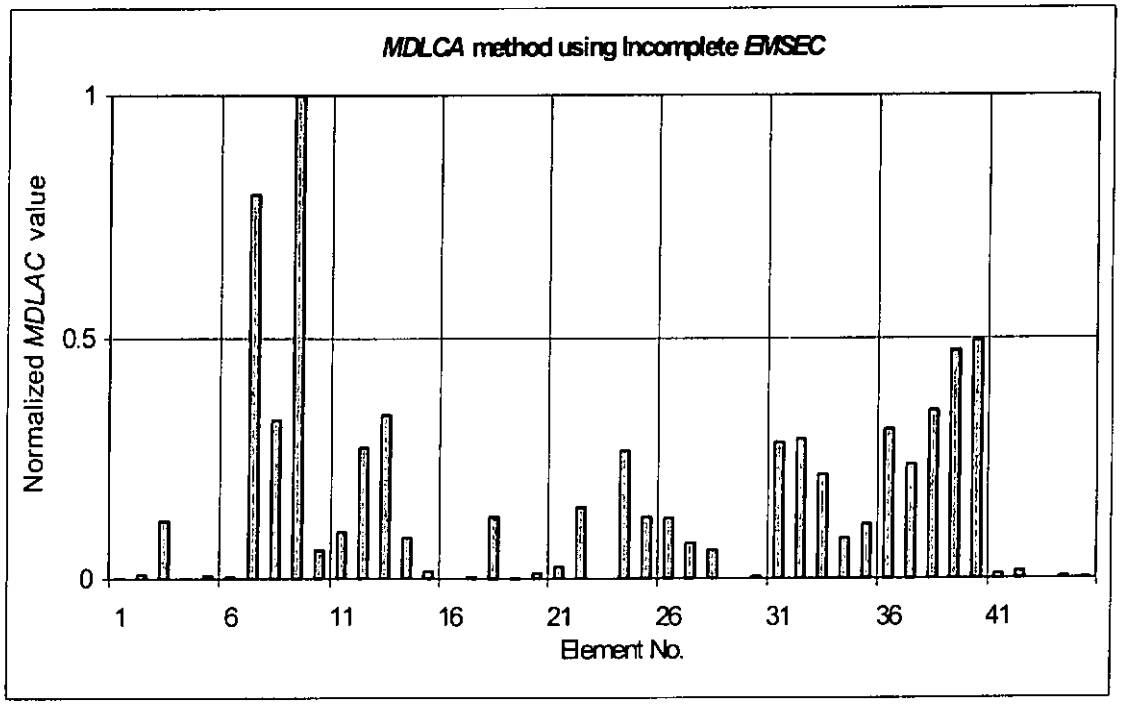

Figure 3.16 - Damage localization chart for scenario L3 with noise level B

Chapter 4

Damage Quantification Method using First Order Analysis

4.1 Introduction

After localization of the damage sites, the damage extent of the final damage sites can be quantified by using the measured eigenvalues. In this chapter, a structural damage quantification method is proposed using only the first order sensitivity terms in the Taylor's expansion. A linear sequential filtering technique is used to relate the analytical and experimental sets of eigenvalues including the measurement noise matrix. Optimum solution of the damage extent is obtained from an unbiased minimum variance error estimation method (Law and Li, 1993). The formulation has the capability to estimate a larger set of eigenvalues from a smaller set of measured eigenvalues. Weight linear least squares method is used to solve the identification equation. Numerical examples on the damage quantification method using first order analysis are conducted on the same three-storey plane frame described in Chapter 3.

4.2 Theory

The equation of motion of an undamped n-degrees-of-freedom structural dynamic system can be expressed as

$$K\Phi = M\Phi\Lambda \tag{4.1}$$

where K and M are the system stiffness and mass matrices and Λ is the diagonal eigenvalue matrix of λ_k; Φ is the matrix of eigenvector of the system. For a small perturbation in the stiffness and mass matrices of the system, the dynamic system in Eqt.(4.1) becomes

$$[(K+\Delta K)-(\lambda_k+\Delta\lambda_k)(M+\Delta M)](\Phi_k+\Delta\Phi_k)=0 \tag{4.2}$$

where the Δ terms represent the perturbations. When the structural perturbations and the corresponding characteristic changes are small, the higher order terms can be neglected, and the first-order perturbation gives the usual sensitivity of the eigenvalues as

$$\Delta\lambda_k = \frac{\Phi_k{}^T(\Delta K - \lambda_k \Delta M)\Phi_k}{\Phi_k{}^T M \Phi_k} \tag{4.3}$$

which relates the change of eigenvalue with the change in the stiffness and mass of the system.

Considering the orthogonal condition $\Phi_k{}^T M\Phi_k = 1$, and for the most general case where a damage in a structural system only involves a change in the stiffness, Eqt.(4.3) becomes

$$\Delta\lambda_k = \Phi_k{}^T \Delta K \Phi_k \tag{4.4}$$

Structural faults will cause changes to several elemental stiffness matrices K_i in general. In the present study, the fractional change of the stiffness matrix is represented by a damage coefficient C_i

$$\Delta K = \sum_{i=1}^{N} C_i K_i \tag{4.5}$$

where $0 \geq C_i \geq -1.0$ and N is the total number of damage elements in the structural system.

Expanding the change in eigenvalue as a Taylor's series and neglecting the higher order terms, we have

$$\Delta\lambda_k = \sum_{i=1}^{N} \frac{\partial \lambda_k}{\partial K_i} \Delta K_i \tag{4.6}$$

where

$$\frac{\partial \lambda_k}{\partial K_i} = \Phi_k{}^T \frac{\partial K}{\partial K_i} \Phi_k \tag{4.7}$$

4.2.1 Identification Equation

Substituting Eqt.(4.7) into Eqt.(4.6) and rewriting in a matrix form for L number of eigenvalues, we have

$$\begin{Bmatrix} \Delta\lambda_1 \\ \Delta\lambda_2 \\ \vdots \\ \vdots \\ \Delta\lambda_L \end{Bmatrix} = \begin{bmatrix} \Phi_1^T K_1 \Phi_1 & \Phi_1^T K_2 \Phi_1 & \cdots & \cdots & \Phi_1^T K_N \Phi_1 \\ \Phi_2^T K_1 \Phi_2 & \Phi_2^T K_2 \Phi_2 & \cdots & \cdots & \Phi_2^T K_N \Phi_2 \\ \cdots & \cdots & \cdots & \cdots & \cdots \\ \cdots & \cdots & \cdots & \cdots & \cdots \\ \Phi_L^T K_1 \Phi_L & \Phi_L^T K_2 \Phi_L & \cdots & \cdots & \Phi_L^T K_N \Phi_L \end{bmatrix} \begin{Bmatrix} C_1 \\ C_2 \\ \vdots \\ \vdots \\ C_N \end{Bmatrix} \tag{4.8}$$

Rearranging in a matrix form, we have the identification equation on the damage coefficient vector C.

$$\Delta\lambda = AC \tag{4.9}$$

This is the most general equation used by many researchers to relate the change in eigenvalues with respect to the damage coefficients with an analytical model. Considering the practical case of having incomplete measured eigenvalues and the existence of measurement noise, the measurement state of the problem can be expressed in terms of the analytical change of eigenvalues as

$$\Delta\bar{\lambda} = D\Delta\lambda + w \tag{4.10}$$

where D is the measurement matrix; w is a random noise vector; $\Delta\bar{\lambda}$ and $\Delta\lambda$ are the vectors of measured and analytical eigenvalues respectively.

4.2.2 Optimal Solution of the Identification Equation

A linear unbiased minimum variance estimation method is used for an optimal solution on Eqts.(4.9) and (4.10). The measurement matrix D is assumed available.

A linear sequential filter of the following form (Sage and White, 1977) is used for the estimation.

$$\Delta\hat{\lambda} = Q\hat{C} + P\Delta\bar{\lambda} \tag{4.11}$$

where $\hat{C}$ is the estimated vector on C; $\Delta\hat{\lambda}$ and $\Delta\bar{\lambda}$ are the last estimated value and the measured value of $\Delta\lambda$ respectively; and P is the gain matrix. It is noted that Eqt.(4.11) enables the use of a smaller number of measured $\Delta\bar{\lambda}$ to estimate a larger number of $\Delta\hat{\lambda}$ which can then be used to estimate the vector C.

The optimal estimation requires

$$E(\hat{C}) = C, \qquad E(\Delta\hat{\lambda}) = \Delta\lambda \tag{4.12}$$

Substituting Eqts.(4.9), (4.10) and (4.12) into Eqt.(4.11), the expected value of $\Delta\hat{\lambda}$ becomes

$$E\left(\Delta\hat{\lambda}\right) = (Q + PDA)C \tag{4.13}$$

with $E(w)$ equals to zero for an assumed white noise distribution. Comparing Eqt.(4.9) with Eqt.(4.13) shows that the necessary condition for Eqt.(4.9) to have an optimal unbiased solution is

$$A = Q + PDA \tag{4.14}$$

4.2.3 The Gain Matrix *P*

Substituting Eqt.(4.14) into Eqt.(4.11) gives the unbiased estimated $\Delta\hat{\lambda}$ as

$$\Delta\hat{\lambda} = A\hat{C} + P(\Delta\overline{\lambda} - DA\hat{C}) \tag{4.15}$$

The errors in the eigenvalue change and coefficient C are defined as

$$\Delta\tilde{\lambda} = \Delta\lambda - \Delta\hat{\lambda}, \qquad \tilde{C} = C - \hat{C} \tag{4.16}$$

Substituting Eqts.(4.9), (4.10) and (4.15) into Eqt.(4.16), we have

$$\Delta\tilde{\lambda} = (A - PDA)\tilde{C} - Pw \tag{4.17}$$

The variance of error $\Delta\tilde{\lambda}$ can be derived as

$$E(\Delta\tilde{\lambda}\Delta\tilde{\lambda}^T) = \overline{A} - \overline{A}D^TP^T - PD\overline{A} + P\overline{D}P^T + PE(ww^T)P^T \tag{4.18}$$

where

$$\overline{A} = AE(\tilde{C}\tilde{C}^T)A^T, \quad \overline{D} = D\overline{A}D^T \tag{4.19}$$

which are symmetrical matrices

The minimum variance in the error $\Delta\tilde{\lambda}$ corresponds to the smallest value in $tr\left[E(\Delta\tilde{\lambda}\Delta\tilde{\lambda}^T)\right]$, where $tr[\bullet]$ denotes the trace operation, i.e.

$$\frac{d\ tr\left[E(\Delta\tilde{\lambda}\Delta\tilde{\lambda}^T)\right]}{dP} = 0 \tag{4.20}$$

Substituting Eqt.(4.18) into Eqt.(4.20)

$$\frac{d\ tr\left[E(\Delta\tilde{\lambda}\Delta\tilde{\lambda}^T)\right]}{dP} = 2P(\overline{D}+R) - 2\overline{A}D^T = 0 \tag{4.21}$$

we have

$$P = (\overline{A}D^T)(\overline{D}+R)^{-1} \tag{4.22}$$

where R equals to $E(ww^T)$ and is the variance matrix of the noise. Eqt.(4.22) gives the optimal gain matrix P, which when substituting into Eqt.(4.15) gives an unbiased estimate of $\Delta\lambda$.

4.2.4 Estimation of Coefficient C

The estimated vector $\Delta\hat{\lambda}$ is then used to estimate the coefficient vector $\hat{C}$ using the weight linear least squares method from Eqt.(4.9).

$$\hat{C} = (A^T\overline{W}A)^{-1}A^T\overline{W}\Delta\hat{\lambda} \tag{4.23}$$

where $\overline{W}$ is the weight matrix on the measured data.

The variance of error in the coefficient C is then given by

$$E(\tilde{C}\tilde{C}^T) = (C-\hat{C})(C-\hat{C})^T \tag{4.24}$$

4.3 Procedure of Implementation

The linear sequential filter is implemented as follows in the identification problem.

Step 1 : Perform the dynamic analysis of the structure to obtain the system matrices and the eigen-parameters.

Step 2 : Calculate the sensitivity matrix A from Eqt.(4.8)

Step 3 : Calculate the matrices $\overline{A}$ and $\overline{D}$ from Eqt.(4.19) with an initial variance matrix $E\left(\tilde{C}\tilde{C}^T\right)$.

Step 4 : Calculate the gain matrix P from Eqt.(4.22) with an assumed variance matrix R.

Step 5 : Calculate the variance of $\Delta\tilde{\lambda}$, $E\left(\Delta\tilde{\lambda}\Delta\tilde{\lambda}^T\right)$, from Eqt.(4.18).

Step 6 : Calculate $\Delta\hat{\lambda}$ from Eqt.(4.15) using the measured $\Delta\overline{\lambda}$ and an initial vector $\hat{C}$.

Step 7 : Calculate the coefficient vector $\hat{C}_i$ for the i-th iteration from Eqt.(4.23) with an assumed weight matrix $\overline{W}$.

Step 8 : Calculate the variance matrix $E\left(\tilde{C}\tilde{C}^T\right)$ from Eqt.(4.24).

Step 9 : Compare $\hat{C}$ and $\hat{C}_i$.

If the difference is larger than a prescribed value, set $\hat{C} = \hat{C}_i$ and go to Step 3 until the difference converges.

4.4 Numerical Examples

A symmetric three-storey plane frame described in Section 3.3 is used to illustrate the damage quantification method using first order analysis. The damage scenarios with small or large damages are the same for the damage localization method mentioned in Section 3.3.3. The eigenvalues are obtained from the analytical finite element model with and without damages for each damage scenario. The ratio of the eigenvalue change to the eigenvalue for each mode is computed and the mode numbers are re-arranged with this ratio in descending order. The variance matrix R, the weight matrix $\overline{W}$ and the variance matrix on the error in the damage coefficient C, $E\left(\tilde{C}\tilde{C}^T\right)$, have been set equal to the identity matrix I and the criteria of convergence in $\hat{C}_i$ is set equal to 0.1% of the last computed value. The noise levels for the eigenvalue and mode shape are assumed to be 0.15% and 3% respectively. The eigenvalues and mode shapes with noise effect are calculated by the method described in Section 3.3.5.

The formulation has the capability to expand the eigenvalue from a smaller measured set to a larger set.

4.4.1 Damage Quantification without Eigenvalue Expansion

The first eight modes with the largest eigenvalue change ratio are shown in Table 4.1 and 4.2 for the small and large damage scenarios respectively.

4.4.1.1 For small damages

The identified results with the actual damage elements in the suspected element group only are shown in Table 4.3. The results show that the damage extent can be quantified correctly whether the results are contaminated by noise or not. Besides, the estimated damage extent without noise effect is more accurate than that with noise effect. Fortunately, the error without and with noise is less than 5% and 6% respectively.

In practice, the number of the suspected damage elements may be greater than the number of the actual damage elements. Then, the suspected element group is expanded to include other undamaged elements as identified in Chapter 3 and the true C value of the undamaged element is zero. The results for different damage scenarios are shown in Tables 4.4 to 4.6.

From Tables 4.4 and 4.5, the results show that the damage extent of the suspected group of elements can be estimated accurately for damage scenarios S1 and S2. Their errors are less than 4% and 7% respectively. The damage extent of the elements in scenario S3 can be estimated with a maximum error of 9%. However, the undamaged element 40 is incorrectly identified to have a damage. The damage extent of this element is just smaller than that of the damage element 39. This is because the undamaged element 40 is just adjacent to the damage element 39, and adjacent elements would naturally exhibit some damage characteristics as they are sharing the same measured mode shapes at the adjacent connecting nodes. From Tables 4.4 to

4.6, the estimated results without noise effect are more accurate than those with noise effect.

4.4.1.2 For large damages

Table 4.7 shows the damage quantification results for large damages with the actual damage elements in the suspected element group only. The results show that the damage extent cannot be estimated correctly for both single or multiple damages when only the actual damage element is included in the suspected element group. This is because the behaviour of the structure is no longer linear with damage when the damage is large, and this method only includes the linear part of the Taylor's expansion. Therefore, this damage quantification method using first order analysis is not suitable for large damage identification.

4.4.2 Damage Quantification with Eigenvalue Expansion

There is an advantage in this damage quantification method where a smaller set of measured eigenvalues can be expanded to a larger set of eigenvalues. In this section, the first five modes with the largest eigenvalue change ratio are expanded into eight modes. The re-arranged mode numbers used are the same as that in Section 4.4.1 and shown in Tables 4.1 and 4.2 for small and large damage scenarios respectively.

4.4.2.1 For small damages

Table 4.8 shows the identified results with the actual damage elements in the set of the suspected elements. From this table, it is found that the damage extent of the actual damage elements can be determined correctly with less than 7% error. The estimated damage extent without noise effect has better performance than that with noise effect. By comparing Tables 4.3 and 4.8, the results from the case without eigenvalue expansion are more accurate than those with eigenvalue expansion when the information is contaminated by measurement noise or not. This is due to the more commonly known errors in the expansion process.

The damage quantification results with inclusion of some additional undamaged elements in the suspected element group are shown in Tables 4.9 to 4.11 for different small damage scenarios. For damage scenarios S1 and S2, the damage extent of the suspected element group can be determined accurately with or without noise effect. From Tables 4.9 and 4.10, the errors in damage scenarios S1 and S2 are less than 5% and 8% respectively. For damage scenario S3, the damage extent of the suspected element group can be estimated, and the error is less than 11% (see Table 4.11). However, the undamaged element 40 is estimated to have a stiffness damage and its extent is similar to that of the damage element 39. Reason of this has been explained in Section 4.4.1.1. From Tables 4.9 to 4.11, it is noted that the identified results without noise effect are more accurate than those with noise effect. By comparing Tables 4.4 to 4.6 and 4.9 to 4.11, the estimation without eigenvalue expansion is better than that with eigenvalue expansion.

4.4.3 Stability Analysis

In the above studies, the initial vector $\hat{C}$ has been set to the true values. However, the true damage coefficient C of each element is unknown. In this study, the initial vector $\hat{C}$ is an arbitrary vector and its components are assumed to be equal in this study. Since the estimation without eigenvalue expansion gives more accurate results than that with eigenvalue expansion, the method without eigenvalue expansion is used for this stability study. The importance of the initial value of $\hat{C}$ to the damage assessment is further studied in damage scenario S3 with five suspected elements. The estimation is performed using different initial vector $\hat{C}$ with its components all equal. The initial vector $\hat{C}$ ranges from -0.01 to -0.1 with 0.01 increments. The same final vector $\hat{C}$ is obtained from different initial vector $\hat{C}$ with less than 9% error, and the results with noise effect are shown in Table 4.12. This indicates that the proposed method is independent of the initial vector $\hat{C}$.

4.5 Conclusions

A structural damage quantification method based on the first order terms of the Taylor's expansion is proposed. A linear sequential filtering technique and an unbiased minimum error estimation method is used in the formulation. A weight linear least squares method is used to solve the identification equation. An eigenvalue expansion is allowed for this method. The effectiveness and accuracy in the identification for small and large damages are studied. Numerical simulations on damage assessment with a three-storey plane frame show that this method is effective and gives an accurate result for small damages. The damage extent of the suspected element group can be estimated correctly with or without noise effect. However, the estimation is not suitable for large damages. In general, the method without eigenvalue expansion has better performance than that with eigenvalue expansion due to the error in the expansion process. And the final results from this method are checked independent of the initial vector $\hat{C}$.

Table 4.1 - The first eight re-arranged mode numbers for small damage scenarios

Damage Scenario	Re-arranged Mode Numbers
S1	10, 11, 7, 5, 9, 12, 3, 8
S2	13, 11, 15, 14, 5, 12, 6 ,1
S3	12, 9, 7, 10, 14, 8, 5, 13

Table 4.2 - The first eight re-arranged mode numbers for large damage scenarios

Damage Scenario	Re-arranged Mode Numbers
L1	10, 11, 7, 5, 9, 12, 3, 8
L2	13, 11, 5, 4, 6, 1, 12 ,10
L3	12, 13,10, 9, 7, 5, 4, 8

Table 4.3 - Damage quantification results for small damages with actual damage elements in the suspected element group only (without eigenvalue expansion)

Damage Scenario	S1	S2		S3		
Element No.	45	17	32	9	13	39
True Damage Extent, C	-0.05	-0.05	-0.03	-0.02	-0.03	-0.03
Estimated C	-0.0506	-0.0487	-0.0311	-0.0210	-0.0309	-0.0303
Error	1.2%	2.6%	3.7%	5.0%	3.0%	1.0%
Estimated C_{noise}	-0.0511	-0.0478	-0.0315	-0.0212	-0.0310	-0.0305
Error $_{noise}$	2.2%	4.4%	5.0%	6.0%	3.3%	1.7%

Subscript $_{noise}$ denotes results from polluted measurements

Table 4.4 - Damage quantification results for damage scenario S1 (without eigenvalue expansion)

Element No.	25	44	45
True Damage Extent, C	0	0	-0.05
Estimated C	0.0001	0.0002	-0.0513
Error	-	-	2.6%
Estimated C_{noise}	0.0001	0.0002	-0.0520
Error $_{noise}$	-	-	4.0%

Table 4.5 - Damage quantification results for damage scenario S2 (without eigenvalue expansion)

Element No.	17	31	32
True Damage Extent, C	-0.05	0	-0.03
Estimated C	-0.0482	0.0103	-0.0313
Error	3.6%	-	4.3%
Estimated C_{noise}	-0.0474	0.0107	-0.0320
Error $_{noise}$	5.2%	-	6.7%

Table 4.6 - Damage quantification results for damage scenario S3 (without eigenvalue expansion)

Element No.	9	13	25	39	40
True Damage Extent, C	-0.02	-0.03	0	-0.03	0
Estimated C	-0.0215	-0.0316	0.0082	-0.0278	-0.0227
Error	7.5%	5.3%	-	7.3%	-
Estimated C_{noise}	-0.0218	-0.0321	0.0093	-0.0275	-0.0238
Error $_{noise}$	9.0%	7.0%	-	8.3%	-

Table 4.7 - Damage quantification results for large damages with actual damage elements in the suspected element group only (without eigenvalue expansion)

Damage Scenario	L1	L2		L3		
Element No.	45	17	32	9	13	39
True Damage Extent, C	-0.3	-0.3	-0.2	-0.15	-0.2	-0.2
Estimated C	-0.4178	-0.9308	-0.2144	-0.3473	-0.1807	-0.2064
Error	39.3%	210.3%	7.2%	131.5%	9.7%	3.2%
Estimated C_{noise}	-0.4275	-0.9349	-0.2145	-0.3497	-0.1810	-0.2072
Error $_{noise}$	42.5%	211.6%	7.3%	133.1%	9.5%	3.6%

Table 4.8 - Damage quantification results for small damages with actual damage elements in the suspected element group only (with eigenvalue expansion)

Damage Scenario	S1	S2		S3		
Element No.	45	17	32	9	13	39
True Damage Extent, C	-0.05	-0.05	-0.03	-0.02	-0.03	-0.03
Estimated C	-0.0510	-0.0486	-0.0314	-0.0212	-0.0311	-0.0304
Error	2.0%	2.8%	4.7%	6.0%	3.7%	1.3%
Estimated C_{noise}	-0.0516	-0.0477	-0.0319	-0.0213	-0.0317	-0.0308
Error $_{noise}$	3.2%	4.6%	6.3%	6.5%	5.7%	2.7%

Table 4.9 - Damage quantification results for damage scenario S1 (with eigenvalue expansion)

Element No.	25	44	45
True Damage Extent, C	0	0	-0.05
Estimated C	0.0002	0.0004	-0.0516
Error	-	-	3.2%
Estimated C_{noise}	0.0002	0.0004	-0.0525
Error $_{noise}$	-	-	5.0%

Table 4.10 - Damage quantification results for damage scenario S2 (with eigenvalue expansion)

Element No.	17	31	32
True Damage Extent, C	-0.05	0	-0.03
Estimated C	-0.0479	0.0121	-0.0318
Error	4.2%	-	6.0%
Estimated C_{noise}	-0.0472	0.0129	-0.0322
Error $_{noise}$	5.6%	-	7.3%

Table 4.11 - Damage quantification results for damage scenario S3 (with eigenvalue expansion)

Element No.	9	13	25	39	40
True Damage Extent, C	-0.02	-0.03	0	-0.03	0
Estimated C	-0.0182	-0.0323	0.0086	-0.0276	-0.0228
Error	9.0%	7.7%	-	8.0%	-
Estimated C_{noise}	-0.0179	-0.0328	0.0099	-0.0272	-0.0240
Error $_{noise}$	10.5%	9.3%	-	9.3%	-

Table 4.12 - Damage quantification results for damage scenario S3 in stability analysis (without eigenvalue expansion)

Element No.	9	13	25	39	40
True Damage Extent, C	-0.02	-0.03	0	-0.03	0
Estimated C_{noise}	-0.0218	-0.0321	0.0093	-0.0275	-0.0238
Error $_{noise}$	9.0%	7.0%	-	8.3%	-

Chapter 5

Damage Quantification Method using Second Order Analysis

5.1 Introduction

The damage quantification method using first order analysis has been shown not suitable for large damages in Chapter 4. The higher order terms in the Taylor's expansion are required to take into account of the non-linear changes. Terms above second order are numerically small and it is computational expensive if they are included in the formulation. Therefore, a damage quantification method using the second order terms in the Taylor's expansion is proposed. The same linear sequential filtering technique and unbiased minimum variance error estimation method (Law and Li, 1993) are use to formulate the identification equation, and weight linear least squares method is used to solve the identification equation. The formulation generates two necessary conditions for the optimal solution. The solution procedure would be similar to that presented in Chapter 4. Numerical examples on the damage quantification method using second order analysis would also be based on the same three-storey plane frame described in Chapter 3.

5.2 Theory

For the sake of clarity in the development of the theory, some of the steps given in Section 4.2 are repeated below.

The equation of motion of an undamped *n*-degrees-of-freedom structural dynamic system can be expressed as

$$K\Phi = M\Phi\Lambda \tag{5.1}$$

where K and M are the system stiffness and mass matrices and Λ is the diagonal eigenvalue matrix of λ_k; Φ is the matrix of eigenvector of the system. For a small perturbation in the stiffness and mass matrices of the system, the dynamic system in Eqt.(5.1) becomes

$$[(K+\Delta K)-(\lambda_k+\Delta\lambda_k)(M+\Delta M)](\Phi_k+\Delta\Phi_k)=0 \tag{5.2}$$

where the Δ terms represent the perturbations. When the structural perturbations and the corresponding characteristic changes are small, the higher order terms can be neglected, and the first-order perturbation gives the usual sensitivity of the eigenvalues as

$$\Delta\lambda_k = \frac{\Phi_k{}^T(\Delta K - \lambda_k \Delta M)\Phi_k}{\Phi_k{}^T M \Phi_k} \tag{5.3}$$

which relates the change of eigenvalue with the change in the stiffness and mass of the system.

Considering the orthogonal condition $\Phi_k^T M \Phi_k = 1$, and for the most general case where a damage in a structural system only involves a change in the stiffness, Eqt.(5.3) becomes

$$\Delta\lambda_k = \Phi_k^T \Delta K \Phi_k \tag{5.4}$$

Structural faults will cause changes to several elemental stiffness matrices K_i in general. In the present study, the fractional change of the stiffness matrix is represented by a damage coefficient C_i

$$\Delta K = \sum_{i=1}^{N} C_i K_i \tag{5.5}$$

where $0 \geq C_i \geq -1.0$ and N is the total number of damage elements in the structural system.

Expanding the change in eigenvalue as a Taylor's series and neglecting the terms above second order, we have

$$\Delta\lambda_k = \sum_{i=1}^{N} \frac{\partial\lambda_k}{\partial K_i}\Delta K_i + \sum_{i=1}^{N}\sum_{j=1}^{N} \frac{1}{2}\frac{\partial^2\lambda_k}{\partial K_i \partial K_j}\Delta K_i \Delta K_j \tag{5.6}$$

where

$$\frac{\partial\lambda_k}{\partial K_i} = \Phi_k^T \frac{\partial K}{\partial K_i}\Phi_k \tag{5.7}$$

$$\frac{\partial^2\lambda_k}{\partial K_i \partial K_j} = \Phi_k^T \left(\frac{\partial K}{\partial K_i} - \frac{\partial\lambda_k}{\partial K_i} M\right)\frac{\partial\Phi_k}{\partial K_j} + \Phi_k^T \left(\frac{\partial K}{\partial K_j} - \frac{\partial\lambda_k}{\partial K_j} M\right)\frac{\partial\Phi_k}{\partial K_i} \tag{5.8}$$

The derivative of eigenvector with respect to the stiffness of the i-th element has been obtained from Rudisill (1974) as

$$\frac{\partial \Phi_k}{\partial K_i} = H_k \left(\frac{\partial K}{\partial K_i} - \Phi_k{}^T \frac{\partial K}{\partial K_i} \Phi_k M \right) \Phi_k \tag{5.9}$$

where

$$H_k = -J_k{}^{-1} [K - \lambda_k M] \tag{5.10}$$

$$J_k = \begin{bmatrix} K - \lambda_k M & 2M\Phi_k \end{bmatrix} \begin{bmatrix} K - \lambda_k M \\ 2\Phi_k{}^T M \end{bmatrix} \tag{5.11}$$

5.2.1 Identification Equation

Substituting Eqts.(5.7) to (5.11) into Eqt.(5.6), the change in eigenvalue becomes

$$\begin{aligned} \Delta\lambda_k = & \sum_{i=1}^{N} \Phi_k{}^T C_i K_i \Phi_k + \\ & \sum_{i=1}^{N} \sum_{j=1}^{N} C_i \left[\frac{1}{2} \Phi_k{}^T \left(K_i - \Phi_k{}^T K_i \Phi_k M \right) H_k \left(K_j - \Phi_k{}^T K_j \Phi_k M \right) \Phi_k + \right. \\ & \left. \frac{1}{2} \Phi_k{}^T \left(K_j - \Phi_k{}^T K_j \Phi_k M \right) H_k \left(K_i - \Phi_k{}^T K_i \Phi_k M \right) \Phi_k \right] C_j \end{aligned} \tag{5.12}$$

and rewriting in a matrix form, we have the identification equation on the damage coefficient vector C.

$$\Delta\lambda_k = A_k C + C^T G C \tag{5.13}$$

where

$$A_k = \left[\Phi_k^T K_1 \Phi_k \quad \Phi_k^T K_2 \Phi_k \quad \cdots \cdots \quad \Phi_k^T K_N \Phi_k\right] \tag{5.14}$$

$$C = \begin{Bmatrix} C_1 \\ C_2 \\ \vdots \\ \vdots \\ C_N \end{Bmatrix} \tag{5.15}$$

and G is an N × N symmetrical matrix with

$$\left[G_{ij}\right]_k = \frac{1}{2}\Phi_k{}^T\left[\left(K_i - \Phi_k{}^T K_i \Phi_k M\right)H_k\left(K_j - \Phi_k{}^T K_j \Phi_k M\right) + \left(K_j - \Phi_k{}^T K_j \Phi_k M\right)H_k\left(K_i - \Phi_k{}^T K_i \Phi_k M\right)\right]\Phi_k \tag{5.16}$$

Eqt.(5.13) is the identification equation but it is non-linear in C. To overcome this problem, the quadratic term C^TGC is expanded in a series about C_0, and the first two terms are taken to become

$$C^T GC = 2C_0{}^T GC - C_0{}^T GC_0 \tag{5.17}$$

where C_0 is the initial value of C.

Substituting Eqt.(5.17) into Eqt.(5.13), we have the identification equation linearized in C as

$$\Delta\lambda_k = \left(A + 2C_0^T G\right)C - C_0^T G C_0 \tag{5.18}$$

which is valid for every eigenvalue of the system. For L number of eigenvalues, we have

$$\begin{Bmatrix} \Delta\lambda_1 \\ \Delta\lambda_2 \\ \vdots \\ \vdots \\ \Delta\lambda_L \end{Bmatrix} = \left(\begin{bmatrix} A_1 \\ A_2 \\ \vdots \\ \vdots \\ A_L \end{bmatrix} + 2 \begin{bmatrix} C_0^T G_1 \\ C_0^T G_2 \\ \vdots \\ \vdots \\ C_0^T G_L \end{bmatrix} \right) C - \begin{bmatrix} C_0^T G_1 \\ C_0^T G_2 \\ \vdots \\ \vdots \\ C_0^T G_L \end{bmatrix} C_0 \tag{5.19}$$

Rearranging in a matrix form, the identification equation on the damage coefficient vector C becomes

$$\begin{aligned} \Delta\lambda &= \left(A + 2B\right)C - BC_0 \\ &= FC - BC_0 \end{aligned} \tag{5.20}$$

where

$$F = A + 2B \tag{5.21}$$

$$\Delta\lambda = \begin{Bmatrix} \Delta\lambda_1 \\ \Delta\lambda_2 \\ \vdots \\ \vdots \\ \Delta\lambda_L \end{Bmatrix}, \qquad C = \begin{Bmatrix} C_1 \\ C_2 \\ \vdots \\ \vdots \\ C_N \end{Bmatrix}, \qquad C_0 = \begin{Bmatrix} C_{10} \\ C_{20} \\ \vdots \\ \vdots \\ C_{N0} \end{Bmatrix} \tag{5.22}$$

$$A = \begin{Bmatrix} \Phi_1^T K_1 \Phi_1 & \Phi_1^T K_2 \Phi_1 & \cdots & \cdots & \Phi_1^T K_N \Phi_1 \\ \Phi_2^T K_1 \Phi_2 & \Phi_2^T K_2 \Phi_2 & \cdots & \cdots & \Phi_2^T K_N \Phi_2 \\ \cdots & \cdots & \cdots & \cdots & \cdots \\ \cdots & \cdots & \cdots & \cdots & \cdots \\ \Phi_L^T K_1 \Phi_L & \Phi_L^T K_2 \Phi_L & \cdots & \cdots & \Phi_L^T K_N \Phi_L \end{Bmatrix}_{L \times N} \tag{5.23}$$

$$B = \begin{Bmatrix} C_0^T G_1 \\ C_0^T G_2 \\ \vdots \\ \vdots \\ C_0^T G_L \end{Bmatrix}_{L \times N} \tag{5.24}$$

Considering the practical case of having incomplete measured eigenvalues and the existence of measurement noise, the measurement state of the problem can be expressed in terms of the analytical change of eigenvalues as

$$\Delta\bar{\lambda} = D\Delta\lambda + w \tag{5.25}$$

where D is the measurement matrix; w is a random noise vector; $\Delta\bar{\lambda}$ and $\Delta\lambda$ are the vectors of measured and analytical eigenvalues respectively.

5.2.2 Optimal Solution of the Identification Equation

A linear unbiased minimum variance estimation method is used for an optimum solution on Eqts (5.20) and (5.25). The measurement matrix D and matrices F and B are assumed available.

A linear sequential filter of the following form (Sage and White, 1977) is used for the estimation.

$$\Delta\hat{\lambda} = Q\hat{C} + P\Delta\bar{\lambda} \tag{5.26}$$

where $\hat{C}$ is the estimated vector on C; $\Delta\hat{\lambda}$ and $\Delta\bar{\lambda}$ are the last estimated value and the measured value of $\Delta\lambda$ respectively; and P is the gain matrix. It is noted that Eqt.(5.26) enables the use of a smaller number of measured $\Delta\bar{\lambda}$ to estimate a larger number of $\Delta\hat{\lambda}$ which can then be used to estimate the vector C.

The optimal estimation requires

$$E(\hat{C}) = C, \qquad E(\Delta\hat{\lambda}) = \Delta\lambda \tag{5.27}$$

Substituting Eqts.(5.20), (5.25) and (5.27) into Eqt.(5.26), the expected value of $\Delta\hat{\lambda}$ becomes

$$E\left(\Delta\hat{\lambda}\right) = (Q + PDF)C - PDBC_0 \tag{5.28}$$

with $E(w)$ equals to zero for an assumed white noise distribution. Comparing Eqt.(5.20) with Eqt.(5.28) shows that the necessary conditions for Eqt.(5.20) to have an optimal unbiased solution are

$$\begin{aligned} &F = Q + PDF \quad \textit{and} \\ &B = PDB \quad \textit{or} \quad PD = I \end{aligned} \tag{5.29}$$

5.2.3 The Gain Matrix P from the First Condition Only

The gain matrix P takes up different form with the use of either the first condition or both conditions in Eqt.(5.29). Substituting the first condition in Eqt.(5.29) into Eqt.(5.26) gives the unbiased estimated $\Delta\hat{\lambda}$ as follow

$$\Delta\hat{\lambda} = F\hat{C} + P(\Delta\bar{\lambda} - DF\hat{C}) \tag{5.30}$$

The errors in the eigenvalue change and coefficient C are defined as

$$\Delta\tilde{\lambda} = \Delta\lambda - \Delta\hat{\lambda}, \qquad \tilde{C} = C - \hat{C} \tag{5.31}$$

Substituting Eqts.(5.20), (5.25) and (5.30) into Eqt.(5.31), we have

$$\Delta\tilde{\lambda} = (F - PDF)\tilde{C} - BC_0 + PDBC_0 - Pw \tag{5.32}$$

The variance of error $\Delta\tilde{\lambda}$ can be derived as

$$E(\Delta\tilde{\lambda}\Delta\tilde{\lambda}^T) = \bar{F} - \bar{F}D^T P^T - PD\bar{F} + P\bar{D}P^T + \bar{B} - \bar{B}D^T P^T - PD\bar{B} + PD\bar{B}D^T P^T + PE\left(ww^T\right)P^T \tag{5.33}$$

where

$$\bar{B} = BC_0 C_0{}^T B^T, \quad \bar{F} = FE(\tilde{C}\tilde{C}^T)F^T \quad and \quad \bar{D} = D\bar{F}D^T \tag{5.34}$$

which are symmetrical matrices

The minimum variance in the error $\Delta\tilde{\lambda}$ corresponds to the smallest value in $tr\left[E(\Delta\tilde{\lambda}\Delta\tilde{\lambda}^T)\right]$, where $tr[\bullet]$ denotes the trace operation, i.e.

$$\frac{d\ tr\left[E(\Delta\tilde{\lambda}\Delta\tilde{\lambda}^T)\right]}{dP} = 0 \tag{5.35}$$

Substituting Eqt.(5.33) into Eqt.(5.35)

$$\frac{d\ tr\left[E(\Delta\tilde{\lambda}\Delta\tilde{\lambda}^T)\right]}{dP} = 2P(D\bar{B}D^T + \bar{D} + R) - 2\bar{B}D^T - 2\bar{F}D^T = 0 \tag{5.36}$$

we have

$$P = (\bar{B}D^T + \bar{F}D^T)(D\bar{B}D^T + \bar{D} + R)^{-1} \tag{5.37}$$

where R equals to $E(ww^T)$ and is the variance matrix of the noise. Eqt.(5.37) gives the optimal gain matrix P, which when substituting into Eqt.(5.30) gives an unbiased estimate of $\Delta\lambda$.

5.2.4 The Gain Matrix P from both the First and Second Conditions

Note that Eqt.(5.37) gives the optimal gain matrix P for the first condition in Eqt.(5.29). When the second condition in Eqt.(5.29) is also included into Eqt.(5.32), we get another eigenvalue change error $\Delta\tilde{\lambda}$ as

$$\Delta\tilde{\lambda} = (F - PDF)\tilde{C} - Pw \tag{5.38}$$

The variance of error $\Delta\tilde{\lambda}$ and the gain matrix P are simplified as

$$E(\Delta\tilde{\lambda}\Delta\tilde{\lambda}^T) = \bar{F} - \bar{F}D^T P^T - PD\bar{F} + P\bar{D}P^T + PE(ww^T)P^T \tag{5.39}$$

$$P = \bar{F}D^T(\bar{D} + R)^{-1} \tag{5.40}$$

5.2.5 Estimation of Coefficient *C*

The estimated vector $\Delta\hat{\lambda}$ is then used to estimate the coefficient vector $\hat{C}$ using the weight linear least squares method from Eqt.(5.20).

$$\hat{C} = (F^T \overline{W} F)^{-1} F^T \overline{W} (\Delta\hat{\lambda} + BC_0) \tag{5.41}$$

where $\overline{W}$ is the weight matrix on the measured data.

The variance of error in the coefficient C is then given by

$$E(\tilde{C}\tilde{C}^T) = (C - \hat{C})(C - \hat{C})^T \tag{5.42}$$

5.3 Procedure of Implementation

The linear sequential filter is implemented as follows in the identification problem.

Step 1 : Perform the dynamic analysis of the structure to obtain the system matrices and the eigen-parameters.

Step 2 : Calculate the sensitivity matrix A and the matrix G from Eqt.(5.23) and Eqt.(5.16) respectively.

Step 3 : Calculate the matrices B and F from Eqt.(5.24) and Eqt.(5.21) respectively with an initial vector C_0.

Step 4 : Calculate the matrix $\overline{B}$ from Eqt.(5.34) with an initial vector C_0.

Step 5 : Calculate the matrices $\overline{F}$ and $\overline{D}$ from Eqt.(5.34) with an initial variance matrix $E\left(\tilde{C}\tilde{C}^T\right)$.

Step 6 : Calculate the gain matrix P from Eqt.(5.37) and Eqt.(5.40) for using the first condition only and using both conditions respectively with an assumed variance matrix R.

Step 7 : Calculate the variance of $\Delta\tilde{\lambda}$, $E\left(\Delta\tilde{\lambda}\Delta\tilde{\lambda}^T\right)$, from Eqt.(5.33) and Eqt.(5.39) for using the first condition only and using both conditions respectively.

Step 8 : Calculate the vector $\Delta\hat{\lambda}$ from Eqt.(5.30) using the measured $\Delta\overline{\lambda}$ and an initial vector $\hat{C}$.

Step 9 : Calculate the coefficient vector $\hat{C}_i$ for the i-th iteration from Eqt.(5.41) with an assumed weight matrix $\overline{W}$.

Step 10 : Calculate the variance matrix $E\left(\tilde{C}\tilde{C}^T\right)$ from Eqt.(5.42).

Step 11 : Compare $\hat{C}$ and $\hat{C}_i$.

If the difference is larger than a prescribed value, set $\hat{C} = \hat{C}_i$ and go to Step 5 until the difference converges.

Otherwise, go to Step 12.

Step 12 : Compare C_0 and $\hat{C}_i$.

If the difference is larger than a prescribed value, set $C_0 = \hat{C}_i$ and go to Step 3 until the difference converges.

5.4 Numerical Examples

The damage quantification method using second order analysis is studied using the symmetric three-storey plane frame described in Section 3.3. The small and large damage scenarios studied in this method are those described in Section 3.3.3, and the mode number is re-arranged with the eigenvalue change ratio in descending order as described in Section 4.4. The variance matrix R, the weight matrix $\overline{W}$, and the variance matrix on the error in the damage coefficient C, $E\left(\tilde{C}\tilde{C}^T\right)$, have been set equal to the identify matrix I. The criteria of convergence in $\hat{C}_i$ is set equal to 0.1% of the last estimated value. The noise levels for the eigenvalue and mode shape are assumed to be 0.15% and 3% respectively. The noisy "measured" eigenvalues and mode shapes are calculated by the method described in Section 3.3.5.

5.4.1 Damage Quantification of Large Damages

The formulation has the capability to expand the eigenvalue from a smaller measured set to a larger set. The first eight modes with the largest eigenvalue change ratio are used when eigenvalue expansion is not applied in this method. When the expansion process is included, the first five modes with the largest eigenvalue change ratio are expanded into eight modes. The re-arranged mode numbers for large damage scenarios are the same as shown in Table 4.2 in Chapter 4.

5.4.1.1 Without eigenvalue expansion

The damage quantification results with the actual damage elements in the set of suspected element only from using the first condition and both conditions are shown in Tables 5.1 and 5.2 respectively. By comparing Tables 5.1 and 5.2, it is found that the results obtained in both cases are equal for different large damage scenarios, and the errors are all less than 5%.

In practice, some undamaged elements are included in the suspected element group and the true C value of the undamaged element is zero. The identification results using the first condition for different large damage scenarios with undamaged elements included in the identification are shown in Tables 5.3 to 5.5. These three tables show that the damage extent of different damage scenarios can be estimated correctly. The errors for damage scenarios L1, L2 and L3 are 2%, 1% and 7% respectively. However from Table 5.5, it is reported that the undamaged element 40 is estimated to have about 11% stiffness damage. Element 40 is adjacent to the damage element 39 and the reason of this mistake is given in Section 4.4.1.1.

Whether the undamaged elements are included in the suspected element group or not, the results without noise effect are more accurate than those with noise effect for all large damage scenarios (see Tables 5.1 to 5.5).

5.4.1.2 With eigenvalue expansion

The results with the actual damage elements in the suspected element group only from using the first condition or both conditions are shown in Tables 5.6 and 5.7 respectively. It is reported that the estimation results using the first condition are slightly better than those using both conditions for different large damage scenarios. The errors using the first condition are less than 6% but the errors using both conditions are less than 7%. The reason is that the inclusion of the second condition in the formulation simplifies the gain matrix P as shown in Eqt.(5.40) as compared to that in Eqt.(5.37) using only the first condition. Hence, the method using the first condition only is used in the subsequent studies.

The identified results with additional undamaged elements in the suspected element group from using the first condition are shown in Tables 5.8 to 5.10. Similar to the case without eigenvalue expansion, the damage extent can be quantified correctly for different large damage scenarios except that the undamaged element 40 is identified as damage element in damage scenario L3.

From Tables 5.6 to 5.10, the identified results without noise effect have better performance than those with noise effect. By comparing Tables 5.1 to 5.5 and Tables 5.6 to 5.10, the quantified results without eigenvalue expansion are more accurate than those with expansion. Therefore, the damage quantification method without eigenvalue expansion from using the first condition is more suitable for the estimation of large damages.

5.4.2 Damage Quantification of Small Damages

After illustrating the damage quantification method with the large damages, the robustness and the accuracy of this method when applied to the identification of small damages are studied. Only the algorithm using the first condition is used. The first eight modes with the largest eigenvalue change ratio are used when eigenvalue expansion is not included. When the expansion process is included, the first five modes with the largest eigenvalue change ratio are expanded into eight modes. The re-arranged mode numbers for small damage scenarios are the same as in Table 4.1 in Chapter 4.

For the cases with actual damage elements only in the suspected element group, the damage quantification results using the first condition without and with eigenvalue expansion are shown in Tables 5.11 to 5.12 respectively. The estimation on the damage extent is accurate and the errors without expansion and with expansion are less than 1% and 2% respectively. From these two tables, the same observations as before are made, i.e. the identified results without noise effect are better than those with noise effect, and the estimation without eigenvalue expansion is more accurate than that with expansion.

The damage extent of the suspected elements, where some additional undamaged elements are included in the identification, is estimated. Tables 5.13 to 5.15 show the damage extent results without eigenvalue expansion and Tables 5.16 to 5.18 show the quantified results with eigenvalue expansion. Tables 5.13 to 5.18 show that the identified results are estimated accurately for all small damage scenarios

whether eigenvalue expansion is included or not. The errors without and with expansion process are less than 5% and 7% respectively. From these six tables, it is also found that the existence of noise makes the results less accurate. By comparing the same damage scenarios with and without eigenvalue expansion, the results indicate that the damage extent without expansion is more accurate. This is due to that errors incurred in the expansion process.

Both the damage quantification method using first order analysis and the method using second order analysis are suitable for the small damage estimation. By comparing Tables 4.3 to 4.11 and Tables 5.11 to 5.18, it is found that the damage extent using second order analysis is more accurate than that using first order analysis whether eigenvalue expansion is included or not. Moreover, the undamaged element 40 in damage scenario S3 using second order analysis is estimated correctly as seen in Table 5.18, but this element is quantified to contain damage under the method using first order analysis. Hence, the method using second order analysis could improve the accuracy of quantification for small damages.

5.4.3 Stability Analysis

In the above studies, the initial vectors $\hat{C}$ and C_0 have been set to the true values. However, the true damage extent of each element is unknown. In this study, the initial vectors $\hat{C}$ and C_0 are arbitrary vectors and their components are taken to be equal. The initial vector C_0 is set equal to the initial vector $\hat{C}$. A study is made on damage scenarios L3 and S3 with five suspected elements and without eigenvalue

expansion. The estimation makes use of different initial vector $\hat{C}$ with its components all equal. For damage scenario L3, the range of the initial vector $\hat{C}$ ranges from -0.05 to -0.4 with 0.05 increments. The same results are obtained from using these different initial vector $\hat{C}$ and the resutls with noise effect are shown in Table 5.19 with less than 7% error. For damage scenario S3, the initial vector $\hat{C}$ is ranging from -0.01 to -0.1 with 0.01 increments. The same damage extent is estimated from these different initial vector $\hat{C}$ and the results are shown in Table 5.20 with less than 5% error. This indicates that the proposed method is independent of the initial vectors $\hat{C}$ and C_0 for both small and large damages.

5.4.4 Damage Quantification with Larger Noise Effect

The noise effect on this proposed damage quantification method is further studied with the inclusion of two more noise levels described in Section 3.3.6 in Chapter 3. Noise level A is 0.25% and 5% for the eigenvalue and mode shape respectively. And Noise level B is 0.5% and 10% for the eigenvalue and mode shape respectively. The noisy eigenvalue and mode shape are calculated using the equations in Section 3.3.5. Damage scenario L3 is used to investigate the effect of larger noise level in this method, and only the algorithm using the first condition is used. The first eight modes with the largest eigenvalue change ratio are used and there is no eigenvalue expansion. When eigenvalue expansion is included, the first five modes with the largest eigenvalue change ratio are expanded into eight modes. The re-arrange mode numbers are the same as shown in Table 4.2 in Chapter 4.

The damage quantification results with the actual damage elements in the suspected element group using noise level A and noise level B are shown in Table 5.21. The error in the identified damage is less than 15.6% and 18.7% for noise level A and noise level B respectively with or without eigenvalue expansion. Besides, the identified results without eigenvalue expansion is more accurate than that with eigenvalue expansion for both noise levels. By comparing Tables 5.1, 5.6 and 5.21, the error of identification is increased when the noise level is increased.

In practice, some undamaged elements are included in the suspected element group. For the damage localization method with larger noise level, the actual damage elements cannot be localized. Hence, the suspected elements in Table 3.6 in Chapter 3 using the noise level 0.15% and 3% for eigenvalue and mode shape are used. The identification results are shown in Tables 5.22 and 5.23 for the case without eigenvalue expansion and with eigenvalue expansion respectively. When there is no eigenvalue expansion (see Table 5.22), we found that the maximum error is 22.7% and 30.7% for noise level A and noise level B respectively. By comparing Tables 5.5 and 5.22, the results indicated that the error is increased with the noise level. When eigenvalue expansion is included, the damage extent of the computation on the suspected damage element does not converge for noise level A. For noise level B, the quantification results converge but the error is larger than 100%. Hence, the proposed damage quantification method with eigenvalue expansion is not effective when the noise level is too high.

5.5 Conclusions

A structural damage quantification method using the second order terms in the Taylor's expansion is developed. A linear sequential filtering technique and an unbiased minimum error estimation method is used in the formulation. A weight linear least squares method is used to solve the identification equation. The robustness and effectiveness of this method to quantify small and large damages are studied. This method permits an eigenvalue expansion in the formulation. Numerical simulations are studied on a three-storey plane frame. The results show that the method using the first necessary condition only and the method using both necessary conditions give the same estimation results when there is no eigenvalue expansion. However, the method using the first necessary condition is more accurate than that using both necessary conditions when eigenvalue expansion is included. The reason is that the accuracy of the estimation is reduced when the gain matrix P is simplified by the second condition in the formulation. The simulation results also show that the method using the first necessary condition only is effective and give an accurate result for assessing small and large damages. Whether noise effect is included or not, most damage extent of elements in the suspected element group with actual damage elements only can be estimated correctly. However, the error increases when the noise level is increased. The method using second order analysis is independent of the initial vectors $\hat{C}$ and C_0. Also, the method using second order analysis has higher accuracy in the estimation of small damages than that using first order analysis.

Table 5.1 - Damage quantification results for large damages with actual damage elements in the suspected element group only from using the first condition (without eigenvalue expansion)

Damage Scenario	L1	L2		L3		
Element No.	45	17	32	9	13	39
True Damage Extent, C	-0.3	-0.3	-0.2	-0.15	-0.2	-0.2
Estimated C	-0.3042	-0.3021	-0.1993	-0.1561	-0.1927	-0.2004
Error	1.4%	0.7%	0.4%	4.1%	3.7%	0.2%
Estimated C_{noise}	-0.3046	-0.3025	-0.1990	-0.1570	-0.1925	-0.2006
Error $_{noise}$	1.5%	0.8%	0.5%	4.7%	3.8%	0.3%

Subscript $_{noise}$ denotes results from polluted measurements

Table 5.2 - Damage quantification results for large damages with actual damage elements in the suspected element group only from using both conditions (without eigenvalue expansion)

Damage Scenario	L1	L2		L3		
Element No.	45	17	32	9	13	39
True Damage Extent, C	-0.3	-0.3	-0.2	-0.15	-0.2	-0.2
Estimated C	-0.3042	-0.3021	-0.1993	-0.1561	-0.1927	-0.2004
Error	1.4%	0.7%	0.4%	4.1%	3.7%	0.2%
Estimated C_{noise}	-0.3046	-0.3025	-0.1990	-0.1570	-0.1925	-0.2006
Error $_{noise}$	1.5%	0.8%	0.5%	4.7%	3.8%	0.3%

Table 5.3 - Damage quantification results for damage scenario L1 (without eigenvalue expansion)

Element No.	25	44	45
True Damage Extent, C	0	0	-0.3
Estimated C	0.0013	0.0034	-0.3051
Error	-	-	1.7%
Estimated C_{noise}	0.0015	0.0038	-0.3058
Error $_{noise}$	-	-	1.9%

Table 5.4 - Damage quantification results for damage scenario L2 (without eigenvalue expansion)

Element No.	17	31	32
True Damage Extent, C	-0.3	0	-0.2
Estimated C	-0.3021	-0.0054	-0.1988
Error	0.7%	-	0.6%
Estimated C_{noise}	-0.3027	0.0092	-0.2015
Error $_{noise}$	0.9%	-	0.8%

Table 5.5 - Damage quantification results for damage scenario L3 (without eigenvalue expansion)

Element No.	7	9	13	39	40
True Damage Extent, C	0	-0.15	-0.2	-0.2	0
Estimated C	0.0063	-0.1579	-0.1907	-0.1888	-0.1061
Error	-	5.3%	4.7%	5.6%	-
Estimated C_{noise}	0.0071	-0.1596	-0.1899	-0.1871	-0.1144
Error $_{noise}$	-	6.4%	5.1%	6.5%	-

Table 5.6 - Damage quantification results for large damages with actual damage elements in the suspected element group only from using the first condition (with eigenvalue expansion)

Damage Scenario	L1	L2		L3		
Element No.	45	17	32	9	13	39
True Damage Extent, C	-0.3	-0.3	-0.2	-0.15	-0.2	-0.2
Estimated C	-0.3074	-0.3071	-0.1979	-0.1563	-0.1909	-0.2005
Error	2.5%	2.4%	1.1%	4.2%	4.6%	0.3%
Estimated C_{noise}	-0.3082	-0.3076	-0.1976	-0.1576	-0.1894	-0.2010
Error $_{noise}$	2.7%	2.5%	1.2%	5.1%	5.3%	0.5%

Table 5.7 - Damage quantification results for large damages with actual damage elements in the suspected element group only from using both conditions (with eigenvalue expansion)

Damage Scenario	L1	L2		L3		
Element No.	45	17	32	9	13	39
True Damage Extent, C	-0.3	-0.3	-0.2	-0.15	-0.2	-0.2
Estimated C	-0.3076	-0.3077	-0.1945	-0.1572	-0.1895	-0.2023
Error	2.5%	2.6%	2.8%	4.8%	5.3%	1.2%
Estimated C_{noise}	-0.3086	-0.3077	-0.1942	-0.1583	-0.1877	-0.2036
Error $_{noise}$	2.9%	2.6%	2.9%	5.5%	6.2%	1.8%

Table 5.8 - Damage quantification results for damage scenario L1 (with eigenvalue expansion)

Element No.	25	44	45
True Damage Extent, C	0	0	-0.3
Estimated C	0.0018	0.0042	-0.3085
Error	-	-	2.8%
Estimated C_{noise}	0.0021	0.0048	-0.3092
Error $_{noise}$	-	-	3.1%

Table 5.9 - Damage quantification results for damage scenario L2 (with eigenvalue expansion)

Element No.	17	31	32
True Damage Extent, C	-0.3	0	-0.2
Estimated C	-0.3077	-0.0109	-0.1972
Error	2.6%	-	1.4%
Estimated C_{noise}	-0.3081	0.0189	-0.2028
Error $_{noise}$	2.7%	-	1.4%

Table 5.10 - Damage quantification results for damage scenario L3 (with eigenvalue expansion)

Element No.	7	9	13	39	40
True Damage Extent, C	0	-0.15	-0.2	-0.2	0
Estimated C	0.0065	-0.1583	-0.1892	-0.1880	-0.1084
Error	-	5.5%	5.4%	6.0%	-
Estimated C_{noise}	0.0078	-0.1606	-0.1885	-0.1852	-0.1191
Error $_{noise}$	-	7.1%	5.8%	7.4%	-

Table 5.11 - Damage quantification results for small damages with actual damage elements in the suspected element group only from using the first condition (without eigenvalue expansion)

Damage Scenario	S1	S2		S3		
Element No.	45	17	32	9	13	39
True Damage Extent, C	-0.05	-0.05	-0.03	-0.02	-0.03	-0.03
Estimated C	-0.0501	-0.0503	-0.0301	-0.0198	-0.0301	-0.0300
Error	0.2%	0.6%	0.3%	1.0%	0.3%	0%
Estimated C_{noise}	-0.0505	-0.0505	-0.0302	-0.0198	-0.0302	-0.0301
Error $_{noise}$	1.0%	1.0%	0.7%	1.0%	0.7%	0.3%

Table 5.12 - Damage quantification results for small damages with actual damage elements in the suspected element group only from using the first condition (with eigenvalue expansion)

Damage Scenario	S1	S2		S3		
Element No.	45	17	32	9	13	39
True Damage Extent, C	-0.05	-0.05	-0.03	-0.02	-0.03	-0.03
Estimated C	-0.0501	-0.0504	-0.0302	-0.0197	-0.0302	-0.0301
Error	0.2%	0.8%	0.7%	1.5%	0.7%	0.3%
Estimated C_{noise}	-0.0506	-0.0506	-0.0302	-0.0196	-0.0303	-0.0301
Error $_{noise}$	1.2%	1.2%	0.7%	2.0%	1.0%	0.3%

Table 5.13 - Damage quantification results for damage scenario S1 (without eigenvalue expansion)

Element No.	25	44	45
True Damage Extent, C	0	0	-0.05
Estimated C	0	0	0.0502
Error	-	-	0.4%
Estimated C_{noise}	0	0	0.0508
Error $_{noise}$	-	-	1.6%

Table 5.14 - Damage quantification results for damage scenario S2 (without eigenvalue expansion)

Element No.	17	31	32
True Damage Extent, C	-0.05	0	-0.03
Estimated C	-0.0504	-0.0021	-0.0303
Error	0.8%	-	1.0%
Estimated C_{noise}	-0.0510	-0.0035	-0.0308
Error $_{noise}$	2%	-	2.7%

Table 5.15 - Damage quantification results for damage scenario S3 (without eigenvalue expansion)

Element No.	9	13	25	39	40
True Damage Extent, C	-0.02	-0.03	0	-0.03	0
Estimated C	-0.0207	-0.0306	0.0013	-0.0302	0.0002
Error	3.5%	2.0%	-	0.7%	-
Estimated C_{noise}	-0.0209	-0.0307	0.0016	-0.0303	0.0005
Error $_{noise}$	4.5%	2.3%	-	1.0%	-

Table 5.16 - Damage quantification results for damage scenario S1 (with eigenvalue expansion)

Element No.	25	44	45
True Damage Extent, C	0	0	-0.05
Estimated C	0	0.0001	-0.0504
Error	-	-	0.8%
Estimated C_{noise}	0	0.0001	-0.0511
Error $_{noise}$	-	-	2.2%

Table 5.17 - Damage quantification results for damage scenario S2 (with eigenvalue expansion)

Element No.	17	31	32
True Damage Extent, C	-0.05	0	-0.03
Estimated C	-0.0509	-0.0037	-0.0305
Error	1.8%	-	1.7%
Estimated C_{noise}	-0.0515	-0.0046	-0.0311
Error $_{noise}$	3.0%	-	3.7%

Table 5.18 - Damage quantification results for damage scenario S3 (with eigenvalue expansion)

Element No.	9	13	25	39	40
True Damage Extent, C	-0.02	-0.03	0	-0.03	0
Estimated C	-0.0189	-0.0293	-0.0025	-0.0290	-0.0018
Error	5.5%	2.3%	-	3.3%	-
Estimated C_{noise}	-0.0186	-0.0292	-0.0032	-0.0288	-0.0026
Error $_{noise}$	7.0%	2.7%	-	4.0%	-

Table 5.19 - Damage quantification results for damage scenario L3 in stability analysis (without eigenvalue expansion)

Element No.	7	9	13	39	40
True Damage Extent, C	0	-0.15	-0.2	-0.2	0
Estimated C_{noise}	0.0071	-0.1596	-0.1899	-0.1871	-0.1144
Error $_{noise}$	-	6.4%	5.1%	6.5%	-

Table 5.20 - Damage quantification results for damage scenario S3 in stability analysis (without eigenvalue expansion)

Element No.	9	13	25	39	40
True Damage Extent, C	-0.02	-0.03	0	-0.03	0
Estimated C_{noise}	-0.0209	-0.0307	0.0016	-0.0303	0.0005
Error $_{noise}$	4.5%	2.3%	-	1.0%	-

Table 5.21 - Damage quantification results for damage scenario L3 with actual damage elements in the suspected element group only from using the first condition

	Without Eigenvalue Expansion			With Eigenvalue Expansion		
Element No.	9	13	39	9	13	39
True Damage Extent, C	-0.15	-0.2	-0.2	-0.15	-0.2	-0.2
Estimated $C_{noise\ A}$	-0.1733	-0.1921	-0.2002	-0.1734	-0.1869	-0.2001
Error $_{noise\ A}$	15.5%	4.0%	0.1%	15.6%	6.6%	0.1%
Estimated $C_{noise\ B}$	-0.1778	-0.1923	-0.1999	-0.1780	-0.1874	-0.1998
Error $_{noise\ B}$	18.5%	3.9%	0.04%	18.7%	6.3%	0.1%

Subscript $_{\text{noise A}}$ denotes results from polluted measurements of noise level A and $_{\text{noise B}}$ denotes results from polluted measurements of noise level B

Table 5.22 - Damage quantification results for damage scenario L3 (without eigenvalue expansion)

Element No.	7	9	13	39	40
True Damage Extent, C	0	-0.15	-0.2	-0.2	0
Estimated $C_{noise\ A}$	-0.0118	-0.1841	-0.1875	-0.1775	-0.1880
Error $_{noise\ A}$	-	22.7%	6.3%	11.3%	-
Estimated $C_{noise\ B}$	0.0192	-0.1960	-0.1881	-0.1787	-0.1769
Error $_{noise\ B}$	-	30.7%	6.0%	10.7%	-

Table 5.23 - Damage quantification results for damage scenario L3 (with eigenvalue expansion)

Element No.	7	9	13	39	40
True Damage Extent, C	0	-0.15	-0.2	-0.2	0
Estimated $C_{noise\ A}$	Does not converge				
Error $_{noise\ A}$	as above				
Estimated $C_{noise\ B}$	0.3913	-0.4290	-0.1986	0.1557	-1.1250
Error $_{noise\ B}$	-	186%	0.7%	177.9%	-

Chapter 6

Study on Eigenvalue Expansion

6.1 Introduction

From the theory on the damage quantification methods presented in Chapters 4 and 5, the formulation has the capability to estimate a larger set of eigenvalues from a smaller set of measured eigenvalues. In this chapter, the effectiveness and accuracy of the eigenvalue expansion is studied. By comparing the identified results from Chapters 4 and 5, it is found that the damage quantification method using second order analysis is more robust and accurate than that using first order analysis for both small and large damages. Hence, the following simulations are performed by the method using second order analysis. Numerical examples are studies to demonstrate the accuracy of the expanded eigenvalue.

6.2 Numerical Examples

The symmetric three-storey plane frame mentioned in Section 3.3 is used to study the eigenvalue expansion. The damage scenarios with small or large damages are the same as for the damage localization described in Section 3.3.3. The first five modes with the largest eigenvalue change ratio are expanded into eight modes. The

estimated and the true natural frequencies are compared. The noise levels for the eigenvalue and mode shape are assumed to be 0.15% and 3% respectively. The eigenvalues and mode shapes with noise effect are calculated by the method described in Section 3.3.5. The subscript $_{noise}$ in the Tables denotes the results obtained from the eigenvalues and mode shapes with noise effect.

6.2.1 For Small Damages

The first eight re-arranged mode numbers for the small damage scenarios S1, S2 and S3 are the same as those used in Section 4.4.1 and they are shown in Table 4.1 in Chapter 4. The estimated damage frequencies for scenarios with different small damages are shown in Tables 6.1 to 6.6. Tables 6.1, 6.3 and 6.5 are the results without undamaged elements in the suspected group and Tables 6.2, 6.4 and 6.6 are the results with some undamaged elements in the suspected group. The group of suspected elements for each scenario are listed in Tables 3.5 and 3.6 in Chapter 3 for the case without and with noise effect respectively. In all these six cases, the estimated frequencies are very closed to the true frequencies with the errors less than 0.015%. Besides, the estimated frequencies without noise effect are more accurate than those with noise effect. Furthermore, the results with undamaged elements in the suspected group give larger error than those without undamaged elements in the suspected group.

6.2.2 For Large Damages

Table 4.2 in Chapter 4 shows the first eight re-arranged mode numbers for the large damage scenarios L1, L2 and L3. In this section, the same re-arranged modes are used. The set of suspected elements for each scenario are listed in Tables 3.5 and 3.6 in Chapter 3 for the case without and with noise effect respectively. Tables 6.7 to 6.12 contain the estimated frequencies for all scenarios with or without undamaged elements in the suspected group. The estimated frequencies have a very high accuracy. The errors are less than 0.5%. The observations are similar to those with small damages, i.e. the estimated frequencies without noise effect are more closed to the true frequencies than those with noise, and the estimated results without undamaged elements in the suspected group are more accurate than those with undamaged elements in the suspected group.

6.3 Conclusions

In the proposed damage quantification method presented in Chapters 4 and 5, the eigenvalues can be expanded from a smaller set of measured eigenvalues to a larger set. In this chapter, the accuracy of the expanded eigenvalues has been studied. Numerical simulations show that the expanded frequencies are estimated with very high accuracy whether the structure contains multiple small or large damages. Moreover, the estimated frequencies with actual damage elements in the suspected group have better accuracy than those with undamaged elements in the suspected group.

Table 6.1 - Eigenvalue expansion results for damage scenario S1
(without undamaged elements in the suspected group)

Mode No.	12	3	8
True Frequency (Hz)	210.733	31.157	151.662
Estimated Frequency (Hz)	210.733	31.157	151.662
Error	0%	0%	0%
True Frequency $_{noise}$ (Hz)	210.745	31.156	151.747
Estimated Frequency $_{noise}$ (Hz)	210.745	31.156	151.747
Error $_{noise}$	0%	0%	0%

Table 6.2 - Eigenvalue expansion results for damage scenario S1
(with undamaged elements in the suspected group)

Mode No.	12	3	8
True Frequency (Hz)	210.733	31.157	151.662
Estimated Frequency (Hz)	210.734	31.157	151.662
Error	-4.75×10^{-4}%	0%	0%
True Frequency $_{noise}$ (Hz)	210.745	31.156	151.747
Estimated Frequency $_{noise}$ (Hz)	210.746	31.156	151.748
Error $_{noise}$	-4.75×10^{-4}%	0%	-6.59×10^{-4}%

Table 6.3 - Eigenvalue expansion results for damage scenario S2
(without undamaged elements in the suspected group)

Mode No.	12	6	1
True Frequency (Hz)	210.554	136.984	7.062
Estimated Frequency (Hz)	210.553	136.981	7.061
Error	4.75×10^{-4}%	0.00219%	0.0142%
True Frequency $_{noise}$ (Hz)	210.567	137.034	7.057
Estimated Frequency $_{noise}$ (Hz)	210.569	137.031	7.056
Error $_{noise}$	-9.50×10^{-4}%	0.00219%	0.0142%

Table 6.4 - Eigenvalue expansion results for damage scenario S2
(with undamaged elements in the suspected group)

Mode No.	12	6	1
True Frequency (Hz)	210.554	136.984	7.062
Estimated Frequency (Hz)	210.557	136.969	7.061
Error	-0.00142%	0.011%	0.0142%
True Frequency $_{noise}$ (Hz)	210.567	137.034	7.057
Estimated Frequency $_{noise}$ (Hz)	210.569	137.047	7.056
Error $_{noise}$	-9.50×10^{-4}%	-0.00949%	0.0142%

Table 6.5 - Eigenvalue expansion results for damage scenario S3
(without undamaged elements in the suspected group)

Mode No.	8	5	13
True Frequency (Hz)	151.545	134.279	374.255
Estimated Frequency (Hz)	151.545	134.279	374.262
Error	0%	0%	-0.00187%
True Frequency $_{noise}$ (Hz)	151.630	134.416	373.991
Estimated Frequency $_{noise}$ (Hz)	151.631	134.416	374.000
Error $_{noise}$	-6.60×10^{-4}%	0%	-0.00241%

Table 6.6 - Eigenvalue expansion results for damage scenario S3
(with undamaged elements in the suspected group)

Mode No.	8	5	13
True Frequency (Hz)	151.545	134.279	374.255
Estimated Frequency (Hz)	151.540	134.280	374.275
Error	0.0033%	-7.45×10^{-4}%	-0.00534%
True Frequency $_{noise}$ (Hz)	151.630	134.416	373.991
Estimated Frequency $_{noise}$ (Hz)	151.624	134.417	374.015
Error $_{noise}$	0.00396%	-7.44×10^{-4}%	-0.00642%

Table 6.7 - Eigenvalue expansion results for damage scenario L1
(without undamaged elements in the suspected group)

Mode No.	12	3	8
True Frequency (Hz)	210.630	31.147	151.618
Estimated Frequency (Hz)	210.627	31.147	151.618
Error	0.00142%	0%	0%
True Frequency $_{noise}$ (Hz)	210.643	31.146	151.704
Estimated Frequency $_{noise}$ (Hz)	210.638	31.146	151.704
Error $_{noise}$	0.00237%	0%	0%

Table 6.8 - Eigenvalue expansion results for damage scenario L1
(with undamaged elements in the suspected group)

Mode No.	12	3	8
True Frequency (Hz)	210.630	31.147	151.618
Estimated Frequency (Hz)	210.633	31.149	151.621
Error	-0.00142%	-0.00642%	-0.00198%
True Frequency $_{noise}$ (Hz)	210.643	31.146	151.704
Estimated Frequency $_{noise}$ (Hz)	210.646	31.148	151.707
Error $_{noise}$	-0.00142%	-0.00642%	-0.00264%

Table 6.9 - Eigenvalue expansion results for damage scenario L2
(without undamaged elements in the suspected group)

Mode No.	1	12	10
True Frequency (Hz)	7.062	210.554	192.706
Estimated Frequency (Hz)	7.030	210.467	192.537
Error	0.453%	0.0413%	0.0877%
True Frequency $_{noise}$ (Hz)	7.024	209.732	191.787
Estimated Frequency $_{noise}$ (Hz)	6.990	209.819	191.958
Error $_{noise}$	0.484%	-0.0415%	-0.0892%

Table 6.10 - Eigenvalue expansion results for damage scenario L2
(with undamaged elements in the suspected group)

Mode No.	1	12	10
True Frequency (Hz)	7.062	210.554	192.706
Estimated Frequency (Hz)	7.030	210.463	192.524
Error	0.453%	0.0432%	0.0944%
True Frequency $_{noise}$ (Hz)	7.024	209.732	191.787
Estimated Frequency $_{noise}$ (Hz)	6.994	209.837	191.600
Error $_{noise}$	0.427%	-0.0501%	0.0975%

Table 6.11 - Eigenvalue expansion results for damage scenario L3
(without undamaged elements in the suspected group)

Mode No.	5	4	8
True Frequency (Hz)	133.399	126.253	150.754
Estimated Frequency (Hz)	133.505	126.287	150.775
Error	-0.0795%	-0.0269%	-0.0139%
True Frequency $_{noise}$ (Hz)	133.532	126.263	150.839
Estimated Frequency $_{noise}$ (Hz)	133.687	126.303	150.875
Error $_{noise}$	-0.116%	-0.0317%	-0.0239%

Table 6.12 - Eigenvalue expansion results for damage scenario L3
(with undamaged elements in the suspected group)

Mode No.	5	4	8
True Frequency (Hz)	133.399	126.253	150.754
Estimated Frequency (Hz)	133.603	126.327	150.590
Error	-0.153%	-0.0586%	0.109%
True Frequency $_{noise}$ (Hz)	133.532	126.263	150.839
Estimated Frequency $_{noise}$ (Hz)	133.764	126.355	150.658
Error $_{noise}$	-0.174%	-0.0729%	0.120%

Chapter 7

Experimental Results

7.1 Introduction

The damage localization method and the damage quantification methods using first order and second order analysis have been described previously and their effectiveness and accuracy are investigated using numerical simulations in Chapters 3, 4 and 5. The simulation results show that the damage localization method and the damage quantification method using second order analysis are robust and effective for both small and large damages, and the damage quantification method using first order analysis is effective only for small damages. A dynamic test is carried out in the laboratory on a five-storey steel plane frame to further verify the damage localization method and the damage quantification methods.

7.2 Descriptions of the Structure

The test structure is a five-storey steel plane frame as shown in Figure 7.1. It consists of two columns and five horizontal interconnecting beams. The beam to column connections and the column to base plate connections are rigidly connected. The overall height of the frame is 2 metres and the height of each storey is 0.4 metre.

The length of each horizontal interconnecting beam is 0.59 metre. The columns are flat steel bars with a cross-sectional dimension of 4.45mm thick × 32.2mm width. The horizontal beams are Tee-beams with an overall height of 30.3mm. The flange of the Tee-beams is 30.55mm width × 4.15mm thick and the web is 3.75mm thick. The Tee-beams are connected to the flat steel column at the mass center of the Tee-beams. The material properties of frame are shown in Figure 7.1, and the physical properties are summarized in Table 7.1.

The finite element model of this structure consists of seventy-five Euler-Bernoulli elements and seventy-two nodes. There are seventy unconstrained nodes and two constrained nodes at the supports. The motion of the frame in the x-z plane is considered. Each unconstrained node has three degrees-of-freedom. They are the displacement in x-direction, z-direction and the rotation about y-axis. Besides, there is no restriction on the elongation of the elements. However, the rotation of each node is difficult to measure. Then, all rotational degrees-of-freedom are not chosen to have incomplete information on the mode shapes for the damage localization method. Moreover, the z-direction displacement of each column node is too small and is not considered to have incomplete information for the damage localization method. Besides, the beams are assumed to vibrate without elongation, and the x-direction displacement of each beam node is taken equal to that at the corresponding column-beam connection node. Therefore, only one degree-of-freedom is measured at each unconstrained node. The displacement in x-direction is measured for the column nodes and the displacement in z-direction is measured for the beam nodes. There are totally seventy measurable degrees-of-freedom.

7.3 Experimental Setup

The setup of the experiment is illustrated in Figure 7.2. A B&K Model 1049 signal generator generates a random force through an exciter. This force is applied to the supporting base plate of the steel frame as shown in Figure 7.3 such that this random force is transmitted to the frame indirectly. The frequency bandwidth of the random excitation force ranges from 2Hz to 100Hz for identifying the lower five modes that are the global modes, and from 30Hz to 316Hz for identifying the remaining higher modes which are the local modes. The force is 100N and 94N for detecting the global modes and the local modes respectively. These two forces are the highest output from the signal generator such that a large and steady vibrational displacement at the monitored degrees-of-freedom is obtained.

Seven B&K Model 8201 accelerometers and seven B&K Model 2635 charge amplifiers are used in this experiment. The number of accelerometers is much less than the number of degrees-of-freedom to be measured. Therefore, eleven sets of measurement are required to measure all the degrees-of-freedom. In each set of measurement, one accelerometer is fixed on a "reference" degree-of-freedom, and the other six accelerometers are arranged on the remaining degrees-of-freedom to measure the acceleration responses until all seventy degrees-of-freedom are measured. The spectrum results from each accelerometer are then normalized to form the full mode shapes.

Small pieces of lump mass are placed at all the unconstrained nodes of the structure during each measurement. The weight of each mass is equal to the weight of the "moving" accelerometers. The lump mass counteracts the mass variation of the system due to the change in location of the moving accelerometers in the different sets of measurement. Hence, the distribution of the mass of the system is the same for different sets of measurement.

Signals from the accelerometers are sampled with the software package GLOBAL LAB through a Data Translation Model DT2829 A/D Card. The sampling frequencies are 249.75025Hz and 2012.0724Hz for the measurement of global and local modes respectively. The frequency resolution of the global mode measurements is 0.061Hz when a length of 4096 data block is used in the subsequent Fast Fourier Analysis. Data of the local mode measurements is re-sampled at a ratio of 1 to 4, and the resulting frequency resolution is 0.0614Hz from the Fast Fourier Analysis. A spectral analysis and a modal analysis are then performed on these digitized signals. Finally, the mode shapes and the corresponding natural frequencies of the frame are obtained.

After the data collection on the undamaged state of the frame is completed, the procedures described in the last few paragraphs are repeated for the three different damage scenarios described below.

7.4 Damage Scenarios

Three damage scenarios on the test structure are studied. The location and the extent of the damages are listed in Table 7.2. Element 59 is located at the second-level interconnecting beam. Element 9 is located at the column in-between the first and second levels. Damage is created by reducing the physical dimensions of a finite element. The beam height of finite element 59 is reduced from 30.3mm to 29.45mm throughout its length in damage scenarios A and B, and it is further reduced to 27.85mm in damage scenario C. The width of finite element 9 is decreased from 32.2mm to 28.95mm throughout its length in damage scenarios B and C. These scenarios are such selected to have both small and large damages in the structure. The damages in elements 59 and 9 are shown in Figure 7.4.

Damage in an element is defined in this study as a scalar reduction in the stiffness of the element. The mass matrix is assumed to be unchanged with the existence of damage. The stiffness of a damage element is expressed as a fraction of its original elemental stiffness matrix. That is,

$$K_i^d = \alpha K_i^u \tag{7.1}$$

where K_i^d is the stiffness matrix of element i with a damage; K_i^u is the stiffness matrix of element i without damage; α is the stiffness reduction factor ranging from zero to one. The damage extent C in Chapters 4 and 5 can be related to the stiffness reduction factor α as

$$C = \alpha - 1 \tag{7.2}$$

7.4.1 Damage at Element 59

The stiffness matrix of element 59 without damage is

$$K_{59}^{u} = \begin{bmatrix} 26292572.03 & 1564408.03 & -26292572.03 & 1564408.03 \\ 1564408.03 & 124109.7 & -1564408.03 & 62054.85 \\ -26292572.03 & -1564408.03 & 26292572.03 & -1564408.03 \\ 1564408.03 & 62054.85 & -1564408.03 & 124109.7 \end{bmatrix} \quad (7.3)$$

7.4.1.1 For damage scenarios A and B

The stiffness matrix of element 59 with damage is

$$K_{59}^{d} = \begin{bmatrix} 24224116.78 & 1441334.95 & -24224116.78 & 1441334.95 \\ 1441334.95 & 114345.91 & -1441334.95 & 57172.95 \\ -24224116.78 & -1441334.95 & 24224116.78 & -1441334.95 \\ 1441334.95 & 57172.95 & -1441334.95 & 114345.91 \end{bmatrix} \quad (7.4)$$

By comparing the stiffness matrices K_{59}^{u} and K_{59}^{d} in Eqts.(7.3) and (7.4), the stiffness reduction factor α, and the damage extent, C, of element 59 are 0.9213 and -0.0787 respectively for all the components of the matrices.

7.4.1.2 For damage scenario C

The stiffness matrix of element 59 with damage is

$$K_{59}^{d} = \begin{bmatrix} 20612796.28 & 1226461.38 & -20612796.28 & 1226461.38 \\ 1226461.38 & 97299.27 & -1226461.38 & 48649.63 \\ -20612796.28 & -1226461.38 & 20612796.28 & -1226461.38 \\ 1226461.38 & 48649.63 & -1226461.38 & 97299.27 \end{bmatrix} \quad (7.5)$$

By comparing the stiffness matrices K_{59}^{u} and K_{59}^{d} in Eqts.(7.3) and (7.5), the stiffness reduction factor α, and the damage extent, C, of element 59 are 0.784 and -0.216 respectively for all the components of the matrices.

7.4.2 Damage at Element 9

The stiffness matrix of element 9 without damage is

$$K_{9}^{u} = \begin{bmatrix} 1108398.53 & 44335.94 & -1108398.53 & 44335.94 \\ 44335.94 & 2364.58 & -44335.94 & 1182.29 \\ -1108398.53 & -44335.94 & 1108398.53 & -44335.94 \\ 44335.94 & 1182.29 & -44335.94 & 2364.58 \end{bmatrix} \quad (7.6)$$

The stiffness matrix of element 9 with damage is

$$K_{9}^{d} = \begin{bmatrix} 996526 & 39861.04 & -996526 & 39861.04 \\ 39861.04 & 2125.92 & -39861.04 & 1062.96 \\ -996526 & -39861.04 & 996526 & -39861.04 \\ 39861.04 & 1062.96 & -39861.04 & 2125.92 \end{bmatrix} \quad (7.7)$$

By comparing the stiffness matrices K_9^u and K_9^d in Eqts.(7.6) and (7.7), the stiffness reduction factor α, and the damage extent, C, of element 9 are 0.8991 and -0.1009 respectively for all the components of the matrices.

7.4.3 Mass Reduction

There is a small change in mass matrix with the small cut made in the structure in the experiment. The mass reduction in element 59 for damage scenarios A and B and damage scenario C is 1.4% and 4.3% respectively. The mass reduction of element 9 for damage scenarios B and C is 6.2%.

For a higher accuracy of damage extent estimation, the change in mass of the system should not be neglected in Eqts.(4.3) and (5.3). And the change in eigenvalue (Eqts.(4.4) and (5.4)) will involve a change in the stiffness and in the mass. The change in eigenvalue should be expanded as a Taylor's series with respect to the stiffness matrix and mass matrix. The identification equation will become much more complicated than the proposed one. Therefore this project limits the study with no change in the mass of the structure with the damages created, and there is no effect on the change in eigenvalue in this experimental study.

7.5 Modal Properties

The experimental natural frequencies for the four different states of the structure and the analytical natural frequencies are listed in Table 7.3. Modes 1 to 5 are the global modes (only four global modes can be identified for the system) and modes 6 to 14 are the local modes. The frequency of mode 4 varies in the different measurements in each scenario and this mode will not be used in this study. The experimental mode shapes for the four different states are shown in Figures 7.5 to 7.8. The analytical mode shapes are shown in Figure 7.9. The spectrum of the structure in the four different states is shown in Figure 7.10.

Figure 7.10 shows the spectrum of signals from nodes 26 and 14 for the global modes, and from nodes 58 and 66 for the local modes. Those from nodes 51 and 14 are presented instead in scenario A for the global modes because the peaks from nodes 51 and 14 are more prominent than those from nodes 26 and 14 in scenario A. The spectrum is obtained from the Fast Fourier Transformation on the measured responses, and the input excitation force is different in the four different states. Therefore the spectral power is different in the different states and they cannot be compared directly. The spectral magnitudes of global modes are not sensitive to structural changes in the different scenarios while the magnitudes of the local beam modes change relatively in the different scenarios. Since nodes 58 and 66 are located on the beams, the spectral peaks should be from those modes dominated by beam vibrations.

The mode shapes in Figures 7.5 to 7.9 show that modes 6 to 9 are local modes dominated by column vibrations, while modes 11 to 14 are local modes dominated by beam vibrations. Mode 10 has both large vibrations in the beam and column members, and it has an adjacent strongly coupling mode as seen from the spectrum for the original state and scenario A (see Figure 7.10). Due to this strongly coupling effect, experimental mode 10 does not look symmetrical or anti-symmetrical in Figures 7.5 to 7.8 and is not similar to the analytical mode 10 in Figure 7.9.

The correlation of the experimental and analytical modes is obtained by matching the natural frequency and the mode shape, and by inspection of the Modal Assurance Criterion (*MAC*). The *MAC* values for the four different states of the structure comparing with the analytical mode shapes are shown in Table 7.4. The *MAC* values of the global modes for the four different states are all greater than 0.99. For the local modes, the *MAC* values are all above 0.75. These show that the correlation between the analytical and experimental mode shapes of the four different states is fairly good.

7.6 Damage Localization

In Chapter 3, the damage localization method using incomplete mode shapes and the method using incomplete Elemental Modal Strain Energy Change (*EMSEC*) are compared. And in the simulation study, it is found that the *MDLAC* method using incomplete *EMSEC* has better performance than the *MDLAC* method using

incomplete mode shapes. Therefore, the proposed damage localization method using incomplete *EMSEC* is verified with the experimental data.

A set of incomplete mode shapes is selected with engineering sense from the middle of each length of the column and beam members, and a total of fifteen elements are monitored. The selected elements are elements 3, 8, 13, 18, 23, 28, 33, 38, 43, 48, 53, 58, 63, 68 and 73.

7.6.1 Selection of Modes

Three global modes and three local modes dominated with beam vibrations are used for the damage localization. They are selected with information from both the beam and column members. Modes 6 to 9 are dominated by column vibrations. Mode 10 has both large vibrations in columns and beams, but it is strongly coupled with an adjacent mode, and is therefore not selected. Modes 11 to 14 are dominated by beam vibrations. A careful inspection shows that modes 11 and 14 are similar with vibrations in all beam members, while modes 12 and 13 has the second level and third level beam member respectively not in motion. Modes 1, 3, 5, 11, 12 and 14 for scenarios A and B, and modes 1, 3, 5, 11, 13 and 14 for scenario C are finally selected after a few trials.

Damage element 59 is at the second level beam, and mode 13 should be sensitive to the damage in this element. Inspection of the spectrum also shows that mode 12 is stronger than mode 13 in scenario B but mode 13 shows a large surge in the amplitude in scenario C. All these observations contribute to the above selection

of modes. But the inclusion of global mode 2 would produce errors in the identification, and the reason of this behaviour cannot be explained from available information. However, the combination of global modes dominated by column vibrations and local modes dominated by beam vibrations should be appropriated for the detection of damages in both beam and column members. Other combinations of modes should be exist for a similar or better damage assessment of the structure.

7.6.2 The *MDLAC* Approach

The *MDLAC* values of each element are shown in Figures 7.11, 7.12 and 7.13 for damage scenarios A, B and C respectively. The potential damage sites are found with a threshold *MDLAC* value of 0.5 for all damage scenarios. It is seen that the actual damage elements are included in the group of potential damage sites as shown in Table 7.5. The *MDLAC* values on the different combinations of the potential damage sites are further computed. The final damage sites are located corresponding to the combination with the largest *MDLAC* value, and they are shown in Table 7.5. It is reported that the actual damage elements are included in the final damage sites although an undamaged element is also included in each final group of suspected elements. Hence, the proposed *MDLAC* method using incomplete *EMSEC* is found robust and effective to localize the damage experimentally and to significantly reduce the number of suspected damage elements. The final damage sites are limited in number and they are used in the subsequent damage quantification.

From Figures 7.11 to 7.13, it is reported that the damage element has the largest *MDLAC* value for all different scenarios. The undamaged elements, which are

adjacent to or near the damage, also contain a larger *MDLAC* value because they exhibit some damage characteristic derived from the mode shape of the adjacent connecting node. The undamaged elements at the same position of the adjacent elements on the other column have a larger *MDLAC* value due to the symmetry of the structure. However, some undamaged elements, which are far away from the damage, contain a larger *MDLAC* value due to the measurement noise and the assumption of a single damage in the computation of the analytical *EMSEC* for finding the potential damage sites.

7.7 Damage Quantification from First Order Analysis

The damage quantification method using first order analysis is suitable for small damages and its effectiveness has been discussed in Chapter 4. The experimental verification of this method is studied in this section.

7.7.1 Damage Quantification without Eigenvalue Expansion

The first six modes with the largest eigenvalue change ratio are used for damage scenario A and the first eight modes with the largest ratio are used for damage scenarios B and C. The re-arranged mode numbers in descending order of the eigenvalue change ratio for the different damage scenarios are shown in Table 7.6.

The quantification results with actual damage elements in the suspected element group are shown in Table 7.7 for different damage scenarios. It is reported that the damage extent of the actual damage element for single damage (damage scenario A) is estimated correctly and the error is 6%. However for multiple damages (damage scenarios B and C), the damage extent of the actual damage elements cannot be quantified and contains a large error.

When an undamaged element is included in the suspected element group, the estimated damage extent is shown in Tables 7.8 to 7.10 for the three damage scenarios. The damage extent of the elements in the suspected group can be estimated for single damage and its error is less than 10% (see Table 7.8). When one large damage occurs in the structure as scenarios B and C, the estimated results are poor (see Tables 7.9 and 7.10). Hence, the damage quantification method using first order analysis is again confirmed to be suitable for small damages only.

7.7.2 Damage Quantification with Eigenvalue Expansion

When eigenvalue expansion is included, the first four modes with the largest eigenvalue change ratio are expanded into six modes for damage scenario A. For damage scenarios B and C, the first five modes with the largest ratio are expanded in eight modes. The re-arranged mode numbers including order of the eigenvalue change ratio are as shown in Table 7.6.

Table 7.11 shows the identified results with the actual damage elements occur in the set of the suspected elements. It is found that the damage extent of the actual

damage element can be determined correctly with 6.1% error for single damage scenario. The accuracy is similar to that obtained from without expansion. However, the quantified results contain large error for the multiple damage scenarios.

Tables 7.12 to 7.14 show the identified results with an undamaged element in the suspected element group. Similar to the cases without eigenvalue expansion, the damage extent can be estimated for single damage scenario but the damage extent cannot be quantified for multiple damage scenarios. The error is 9.9% for the single damage scenario and is similar to that obtained from without expansion.

By comparing Tables 7.7 to 7.10 and 7.11 to 7.14, it is noted that the results without eigenvalue expansion are more accurate than those with eigenvalue expansion. This is due to an error generated in the expansion process.

7.8 Damage Quantification from Second Order Analysis

The proposed damage quantification method using second order analysis has been proved to be robust in determining the damage extent for both small and large damages in the simulation studies. Results in Chapter 5 show that this method could give an accurate estimation of the damage extent. In this section, the proposed method is further verified with the experimental data.

7.8.1 Damage Quantification without Eigenvalue Expansion

The same vibration modes for the quantification basing on the first order analysis are used for each of the three damage scenarios. The re-arranged mode numbers can be referred to Table 7.6.

The identified results with only the actual damage elements in the suspected element group are shown in Table 7.15. The results show that the damage extent is estimated with a high accuracy for all damage scenarios. The error is less than 7%.

The estimated damage extent with an undamaged element in the suspected element group is listed in Tables 7.16 to 7.18 for the three damage scenarios. From these three tables, it is found that the method using second order analysis is effective for both small and large damages with a maximum error of 10%.

7.8.2 Damage Quantification with Eigenvalue Expansion

The first four modes with the largest eigenvalue change ratio are expanded to six modes for damage scenario A when eigenvalue expansion is included. The first five modes with the largest ratio are expanded to eight modes for damage scenarios B and C. The mode numbers used are referred to Table 7.6.

The damage quantification results without undamaged element in the suspected element group are shown in Table 7.19. The damage extent of the actual damage elements is determined correctly and the error is less than 8.5%.

Tables 7.20 to 7.22 show the estimation results with an undamaged element in the suspected element group for different damage scenarios. For single damage, the damage extent can be estimated with a high accuracy and its error is 2% (see Table 7.20). For multiple damages, the damage extent of element 59 can also be quantified with less than 5% error but the damage extent of element 9 is identified with a larger error of 12.8% (see Tables 7.21 and 7.22).

The identified results with or without eigenvalue expansion are acceptable in all damage scenarios. By comparing Tables 7.15 to 7.18 and 7.19 to 7.22, the estimation without eigenvalue expansion gives more accurate results than that with eigenvalue expansion. This observation shows that error from the eigenvalue expansion has been passed onto the damage quantification.

By comparing the results using first order analysis and using second order analysis, it is found that the damage quantification method using second order analysis is more effective than that using first order analysis for both small and large damages.

7.9 Study on Eigenvalue Expansion

In the damage quantification methods, the eigenvalues can be expanded from a smaller set of measured eigenvalues to a larger set. And the accuracy of such expansion is studied in this section. The first four modes with the largest eigenvalue

change ratio are expanded to six modes for damage scenario A and the first five modes with the largest ratio are expanded to eight modes for damage scenarios B and C. The mode numbers used are referred to Table 7.6.

7.9.1 From Damage Quantification Method using First Order Analysis

This method can only estimate the damage extent for damage scenario A correctly. Hence, the eigenvalue expansion for damage scenario A is studied. The estimated frequencies using first order analysis for damage scenario A are shown in Table 7.23. The estimated frequencies, which are the 5th and 6th frequencies listed in Table 7.6, are very closed to the measured frequencies and the error is less than 0.01%. Moreover, the results without undamaged element in the suspected element group are more accurate than those with undamaged element in the group.

7.9.2 From Damage Quantification Method using Second Order Analysis

The estimated frequencies for different damage scenarios are shown in Tables 7.24 to 7.26. For each damage scenario, the frequencies are estimated without or with an undamaged element in the suspected element group. In these six cases, the estimated frequencies are very closed to the measured frequencies. The errors are less than 0.04%. The estimated frequencies without undamaged element in the set of suspected elements have higher accuracy than those with undamaged element.

7.10 Conclusions

The proposed damage localization method and damage quantification methods are verified experimentally in this chapter. Three damage scenarios are investigated on the test structure. They following conclusions are drawn.

For the proposed damage localization method, the experimental results show that the *MDLAC* method using incomplete Elemental Modal Strain Energy Change (*EMSEC*) can successfully localize the single or multiple damages in the test structure. The actual damage elements are included in the final damage sites although an undamaged element is also grouped together. This method has the advantage that only a limited number of sensor information is required to calculate the change of the elemental modal strain energy between the undamaged and damaged states. This is an attractive method for structural damage assessment. From the experimental results, the damage element has the largest *MDLAC* value. The undamaged elements, which are adjacent to or near the damage, or at the same position of the adjacent elements on the other column, also contain a larger *MDLAC* value due to symmetry. However, some undamaged elements, which are far away from the damage, are identified as potential damage sites due to measurement noise.

For the proposed damage quantification method using first order analysis, the experimental results show that the estimated results are correctly identified for small damages only. When the damage is increased, this method fails in determining the damage extent. The reason is that this method only includes the linear part of the

Taylor's expansion while the effect of a larger damage on the vibration mode shapes is non-linear. Hence, this quantification method using first order analysis is suitable for small damages only.

For the proposed damage quantification method using second order analysis, the experimental results show that this method can estimate the damage extent for both small and large damages. This is because the second-order terms of the Taylor's expansion are included in the formulation. Under the experimental conditions, it is noted that the estimated damage extent using second order analysis is more accurate than that using first order analysis for both small and large damages.

There is a special feature in the damage quantification methods. The formulation on the identification equation has the capability to estimate a larger set of eigenvalues from a smaller set of measured eigenvalues. For the method using first order analysis, the frequencies can be estimated for damage scenario A with a single damage. For the method using second order analysis, the expanded frequencies are identified with a high accuracy for all the damage scenarios. And this method can be used for eigenvalue expansion in practice since the error involved is far below the resolution error due to measurements.

All experimental results show that the estimated frequencies without undamaged element in the suspected element group are more accurate than those with undamaged element under the two proposed damage quantification methods with eigenvalue expansion.

Table 7.1 - Physical properties of column and beam elements

	Column Element	Beam Element
Axial Area, A (m^2)	143.29×10^{-6}	224.85×10^{-6}
Poison Ratio, ν	0.3	0.3
Moment of Inertia, I (m^4)	2.365×10^{-10}	1.846×10^{-8}

Table 7.2 - Damage scenarios for five-storey steel plane frame

Scenario A		Scenario B		Scenario C	
Element No.	Damage	Element No.	Damage	Element No.	Damage
59	7.87%	9	10.09%	9	10.09%
		59	7.87%	59	21.6%

Table 7.3 - Natural frequencies for the four different states of the structure

	Mode No.	Analytical (Hz)	Undamaged (Hz)	Scenario A (Hz)	Scenario B (Hz)	Scenario C (Hz)
Global Modes	1	4.286	4.146	4.146	4.146	4.146
	2	12.73	12.5	12.5	12.5	12.5
	3	20.752	20.304	20.304	20.304	20.304
	4	27.573	26.707 - 27.377	26.829 - 27.012	26.829 - 26.951	26.829 - 27.012
	5	32.442	31.524	31.524	31.524	31.524
Local Modes	6	120.038	117.588	117.526	117.465	117.219
	7	122.014	120.412	120.351	120.29	120.167
	8	145.365	145.649	145.649	145.588	145.588
	9	154.582	154.369	154.369	154.307	154.246
	10	162.853	161	161	160.939	160.939
	11	186.199	183.228	182.614	182.553	180.956
	12	191.614	190.658	190.597	190.597	190.412
	13	196.284	196.491	196.123	196.123	195.386
	14	199.76	200.974	200.544	200.544	199.991

Table 7.4 - Modal Assurance Criterion (*MAC*) values for the four different states

	Mode No.	Undamaged	Scenario A	Scenario B	Scenario C
Global Modes	1	1.000	0.998	0.998	0.999
	2	0.998	0.997	0.995	0.999
	3	0.999	0.998	0.998	0.998
	4	-	-	-	-
	5	0.998	0.998	0.998	0.999
Local Modes	6	0.882	0.850	0.931	0.755
	7	0.938	0.896	0.874	0.892
	8	0.966	0.908	0.921	0.925
	9	0.937	0.897	0.853	0.899
	10	0.949	0.881	0.951	0.942
	11	0.939	0.868	0.903	0.845
	12	0.976	0.942	0.980	0.952
	13	0.955	0.948	0.945	0.854
	14	0.959	0.879	0.828	0.777

Table 7.5 - Potential and final damage sites by using incomplete *EMSEC*

	Potential Damage Sites	Final Damage Sites	*MDLAC* value
Scenario A	13, 16, 36, 59, 60	13, 59	0.321
Scenario B	8, 9, 19, 59, 60	8, 9, 59	0.342
Scenario C	9, 10, 34-36, 56-60	9, 59, 60	0.382

Table 7.6 - The re-arranged mode numbers for different damage scenarios

Damage Scenario	Re-arranged Mode Numbers
A	10, 13, 12, 5, 6, 11
B	10, 13, 12, 5, 6, 7, 8, 9, 11
C	10, 12, 13, 5, 6, 11, 8, 7, 9

Table 7.7 - Damage quantification results using first order analysis (without eigenvalue expansion)

Damage Scenario	A	B		C	
Element No.	59	9	59	9	59
True Damage Extent, C	-0.0787	-0.1009	-0.0787	-0.1009	-0.2160
Estimated C	-0.0834	-0.1183	-0.0823	-0.2412	-0.2468
Error	6.0%	17.2%	4.6%	139.0%	14.3%

Table 7.8 - Damage quantification results using first order analysis for damage scenario A (without eigenvalue expansion)

Element No.	13	59
True Damage Extent, C	0	-0.0787
Estimated C	0.0379	-0.0864
Error	-	9.8%

Table 7.9 - Damage quantification results using first order analysis for damage scenario B (without eigenvalue expansion)

Element No.	8	9	59
True Damage Extent, C	0	-0.1009	-0.0787
Estimated C	0.0568	-0.2079	-0.0807
Error	-	106.0%	2.5%

Table 7.10 - Damage quantification results using first order analysis for damage scenario C (without eigenvalue expansion)

Element No.	9	59	60
True Damage Extent, *C*	-0.1009	-0.2160	0
Estimated *C*	-0.3781	-0.2802	0.4091
Error	274.7%	29.7%	-

Table 7.11 - Damage quantification results using first order analysis (with eigenvalue expansion)

Damage Scenario	A	B		C	
Element No.	59	9	59	9	59
True Damage Extent, *C*	-0.0787	-0.1009	-0.0787	-0.1009	-0.2160
Estimated *C*	-0.0835	-0.1769	-0.0896	-0.6081	-0.2597
Error	6.1%	75.3%	13.9%	502.7%	20.2%

Table 7.12 - Damage quantification results using first order analysis for damage scenario A (with eigenvalue expansion)

Element No.	13	59
True Damage Extent, *C*	0	-0.0787
Estimated *C*	0.0403	-0.0865
Error	-	9.9%

Table 7.13 - Damage quantification results using first order analysis for damage scenario B (with eigenvalue expansion)

Element No.	8	9	59
True Damage Extent, C	0	-0.1009	-0.0787
Estimated C	-0.0932	-0.3508	-0.0511
Error	-	247.7%	76.3%

Table 7.14 - Damage quantification results using first order analysis for damage scenario C (with eigenvalue expansion)

Element No.	9	59	60
True Damage Extent, C	-0.1009	-0.2160	0
Estimated C	-0.6796	-0.3064	0.8614
Error	573.5%	41.9%	-

Table 7.15 - Damage quantification results using second order analysis (without eigenvalue expansion)

Damage Scenario	A	B		C	
Element No.	59	9	59	9	59
True Damage Extent, C	-0.0787	-0.1009	-0.0787	-0.1009	-0.2160
Estimated C	-0.0797	-0.0971	-0.0796	-0.1077	-0.2254
Error	1.3%	3.8%	1.1%	6.7%	4.4%

Table 7.16 - Damage quantification results using second order analysis for damage scenario A (without eigenvalue expansion)

Element No.	13	59
True Damage Extent, C	0	-0.0787
Estimated C	0.0102	-0.0803
Error	-	2.0%

Table 7.17 - Damage quantification results using second order analysis for damage scenario B (without eigenvalue expansion)

Element No.	8	9	59
True Damage Extent, C	0	-0.1009	-0.0787
Estimated C	-0.0044	-0.0914	-0.0797
Error	-	9.4%	1.3%

Table 7.18 - Damage quantification results using second order analysis for damage scenario C (without eigenvalue expansion)

Element No.	9	59	60
True Damage Extent, C	-0.1009	-0.2160	0
Estimated C	-0.1110	-0.2257	0.0125
Error	10.0%	4.5%	-

Table 7.19 - Damage quantification results using second order analysis (with eigenvalue expansion)

Damage Scenario	A	B		C	
Element No.	59	9	59	9	59
True Damage Extent, *C*	-0.0787	-0.1009	-0.0787	-0.1009	-0.2160
Estimated *C*	-0.0797	-0.1052	-0.0798	-0.1092	-0.2261
Error	1.3%	4.3%	1.4%	8.2%	4.7%

Table 7.20 - Damage quantification results using second order analysis for damage scenario A (with eigenvalue expansion)

Element No.	13	59
True Damage Extent, *C*	0	-0.0787
Estimated *C*	0.0096	-0.0803
Error	-	2.0%

Table 7.21 - Damage quantification results using second order analysis for damage scenario B (with eigenvalue expansion)

Element No.	8	9	59
True Damage Extent, *C*	0	-0.1009	-0.0787
Estimated *C*	-0.0092	-0.0901	-0.0816
Error	-	10.7%	3.7%

Table 7.22 - Damage quantification results using second order analysis for damage scenario C (with eigenvalue expansion)

Element No.	9	59	60
True Damage Extent, C	-0.1009	-0.2160	0
Estimated C	-0.1138	-0.2268	0.0241
Error	12.8%	5.0%	-

Table 7.23 - Eigenvalue expansion results using first order analysis for damage scenario A

Mode No.	6	11
Measured Frequency (Hz)	120.351	190.597
(a) Without undamaged elements in suspected group		
Estimated Frequency (Hz)	120.354	190.592
Error	-0.00249%	0.00262%
(b) With undamaged elements in suspected group		
Estimated Frequency (Hz)	120.360	190.607
Error	-0.00748%	-0.00525%

Table 7.24 - Eigenvalue expansion results using second order analysis for damage scenario A

Mode No.	6	11
Measured Frequency (Hz)	120.351	190.597
(a) Without undamaged elements in suspected group		
Estimated Frequency (Hz)	120.353	190.594
Error	-0.00166%	0.00157%
(b) With undamaged elements in suspected group		
Estimated Frequency (Hz)	120.355	190.594
Error	-0.00332%	0.00157%

Table 7.25 - Eigenvalue expansion results using second order analysis for damage scenario B

Mode No.	7	8	9
Measured Frequency (Hz)	145.588	154.307	160.939
(a) Without undamaged elements in suspected group			
Estimated Frequency (Hz)	145.592	154.284	160.951
Error	-0.00275%	0.0149%	-0.00746%
(b) With undamaged elements in suspected group			
Estimated Frequency (Hz)	145.612	154.251	160.976
Error	-0.0165%	0.0363	-0.0230%

Table 7.26 - Eigenvalue expansion results using second order analysis for damage scenario C

Mode No.	11	8	7
Measured Frequency (Hz)	190.415	154.246	145.588
(a) Without undamaged elements in suspected group			
Estimated Frequency (Hz)	190.418	154.271	145.569
Error	-0.00315%	-0.0162%	0.0131%
(b) With undamaged elements in suspected group			
Estimated Frequency (Hz)	190.440	154.276	145.566
Error	-0.0147%	-0.0194%	0.0151%

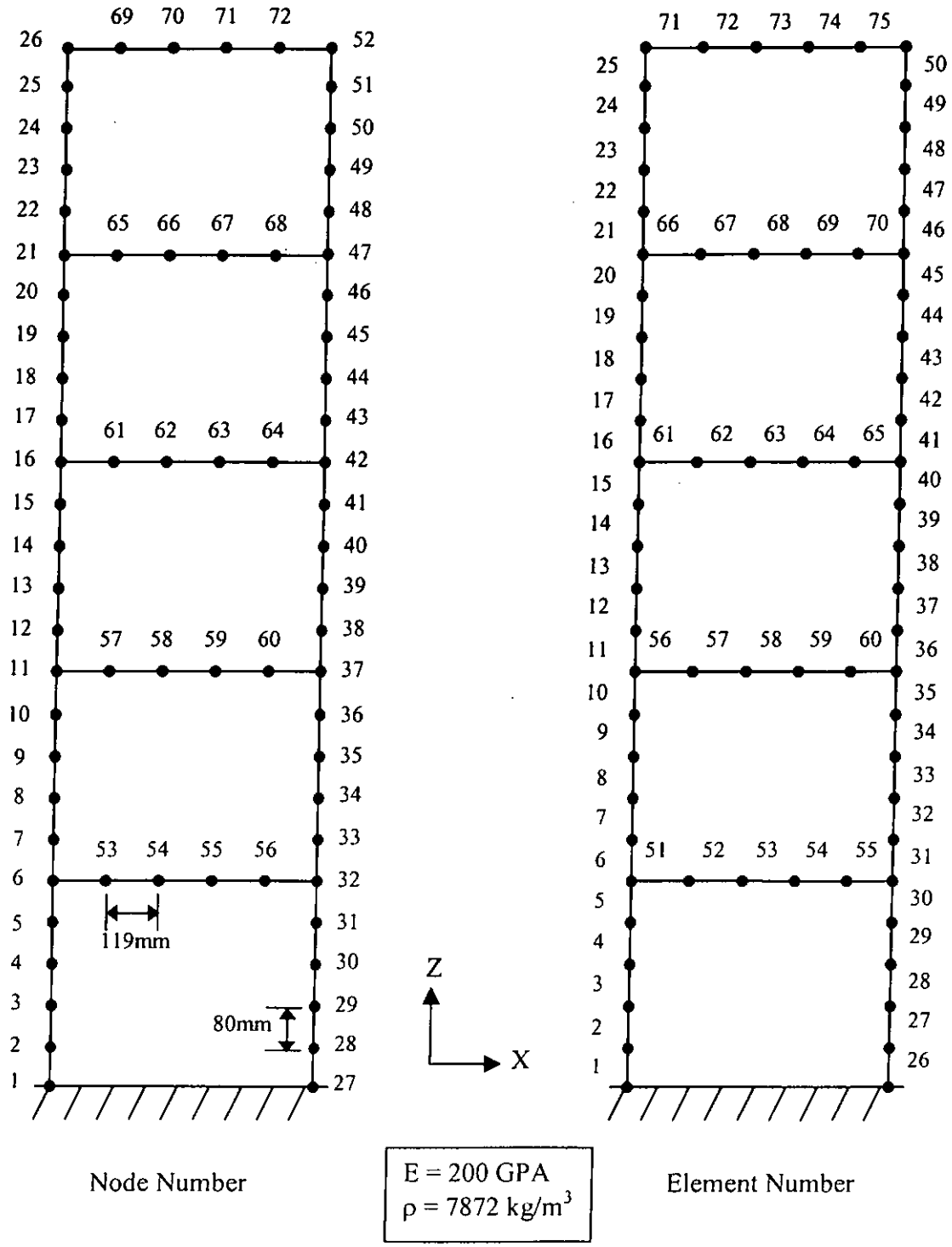

Figure 7.1 - Evaluation view of five-storey steel plane frame

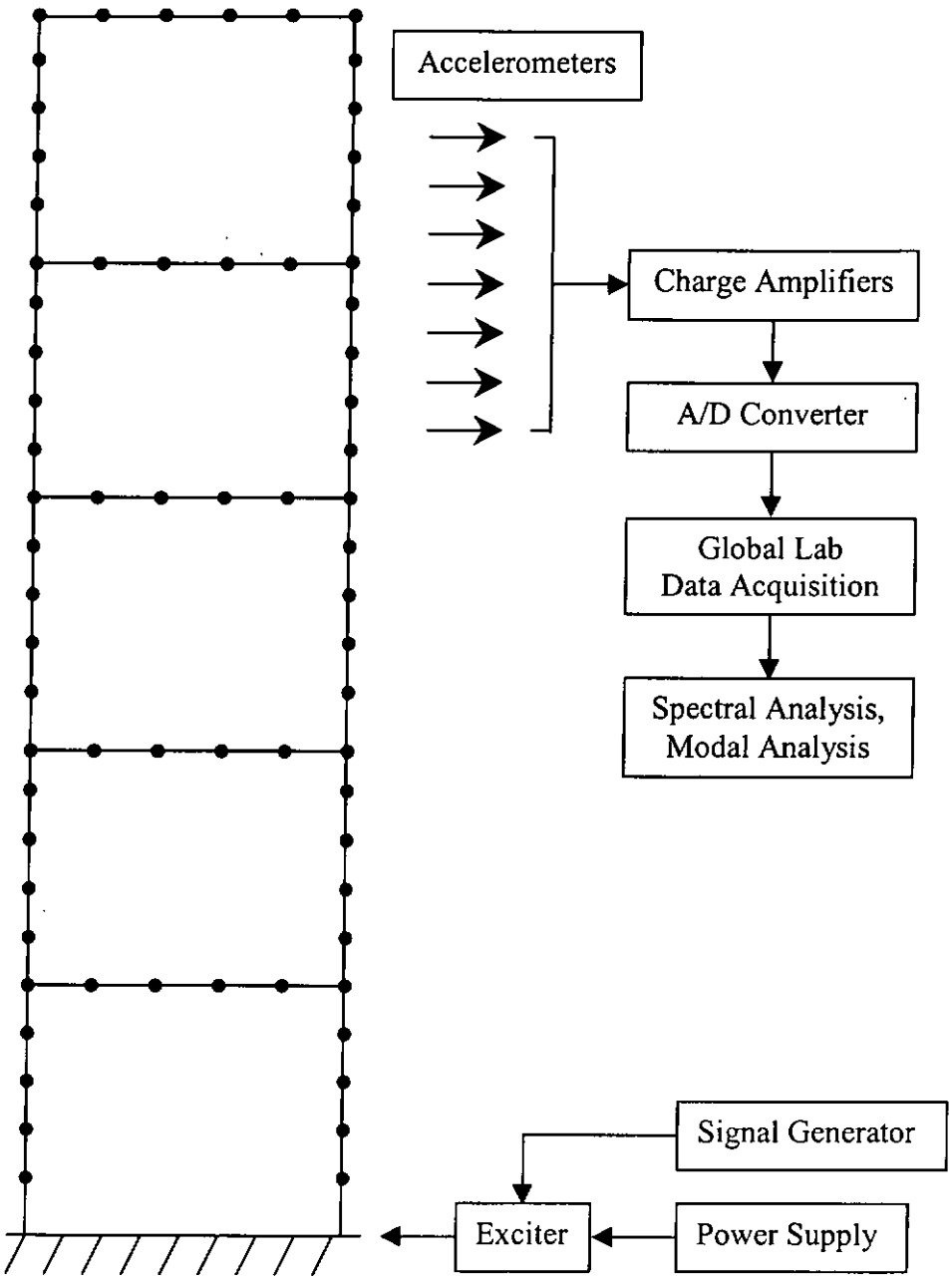

Figure 7.2 - Experimental setup

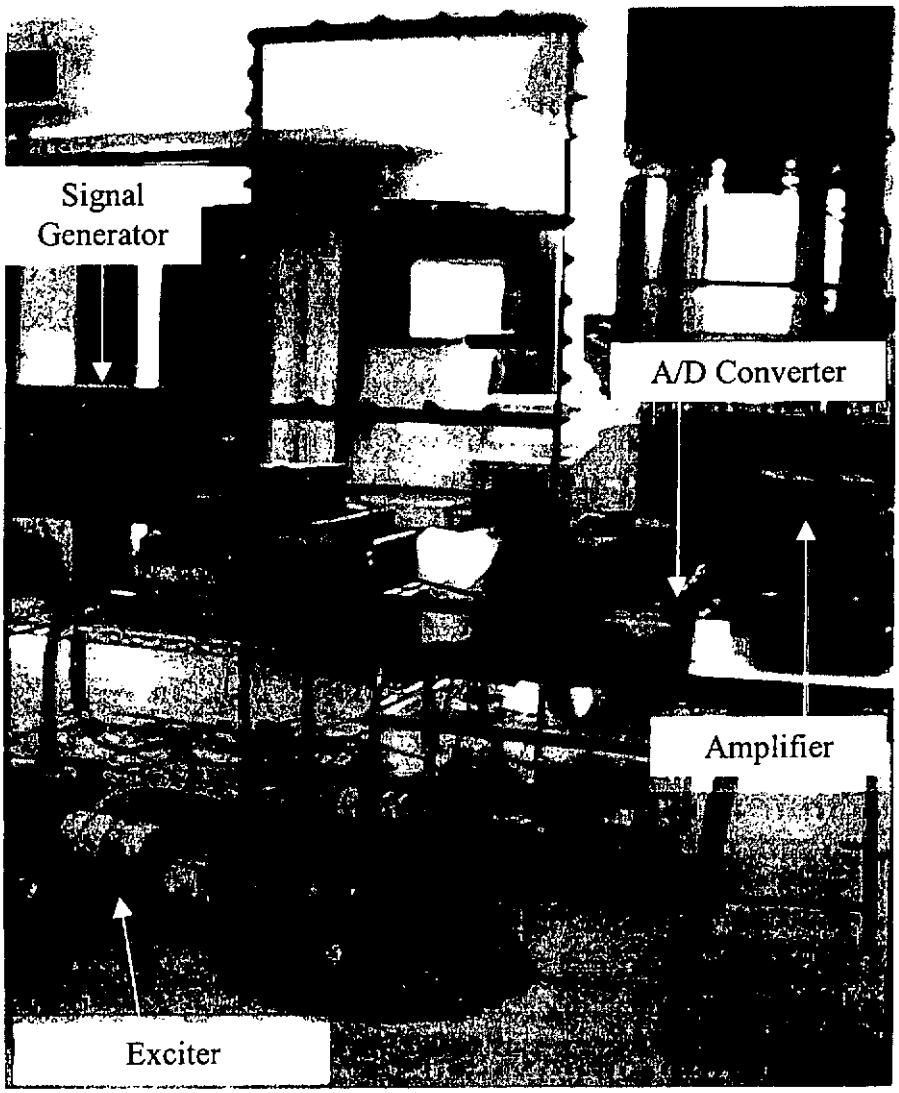

Figure 7.3 - Photograph of experimental setup

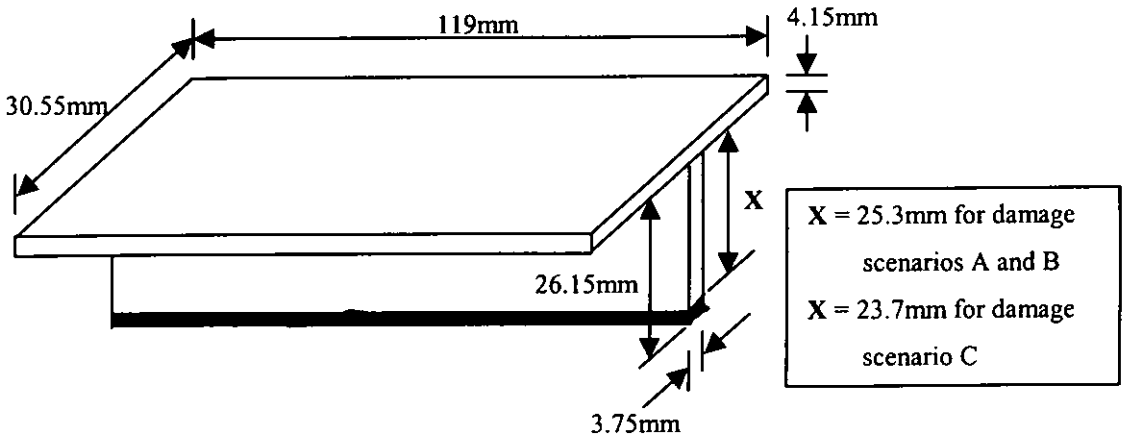

Element 59

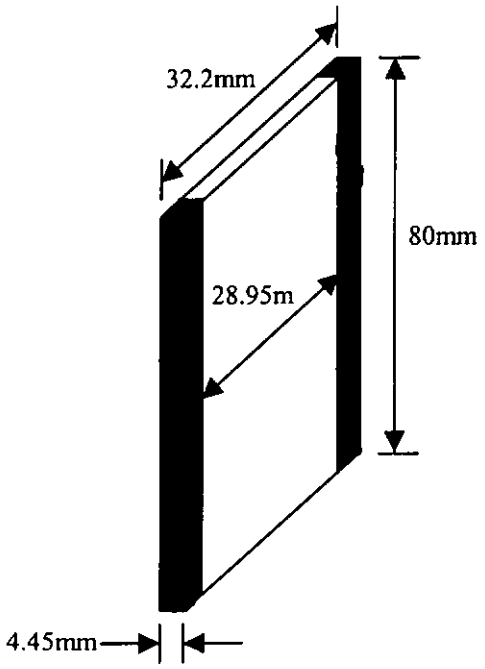

Element 9

Figure 7.4 - Damages in elements 59 and 9

(The part filled with black colour is cut out)

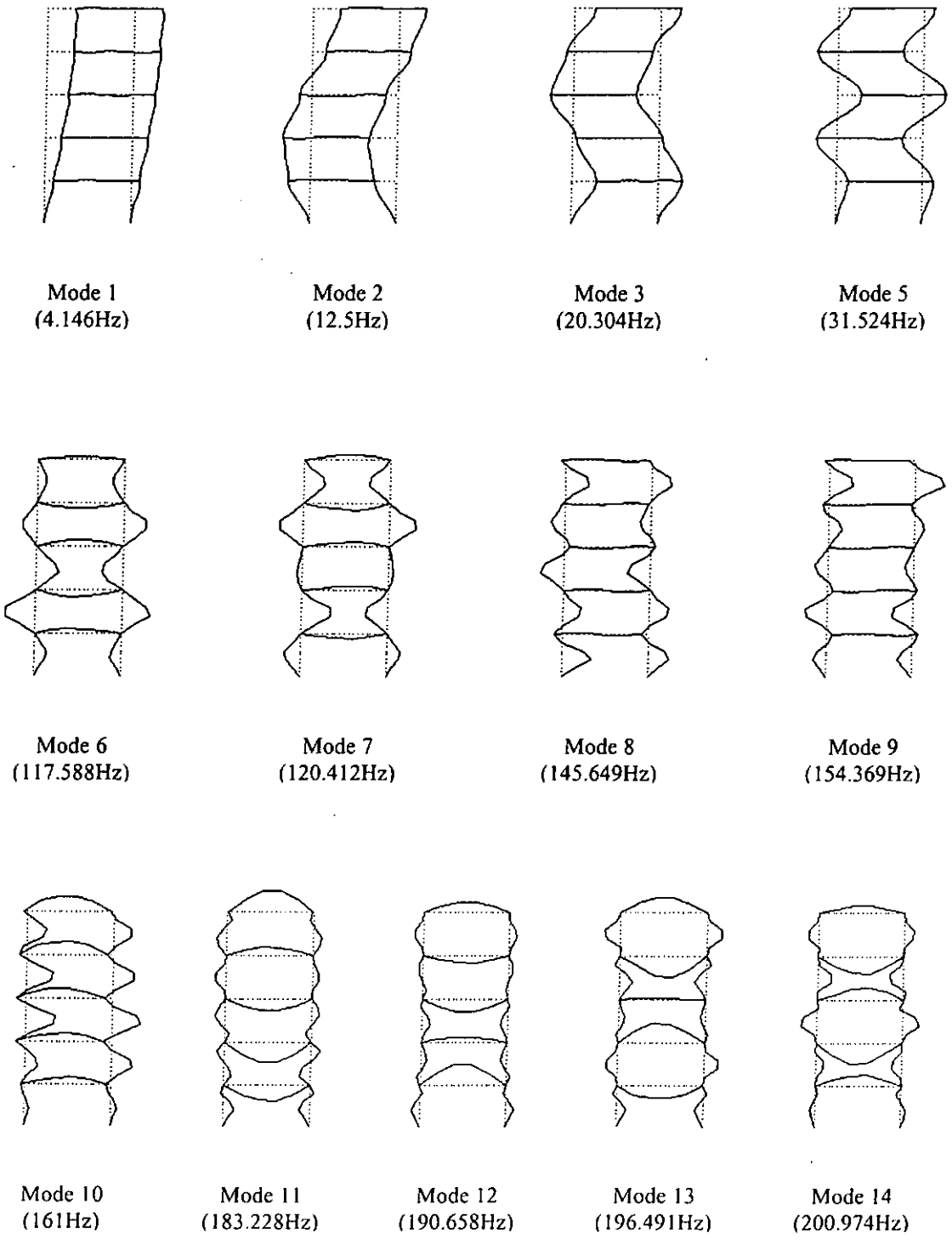

Figure 7.5 - Experimental mode shapes of undamaged five-storey steel plane frame

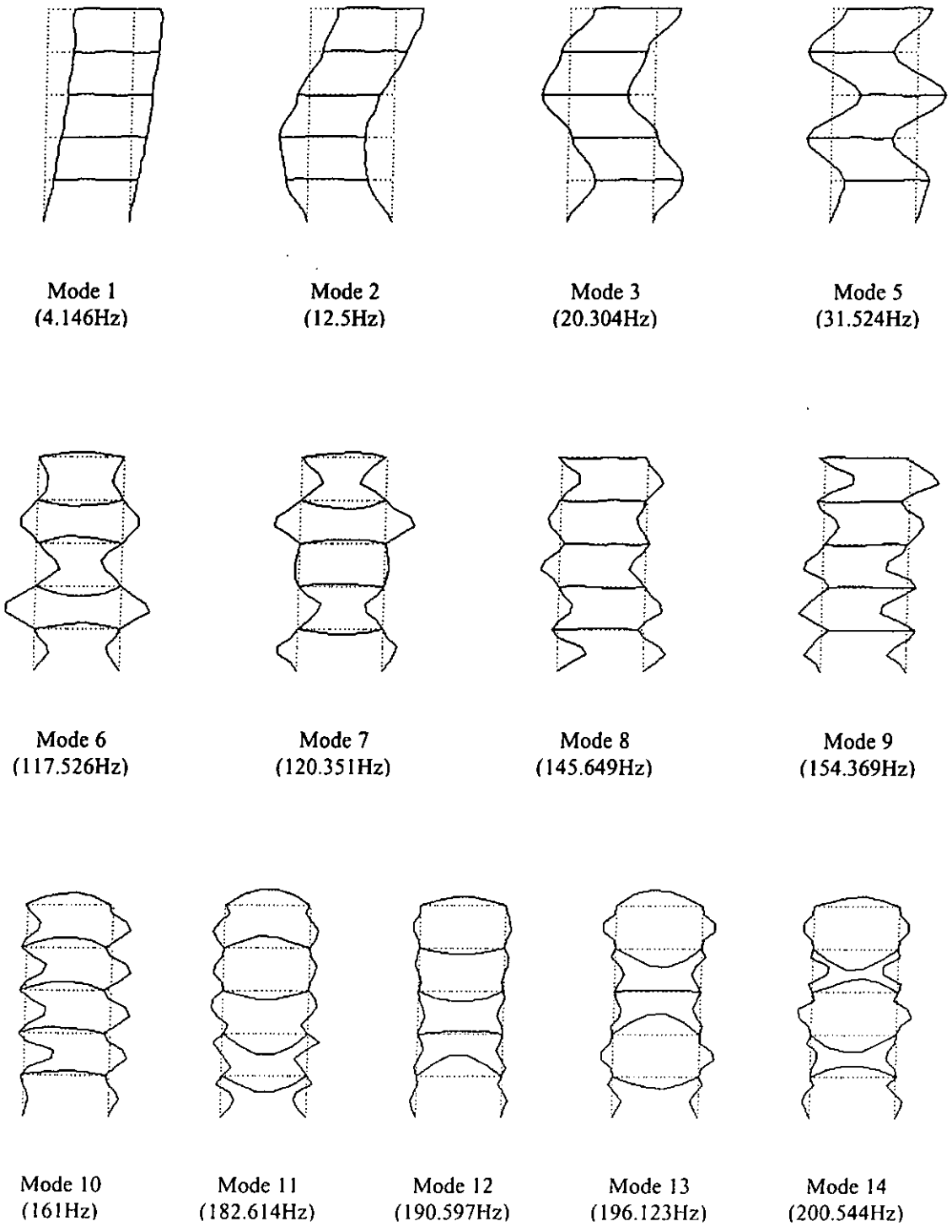

Figure 7.6 - Experimental mode shapes for damage scenario A

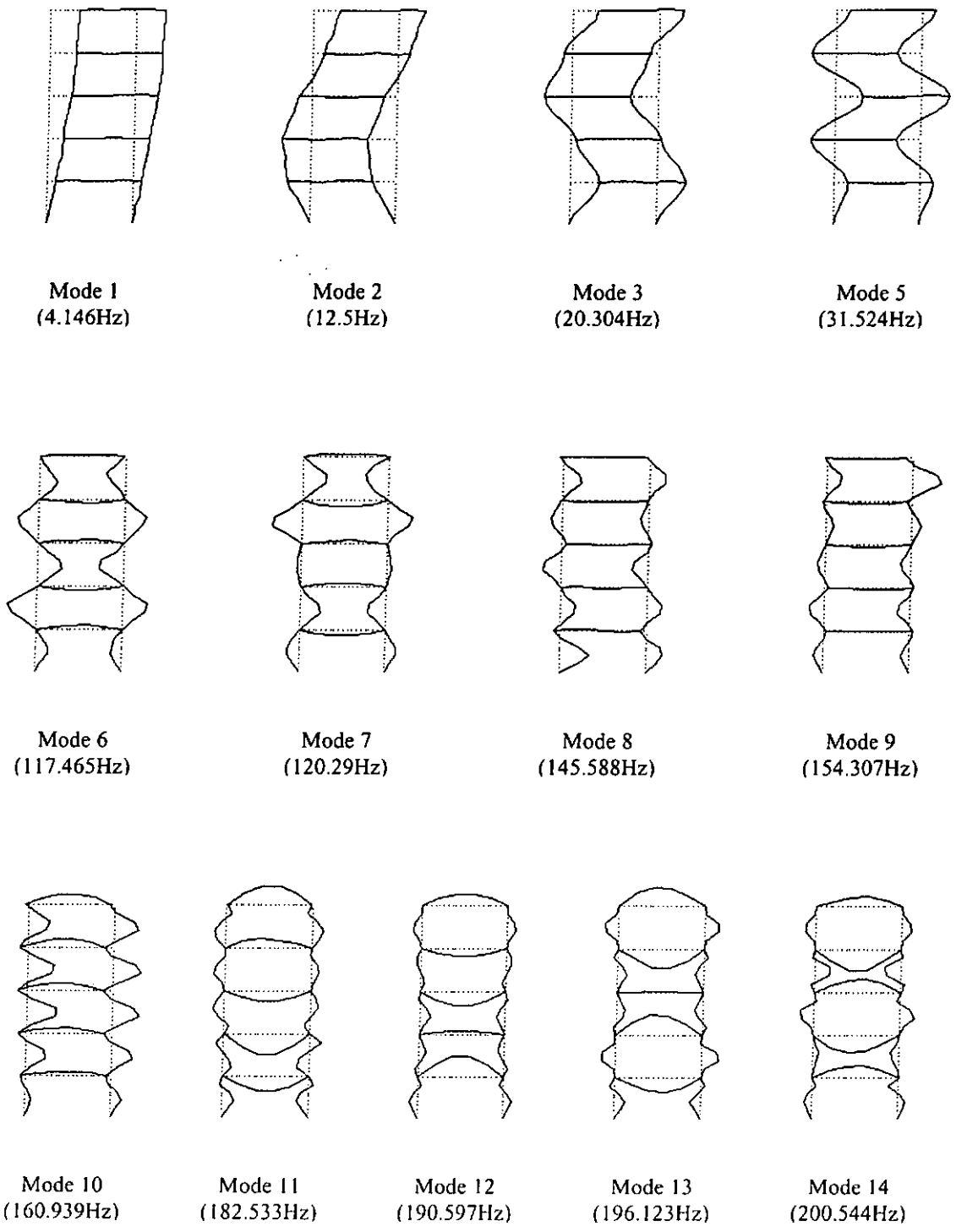

Figure 7.7 - Experimental mode shapes for damage scenario B

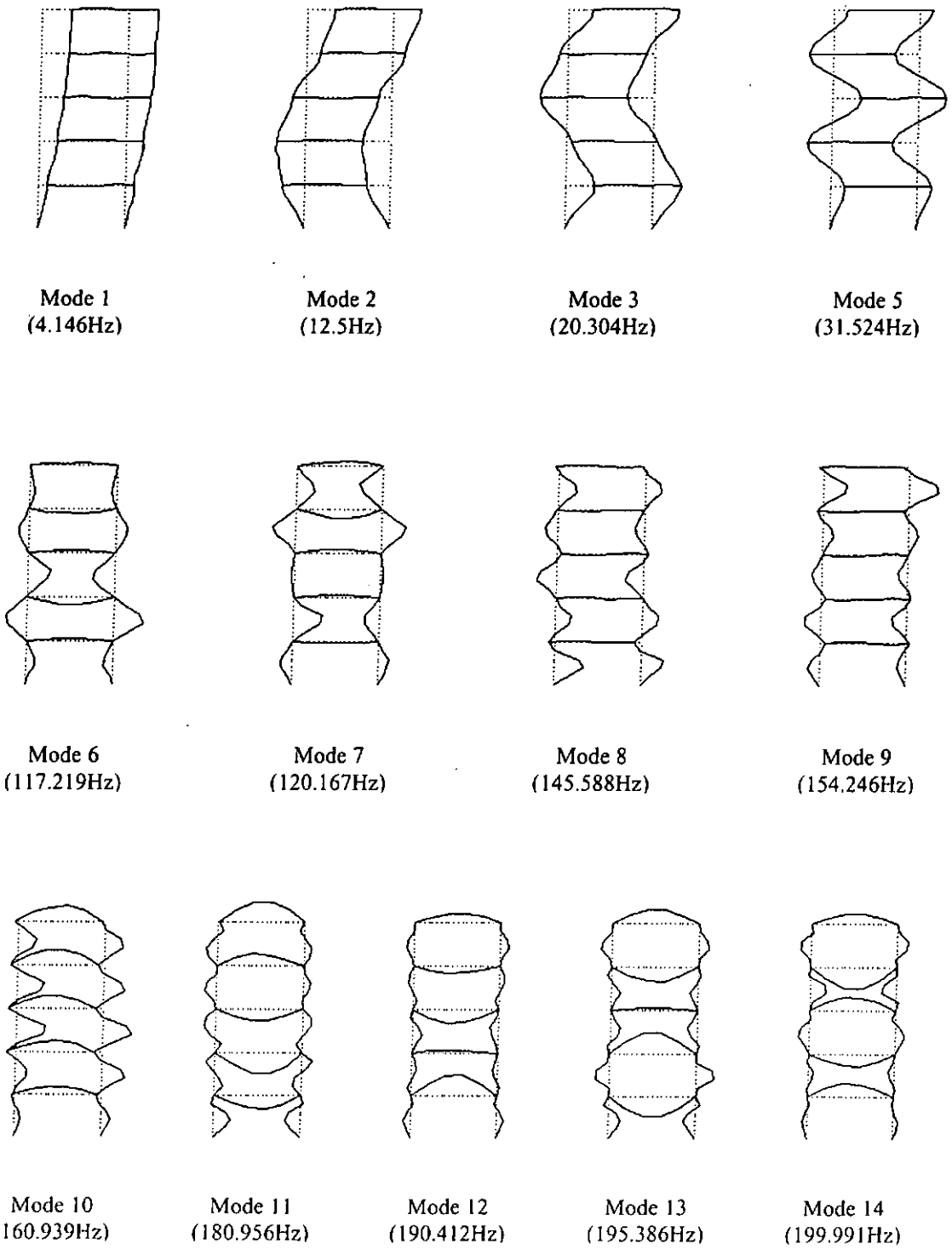

Figure 7.8 - Experimental mode shapes for damage scenario C

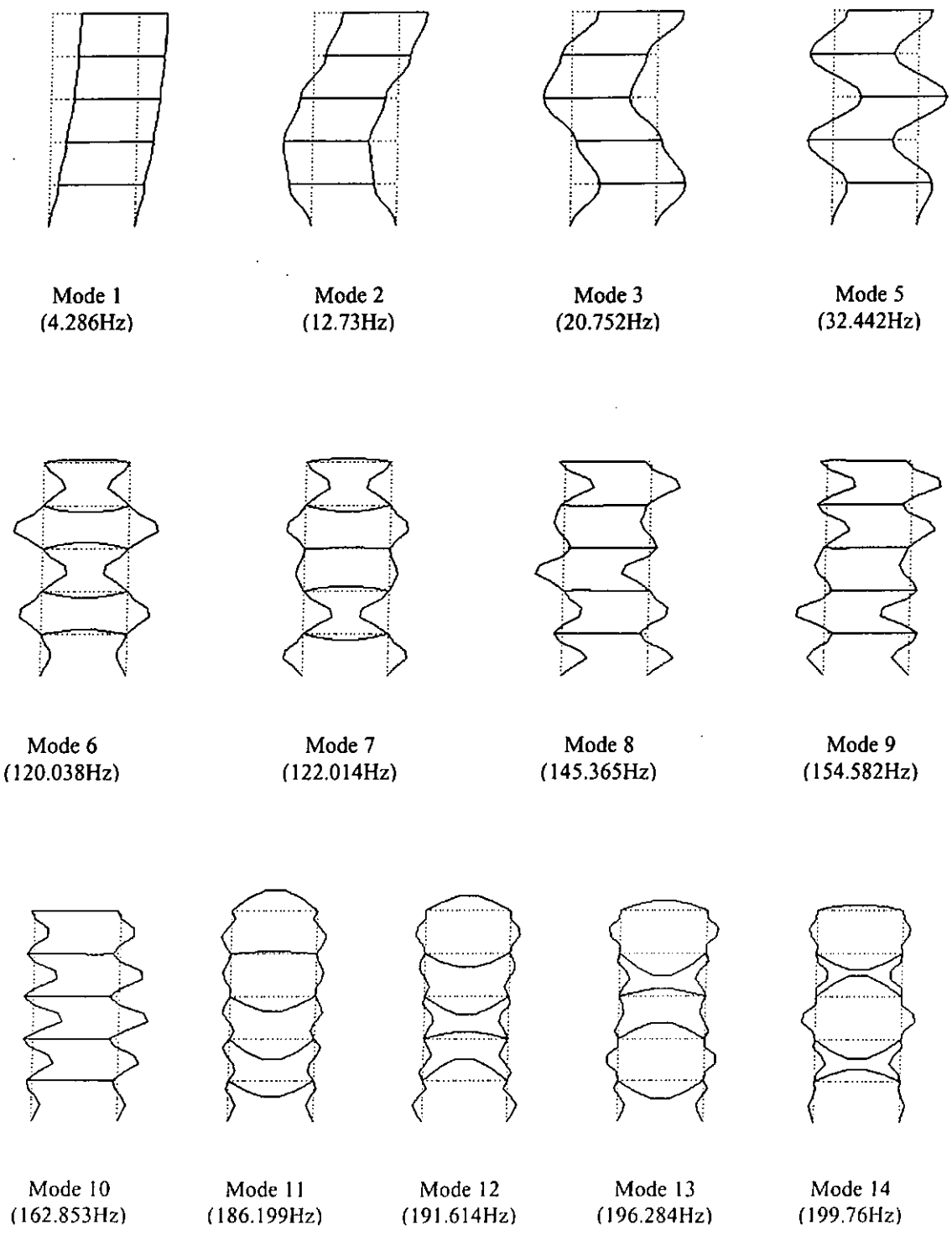

Figure 7.9 - Analytical mode shapes of five-storey steel plane frame

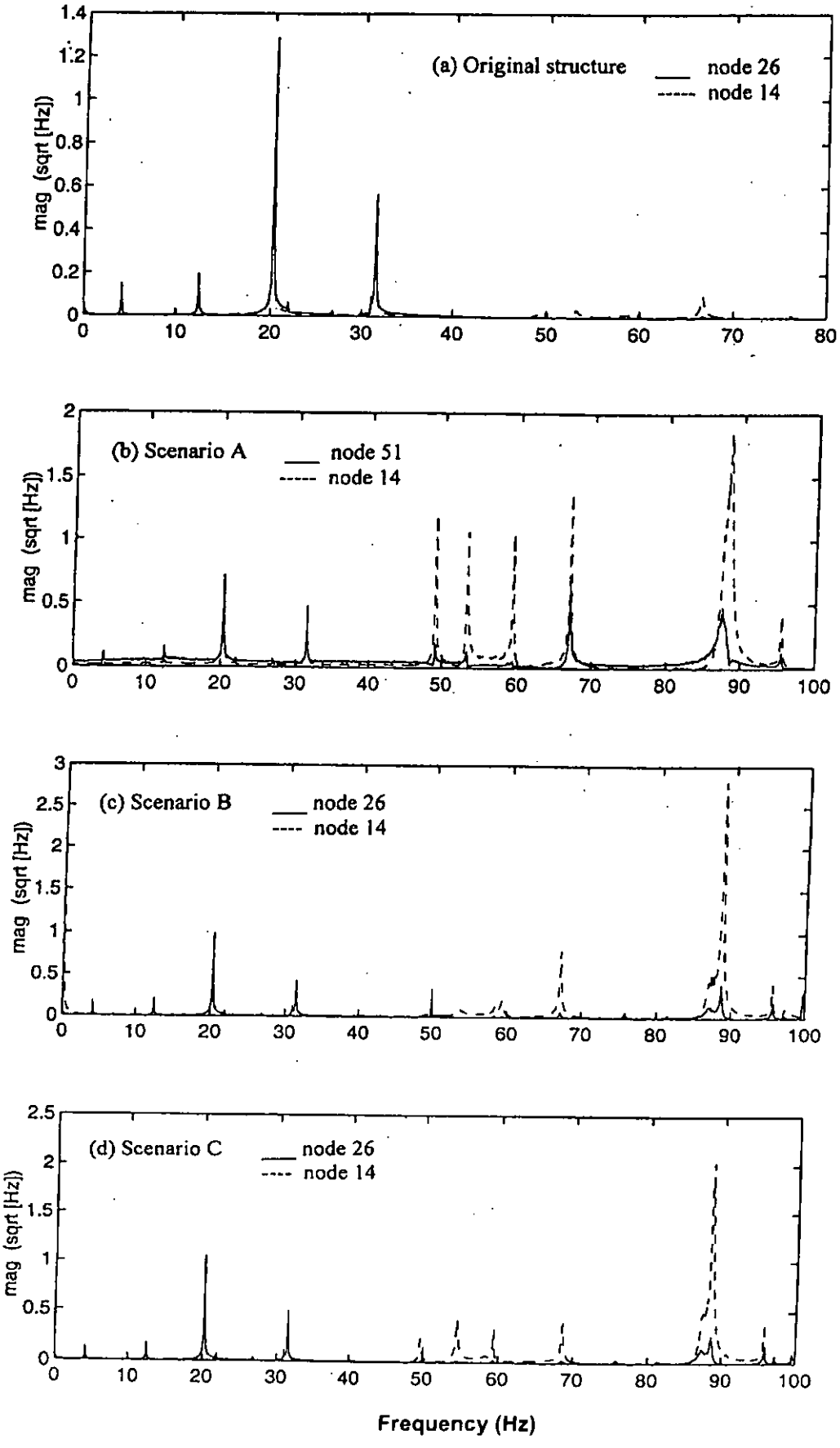
(a) Original structure
node 26
node 14
(b) Scenario A
node 51
node 14
(c) Scenario B
node 26
node 14
(d) Scenario C
node 26
node 14
mag (sqrt [Hz])
Frequency (Hz)

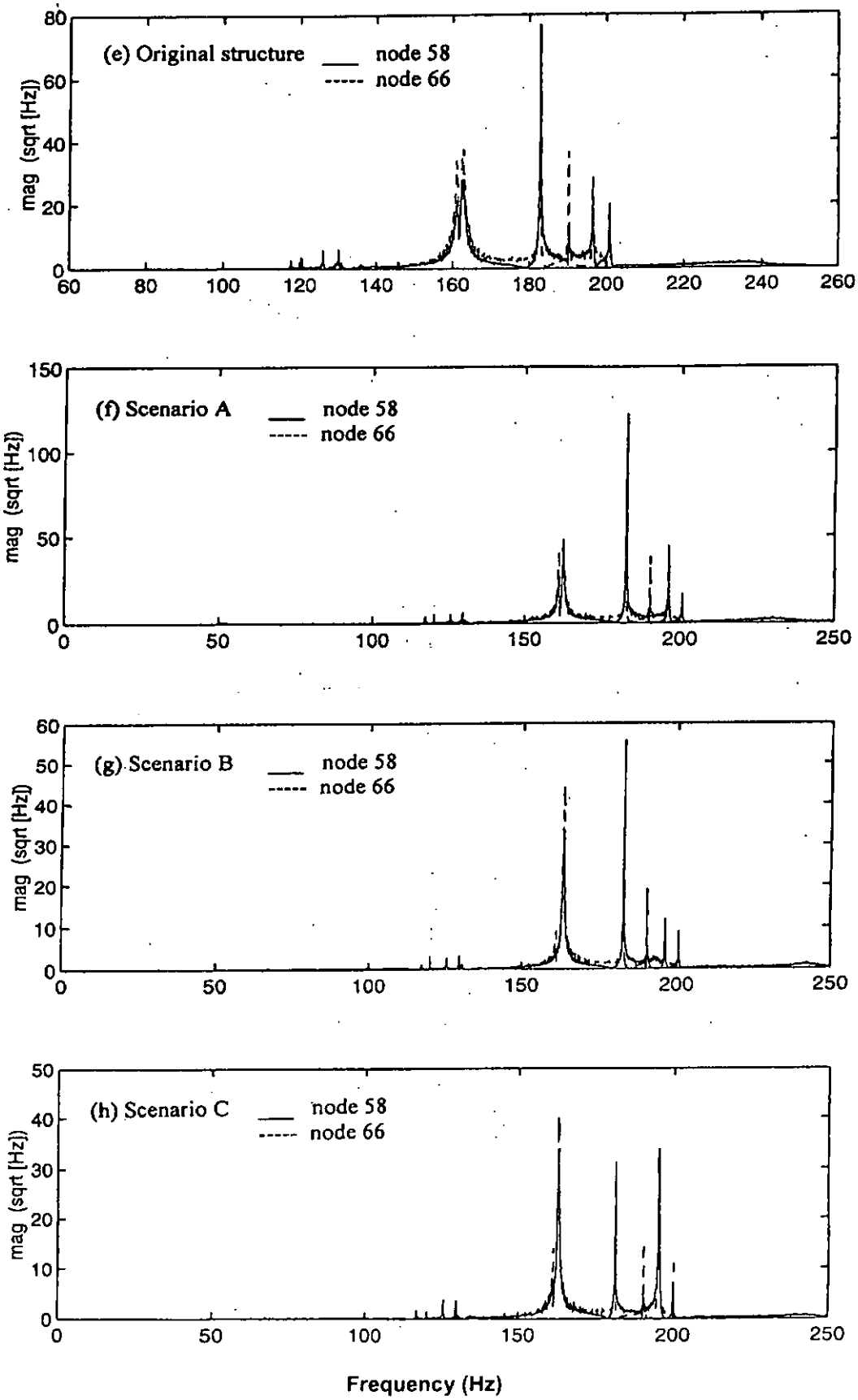

Figure 7.10 - Power spectrum of acceleration responses
(a-d) for global modes; (e-h) for local modes

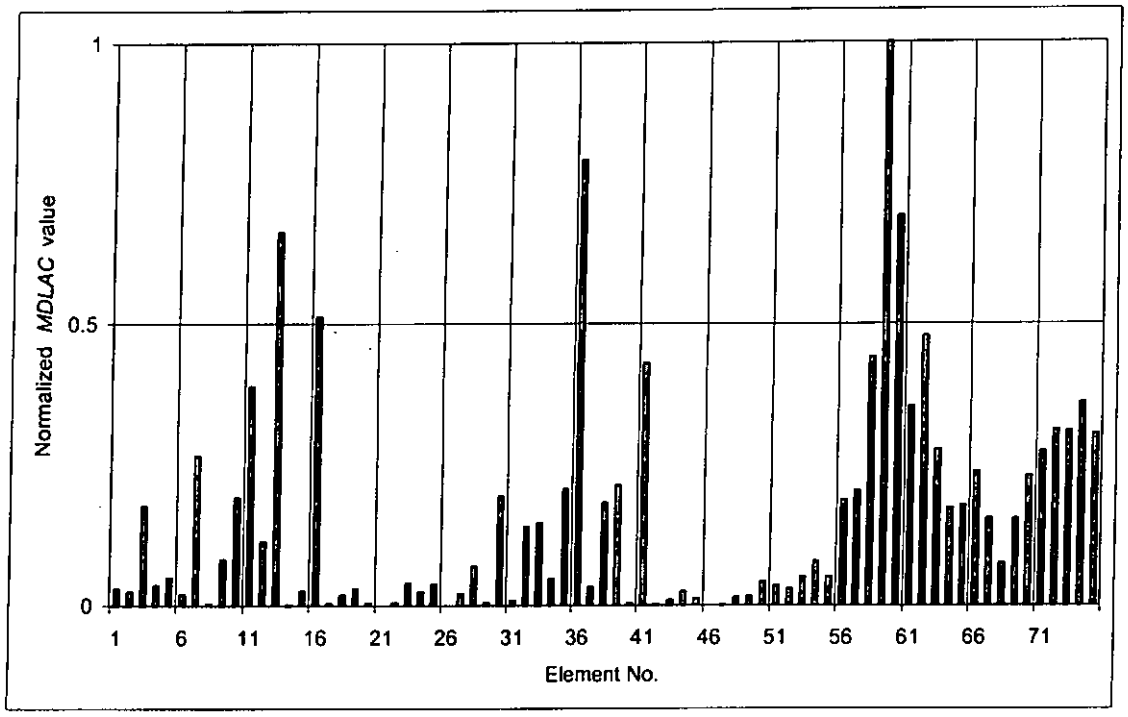

Figure 7.11 - Damage localization chart for damage scenario A

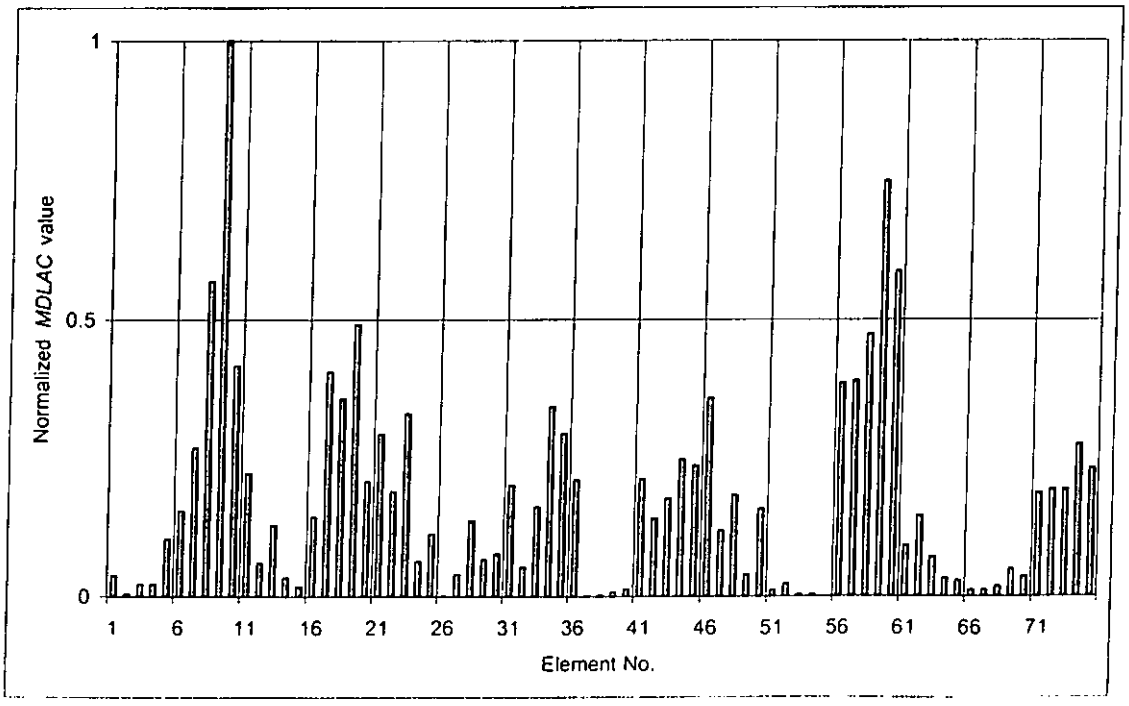

Figure 7.12 - Damage localization chart for damage scenario B

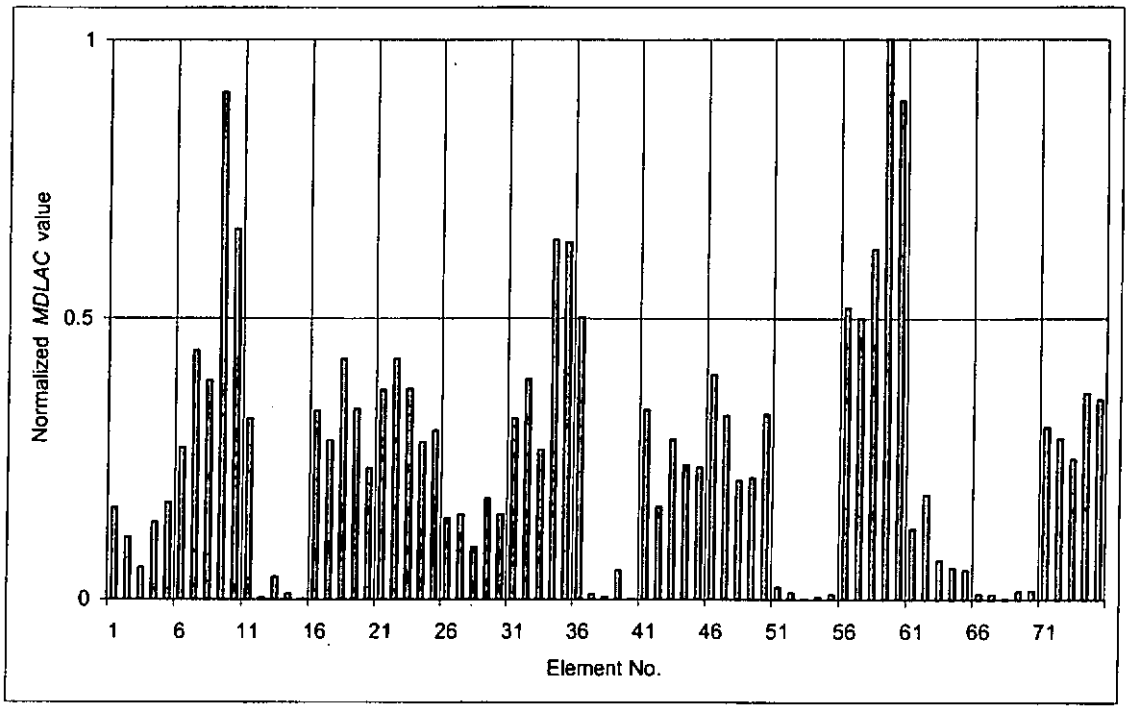

Figure 7.13 - Damage localization chart for damage scenario C

Chapter 8

Conclusions and Recommendations

8.1 Conclusions on the Proposed Damage Localization Method

A damage localization method using incomplete Elemental Modal Strain Energy Change (*EMSEC*) is proposed to localize the structural damage. It is an extension of the Multiple Damage Location Assurance Criterion (*MDLAC*) method. The damage indicator *MDLAC* is used to check the correlation between the analytical *EMSEC* for various damage scenarios and the true measured *EMSEC*. At first, only one element of the structure is assumed to be damaged so that the number of damage scenarios is equal to the number of total element of the structure. The potential damage sites are identified as those elements with higher *MDLAC* values. The final damage sites are then determined by finding those combined sites among the potential damage sites with the highest *MDLAC* values. The advantage of this *MDLAC* method is that only limited information (incomplete *EMSEC*) is used to localize the damage. Simulation results on a three-storey plane frame show that the proposed *MDLAC* method using incomplete *EMSEC* is effective to localize both small and large damages even if the eigenvalues and mode shapes are contaminated with measurement noise up to 0.15% and 3% respectively. The proposed damage localization method is verified on a five-storey steel plane frame experimentally. The

experimental results show that this method can be successfully used to localize single and multiple damages in the test structure.

Comparison with the *MDLAC* method using incomplete mode shape in the simulated three-storey plane frame is also studied. Numerical examples show that the *MDLAC* method using incomplete *EMSEC* has better accuracy than the *MDLAC* method using incomplete mode shapes in damage localization.

Simulation and experimental results show that the damage element usually has the largest *MDLAC* value. The undamaged elements, which are adjacent to or near the damage, have a larger *MDLAC* value because they share the same measured mode shapes of the damage element and have some damage characteristic. The undamaged elements, which symmetrically locate on the other side of the adjacent elements, are identified as potential damage sites due to symmetry of the structure. The undamaged elements, which are far away from the damage, also contain a large *MDLAC* value due to the measurement noise and the assumption of a single damage in the calculation of the analytical *EMSEC* for identifying the potential damage sites. Although some undamaged elements are included in the group of final damage sites, the actual damage elements can be localized after the estimation of the damage extent in the final damage sites by the damage quantification method using second order analysis.

8.2 Conclusions on the Two Proposed Damage Quantification Methods

After damage localization, the damage extent of the damage sites can be determined using the measured eigenvalues that are less contaminated by measurement noise and with better accuracy than mode shapes.

At first, the damage quantification method using first order analysis is developed. The formulation of this method includes the first order terms of the Taylor's expansion of the eigenvalue change. Numerical results on the three-storey plane frame show that this method can estimate the damage extent with a high accuracy for small damage only. When the eigenvalues and mode shapes are contaminated by measurement noise, the damage extent can also be correctly estimated for small damage. The accuracy of identification will be reduced substantially for large damage. Therefore, the method using first order analysis is only suitable for small damage.

There is a special feature in this method, that a smaller set of measured eigenvalues can be expanded into a larger set of eigenvalues. The damage extent can also be correctly estimated for small damage when eigenvalue expansion is allowed. However, the method without eigenvalue expansion has better accuracy than that with eigenvalue expansion because this expansion introduces error in the expanded eigenvalues and decreases the accuracy of the estimation. Another feature in this method is that the final identification result is independent of the initial estimate of the damage extent $\hat{C}$. Experimental results on the five-storey steel plane frame indicate

that the damage quantification method using first order analysis is effective for small damage only.

In order to increase the accuracy in identification for large damage, the second order terms in the Taylor's expansion are included in the formulation of the second order analysis. Two necessary conditions are developed in this method for the optimal solution.

This method also has two features. (1) Eigenvalue expansion is permitted in the formulation; and (2) This method is independent of the initial estimate of damage extent $\hat{C}$ and the value of C_0 around which the Taylor's expansion is taken. Simulations on the three-storey plane frame are studied. The simulated results show that the method using the first necessary condition only or using both necessary conditions can obtain the same results when there is no eigenvalue expansion. When the expansion is included, the method using the first necessary condition is more accurate than that using both necessary conditions. This is because the gain matrix P is simplified when both conditions are included in the formulation so that the accuracy of the damage extent is decreased. The identified results also indicate that the method using the first necessary condition only is robust and effective to detect the damage extent for small and large damages. The damage extent of the suspected elements can be determined correctly even when the modal information is affected by measurement noise. The estimation results without eigenvalue expansion are more accurate than those with eigenvalue expansion. This method is verified by the experimental results of the five-storey steel plane frame. The experimental results

indicate that the damage quantification method using second order analysis and the first necessary condition can estimate correctly the damage extent for small and large damages. The method using both conditions give less accurate identification results in the different cases studied.

By comparing the two proposed damage quantification methods for small damage, the simulation results show that the method using second order analysis gives more accurate estimation than the method using first order analysis. The experimental results also support this conclusion.

8.3 Conclusions on the Eigenvalue Expansion Study

Two damage quantification methods studied in this thesis enable eigenvalue expansion from a small set of measured eigenvalues. The simulation results on the three-storey plane frame show that the estimated frequencies are very close to the true frequencies for both small and large damages. Moreover, the estimation without undamaged elements in the suspected element group has better performance than that with undamaged elements in the suspected group. The expanded frequencies from the eigenvalue expansion process are verified with the experimental data of the five-storey steel plane frame. The experimental results show that the expanded frequencies are estimated correctly.

8.4 Recommendations

Following are some recommendations for further research

1. In practice, incomplete information is used directly without any expansion or reduction to localize the structure damages. Many sensor placement methods (Chen and Graba, 1985; Kammer, 1991; Hemez and Farhat, 1994; Cobb and Liebst, 1997 and Kashangaki, 1992) have been proposed to select the sensor locations such that the useful degrees-of-freedom are selected. However in this dissertation, the sensor locations are selected with the engineering sense. Hence, the effectiveness of the *MDLAC* method using incomplete *EMSEC* can be further investigated by using different sensor placement methods.

2. In the damage localization method, three global modes and three local modes are used to detect the structure damages in the three-storey plane frame. However, the number of modes and which of them are most suitable modes are not known, and this information varies for different structure. Some criteria or methods should be developed to select the optimum modes and number of modes.

3. In the damage quantification methods, the first five modes with the largest eigenvalue change ratio are expanded into eight modes in the three-storey plane frame. However, the requirement of the minimum number of measured eigenvalues and the maximum number of the expanded eigenvalues can be further studied.

4. A practical structure is large and complex. It consists of different structural components made of different materials. In this dissertation, the test structure only consists of two structural components and is made of steel. Structures with more structural components made of concrete or composite materials can be used to further investigate the three proposed methods in this thesis.

5. In reality, structures are much larger and complex. The number of unknowns may be much larger, and the least-squares method cannot handle the ill-conditioned problem. Under this situation, different regularization techniques can be used to solve this problem.

References

1. Adelman, H.M. and Haftka, R.T. "Sensitivity analysis of discrete structural systems". *AIAA Journal*, Vol. 24, No. 5, pp.823-832 (1986)
2. Allemang, R.J. and Brown, D.L. "A correlation coefficient for modal vector analysis". *Proceedings International Modal Analysis Conference*, pp.110-116 (1982)
3. Baruch, M. and Bar Itzhack, I.Y. "Optimum weighted orthogonalization of measured modes". *AIAA Journal*, Vol. 16, No. 4, pp.346-351 (1978)
4. Berger, H., Chaquin, J.P. and Ohayon, R. "Finite element model adjustment using experimental vibration data". *Proceedings of the 2nd International Modal Analysis Conference*, Orlando, FL, February, 1984, pp.638-642 (1984)
5. Berman, A. and Flannelly, W.G. "Theory of incomplete models of dynamic structures". *AIAA Journal*, Vol. 9, No. 8, pp.1481-1487 (1971)
6. Berman, A. and Nagy, E.J. "Improvement of a large analytical model using test data". *AIAA Journal*, Vol. 21, No. 8, pp.1168-1173 (1983)
7. Brock, J.E. "Optimal matrices describing linear systems". *AIAA Journal*, Vol. 6, No. 7, pp.1292-1296 (1968)
8. Cawley, P. and Adams, R.D. "The location of defects in structures from measurements of natural frequencies". *Journal of Strain Analysis*, Vol. 14, No. 2, pp.49-57 (1979)
9. Ceravolo, R., Stefano, A.D. and Torino, P.D. "Damage location in structures through a connectivistic use of FEM modal analysis". *The International Journal of Analytical and Experimental Modal Analysis*, Vol. 10, No. 3, pp.178-186 (1995)
10. Chen, J.C. and Garba, J.A. "Analytical model improvement using modal test results". *AIAA Journal*, Vol. 18, No. 6, pp.684-690 (1980)
11. Chen, J.C. and Garba, J.A. "Structural analysis model validation using modal test data". *Joint ASCE/ASME Mechanics Conference*, Albuquerque, NM, pp.109-137 (1985)

12. Cobb, R.G. and Liebst, B.S. "Sensor placement and structural damage identification from minimal sensor information". *AIAA Journal*, Vol. 35, No. 2, pp.369-374 (1997)
13. Doebling, S.W., Hemez, F.M., Barlow, M.S., Peterson, L.D. and Farhat, C. "Damage detection in a suspended scale model truss via model update". *Proceedings of the 11th International Modal Analysis Conference*, Orlando, FL, February, 1993, pp.1083-1094 (1993)
14. Doebling, S.W., Hemez, F.M., Peterson, L.D. and Farhat, C. "Improved damage location accuracy using strain energy-based mode selection criteria". *AIAA Journal*, Vol. 35, No. 4, pp.693-699 (1997)
15. Farrar, C.R. and Cone, K.M. "Vibration testing of the I-40 bridge before and after the introduction of damage". *Proceedings of the 13th International Modal Analysis Conference*, pp.203-209 (1995)
16. Farhat, C. and Hemez, F.M. "Updating finite element dynamic models using an element-by-element sensitivity methodology". *AIAA Journal*, Vol. 31, No. 9, pp.1702-1711 (1993)
17. Friswell, M.I., Panny, J.E.T. and Wilson, D.A.L. "Using vibration data and statistical measures to locate damage in structures". *The International Journal of Analytical and Experimental Modal Analysis*, Vol. 9, No. 4, pp. 239-254 (1994)
18. Guyan, R.J. "Reduction of stiffness and mass matrices". *AIAA Journal, Technical Note*, Vol. 3, No. 2, pp.380 (1965)
19. Hajela, P. and Soeiro, F.J. "Recent developments in damage detection based on system identification methods". *Structural Optimization*, Vol. 2, pp.1-10 (1990)
20. He, J. and Ewins, D.J. "Compatibility of measured and predicted vibration modes in model improvement studies". *AIAA Journal*, Vol. 29, No. 5, pp.798-803 (1991)
21. Hearn, G. and Testa, R.B. "Modal analysis for damage detection in structures". *Journal of Structural Engineering*, Vol. 17, No. 10, pp.3042-3063 (1991)
22. Hemez, F.M. and Farhat, C. "An energy based optimum sensor placement criterion and its application to structural damage detection". *Proceedings of the 12th International Modal Analysis Conference*, pp.1568-1575 (1994)
23. Imregun, M. and Ewins, D.J. "An investigation into mode shape expansion techniques". *Proceedings of the 11th International Modal Analysis Conference*, Orlando, FL, February, 1993, pp.168-175 (1993)

24. Inman, D.J. and Minas, C. "Matching analytical models with experimental modal data in mechanical systems". *Control and Dynamics Systems*, Vol. 37, pp.327-363 (1990)
25. Ju, F.D. and Mimovich, M. "Modal frequency method in diagnosis of fracture damage in structures". *Proceedings of the 4th International Modal Analysis Conference*, Los Angeles, Vol. 2, pp.1168-1174 (1986)
26. Ju, F.D. and Mimovich, M.E. "Experimental diagnosis of fracture damage in structures by the modal frequency method". *Modal Testing and Analysis, ASME*, pp.29-36 (1987)
27. Kabe, A.M. "Stiffness matrix adjustment using mode data". *AIAA Journal*, Vol. 23, No. 9, pp.1431-1436 (1985)
28. Kammer, D.C. "Optimum approximation for residual stiffness in linear system identification". *AIAA Journal*, Vol. 26, No. 1, pp.104-112 (1988)
29. Kammer, D.C. "Sensor placement for on-orbit modal identification and correlation of large space structures". *Journal of Guidance, Control and Dynamics*, Vol. 14, No. 2, pp.251-259 (1991)
30. Kaouk, M. and Zimmerman, D.C. "Structural damage assessment using a generalized minimum rank perturbation theory". *AIAA Journal*, Vol. 32, No. 4, pp.836-842 (1994)
31. Kaouk, M. and Zimmerman, D.C. "Evaluation of the minimum rank update in damage detection: an experimental study". *Proceedings of the 11th International Modal Analysis Conference*, Orlando, FL, February, 1993, pp.1061-1068 (1993)
32. Kashangaki. T.A.L. "Mode selection for damage detection using the modal sensitivity parameter". *Proceedings of the 13th Structures, Structural Dynamics and Materials Conference*, AIAA, Washington, DC, pp.1535-1542 (1992)
33. Koh, C.G., See, L.M. and Balendre, T. "Damage detection of buildings: numerical and experimental studies". *Journal of Structural Engineering, ASCE*, Vol. 121, pp.1155-1160 (1995)
34. Kudva, J.N., Munir, N. and Tan, P.W. "Damage detection in smart structures using neural networks and finite-element analyses". *Smart Materials and Structures*, Vol. 1, pp.108-112 (1992)

35. Law, S.S. and Li, X. "Structural damage detection based on higher order analysis". *Asia-Pacific Vibration Conference, Session: Modal Analysis & Identification*, pp.640-643 (1993)
36. Law, S.S., Shi, Z.Y. and Zhang, L.M. "Structural damage detection from incomplete and noisy modal test data". *Journal of Engineering Mechanics*, Vol. 124, No. 11, pp.1280-1288 (1998)
37. Lieven, N.A.J. and Ewins, D.J. "Spatial correlation of mode shapes, the Co-ordinate Modal Assurance Criterion (COMAC)". *Proceedings of the 6th International Modal Analysis Conference*, pp.690-695 (1988)
38. Lim, T.W. and Kashangaki, T.A.L. "Structural damage detection of space truss structures using best achievable eigenvectors". *AIAA Journal*, Vol. 35, No. 5, pp.1049-1057 (1994)
39. Lin, C.S. "Location of modeling errors using modal test data". *AIAA Journal*, Vol. 28, No. 9, pp.1650-1654 (1990)
40. Messina, A., Jones, I.A. and Williams, E.J. "Damage detection and localization using natural frequency changes". *International Conference on Identification in Engineering Systems*, Swansea, Wales, U.K., pp.67-76 (1996)
41. Messina, A., Williams, E.J. and Contursi, T. "Structural damage detection by a sensitivity and statistical-based method". *Journal of Sound and Vibration*, Vol. 216, No. 5, pp.791-808 (1998)
42. Paul, L.H.F. "Detection of damage location based on sensitivity and experimental modal analysis". *M.Phil. Thesis*, Civil and Structural Engineering Department, The Hong Kong Polytechnic University (1994)
43. Ricles, J.M. and Kosmatka, J.B. "Damage detection in elastic structures using vibratory residual forces and weighted sensitivity". *AIAA Journal*, Vol. 30, No. 9, pp.2310-2316 (1992)
44. Rodden, W.P. "A method for deriving structural influence coefficients from ground vibration tests". *AIAA Journal*, Vol. 5, No. 5, pp.991-1000 (1967)
45. Rudisill, C.S. "Derivatives of eigenvalues and eigenvectors for a general matrix". *Journal of AIAA*, Vol. 12, No. 5, pp.721-722 (1974)
46. Sage, A.P. and White, III C.C. "Optimum state estimation". *Optimum Systems Control*, Prentice-Hall, Inc., United States of America, pp.198-201 (1977)

47. Shi, Z.Y., Ding, X.H. and Gu, H.Z. "A new model reduction and expansion method". *Proceedings of the International Conference on Structural Dynamics, Vibration, Noise and Control*, Hong Kong, Vol. 2, pp.847-852 (1995)
48. Shi, Z.Y., Law, S.S. and Zhang, L.M. "Structural damage localization from modal strain energy change". *Journal of Sound and Vibration*, Vol. 218, No. 5, pp.825-844 (1998)
49. Shi, Z.Y., Law, S.S. and Zhang, L.M. "Damage localization by directly using incomplete mode shapes". *Journal of Engineering Mechanics, ASCE*, Vol. 126, No. 6, pp.656-660 (2000)
50. Shi, Z.Y., Law, S.S. and Zhang, L.M. "Improved damage quantification from modal strain energy change". *Journal of Engineering Mechanics, ASCE*, (submitted)
51. Smith, S.W. and Beattie, C.A. "Simultaneous expansion and orthogonalization of measured modes for structure identification". *Proceedings of the 31st AIAA Dynamics Specialist Conference*, 1990, pp. 261-270 (1990)
52. Smith, S.W. and Beattie, C.A. "Secant-method adjustment for structural models". *AIAA Journal*, Vol. 29, No. 1, pp.119-126 (1991)
53. Stubbs, N. and Kim, J.T. "Damage localization in structures without baseline modal parameters". *AIAA Journal*, Vol. 34, No. 8, pp.1644-1649 (1996)
54. Topole, K.G. and Stubbs, N. "Non-destructive damage evaluation in complex structures from a minimum of modal parameters". *The International Journal of Analytical and Experimental Modal Analysis*, Vol. 10, pp.95-103 (1995)
55. Worden, K., Ball, A.D. and Tomlinson, G.R. "Fault location in a framework structure using neural networks". *Smart Materials and Structures*, Vol. 2, pp.189-200 (1993)
56. Wu, X., Ghaboussi, J. and Garrett, J.H. "Use of neural networks in detection of structural damage". *Computers and Structures*, Vol. 42, No. 4, pp.649-659 (1992)
57. Yuen, M.M.F. "A numerical study of the eigenparameters of a damaged cantilever". *Journal of Sound and Vibration*, Vol. 103, No. 3, pp.301-310 (1985)
58. Zimmerman, D.C. and Kaouk, M. "Structural damage detection using a subspace rotation algorithm". *Proceedings of the AIAA 33rd Structures, Structural Dynamics, and Materials Conference, AIAA*, Washington, DC, 1992, pp.2341-2350 (1992)

59. Zimmerman, D.C. and Widengren, M. "Correcting finite element models using a symmetric eigenstructure assignment technique". *AIAA Journal*, Vol. 28, No. 9, pp.1670-1676 (1990)